Kinematic Analysis of Hurricane Frederick (1979) Using Satellite, Aircraft and Rawinsonde Data

Final Report on NASA Grant NAG5-102

William M. Frank
Department of Meteorology
The Pennsylvania State University

Edward B. Rodgers
Severe Storms Branch
Goddard Laboratory for Atmospheric Sciences
National Aeronautics and Space Administration

Abstract

This report presents results of kinematic analyses of Hurricane Frederick (1979) performed using satellite wind vectors, aircraft measurements and rawinsonde data. The data were gathered, reduced, preliminarily integrated and used to analyze the structure of the storm in the inflow and outflow layers. The mean structure at large radii is in good agreement with composite analyses of tropical cyclones. Changes in the storm structure from 11 to 12 SEP 79 suggest that remote sensing techniques may be useful in monitering storm intensity. A more sophisticated integration of the various data, including determination of optimum heights for satellite wind vectors, is underway as part of the continuation of this research.

1. Introduction

As Hurricane Frederick crossed the Gulf of Mexico on 11-12 Sept. 1979, it was probed by a wide variety of direct and remote sensing instruments. These included continuous monitoring of the low level core by instrumented aircraft, visible satellite imagery, ocean measurements from aircraft-deployed bathothermographs, rawinsondes from land based stations, and surface reports from ships and buoys. This accumulation of measurements is the most extensive and highest quality data set ever assembled for a single tropical cyclone. As such, it offers a unique opportunity to explore the three-dimensional structure, dynamics and energetics of a tropical cyclone over an area extending from its center to approximately 800 km radius.

The available satellite data for Hurricane Frederick included rapid-scan visible imagery on 11-12 Sept. 1979 at five observation times. These special observations allow tracking of low-level cumulus clouds and upper level cirrus to estimate wind speeds. Satellite-wind vectors of this nature have been used in several previous studies of tropical cyclones (Rodgers et al., 1979; Rogers and Gentry, 1981). They have often been the only available data for these storms which are usually far from traditional rawinsonde networks and are often beyond the range of instrumented aircraft.

There are a number of problems concerning the analysis of tropical cyclones using satellite-derived winds. Among the most significant are:

- Inability to estimate winds near the center due to the typical dense cirrus overcast.
- Large areas of suppressed convection with few or no visible clouds.
- Limited vertical resolution.
- Significant problems in determining the heights of the satellite winds.

This study was designed to improve upon previous satellite analyses by making use of the unusually abundant aircraft data near the storm center and rawinsonde data around the perimeter to alleviate some of the above problems. The proposed procedure was to obtain satellite winds using NASA's interactive computer system and then to integrate those winds with aircraft, rawinsonde, ship and buoy data to obtain a comprehensive data set. The goal was to analyze the integrated data set to determine whether the observed slow, steady strengthening of the core on 11-12 Sept. 1979 could be related to observed circulation features at larger radii.

2. Summary of Work Completed

The major data reduction task was to obtain ten sets of satellite-wind vectors (five from low-level cumulus and five from cirrus). Several delays were encountered, due in part to a reconfiguration of the NASA AOIPS (Atmospheric and Oceanic Information Processing System) computer system. The ten satellite-wind sets were completed near the end of the original research period (30 Nov. 1982). Rawinsonde data were obtained and analyzed according to procedures outlined in section 3. The principal investigator (P.I.) had completed a composite analysis of the core of Hurricane Frederick using aircraft data (Frank, 1983), and that aircraft data was ready for incorporation into the integrated analysis. Powell (1982) performed a surface level analysis of the storm's winds using ship, buoy and aircraft data, and he provided his data set for inclusion in the current analysis.

At the end of the original project, all of the available data sets had been reduced and analyzed independently. The remaining tasks were to integrate the data and to analyze the final wind fields. During the eight month extension period the data were combined using compositing techniques similar to those used in previous tropical cyclone studies (Frank, 1977a,b; Frank, 1983; McBride, 1981). The analysis procedures are described in section 3. Several interesting results were obtained. However, it became clear that there were significant problems in assigning the appropriate heights to the satellite-winds. Tropical cyclones exhibit strong vertical shears of the radial wind component in their inflow and outflow layers, and without accurate vertical assignments of the wind vectors in these critical layers, many quantitative analyses cannot be performed. A detailed analysis of all available data sources to estimate the height of each wind vector is necessary to obtain an integrated data set which makes optimum use of the available measurements. Such an analysis is being performed as a continuation

of the current study under NASA sponsorship. The current report focuses on the preliminary results obtained using "bulk integration" techniques where all of the low level satellite-winds were assigned to a single level. The upper level winds were analyzed in a similar fashion.

3. Data and Analysis

3.1 Aircraft Data

Research aircraft from the National Hurricane Research Laboratory (NHRL) were deployed in a long-term monitoring made on 11-12 Sept. 1979. Rather than sampling limited areas at several vertical levels simultaneously, the aircraft flew sequential patterns, primarily at altitudes of 560 m and 1600 m. This provided nearly continuous monitoring of the storm from 11 Sept. 1979 1200 GMT through 13 Sept. 1979 0000 GMT. During this 36 h period the storm central pressure deepened only slightly (Fig. 1), the large scale divergence field remained nearly constant (shown later) and the large scale area-averaged vorticity changed gradually (shown later). Therefore, the aircraft data were suitable for compositing. Table 1 contains a summary of the aircraft reconnaissance flights into Hurricane Frederick. The aircraft primarily flew radial legs into and out of the storm within about 150 km of the center.

The research aircraft sampled a number of kinematic and thermodynamic parameters at 1-s intervals (Table 2). Radar data was available on some flights as well. Frank (1983) composited the flight data at altitudes of 560 m, 1600 m and 6400 m. A brief summary of the compositing procedure is presented below, and a more detailed description is presented in the referenced report. The composited aircraft data were needed to provide data within about 150 km of the storm center where cirrus overcast prevented the determination of a significant number of wind vectors. Rawinsonde reports were unavailable in that region.

All radial legs at each analysis level were combined into a single composite for that level. All portions of a leg within 150 km radius were used except those where the aircraft was turning faster than 1° of

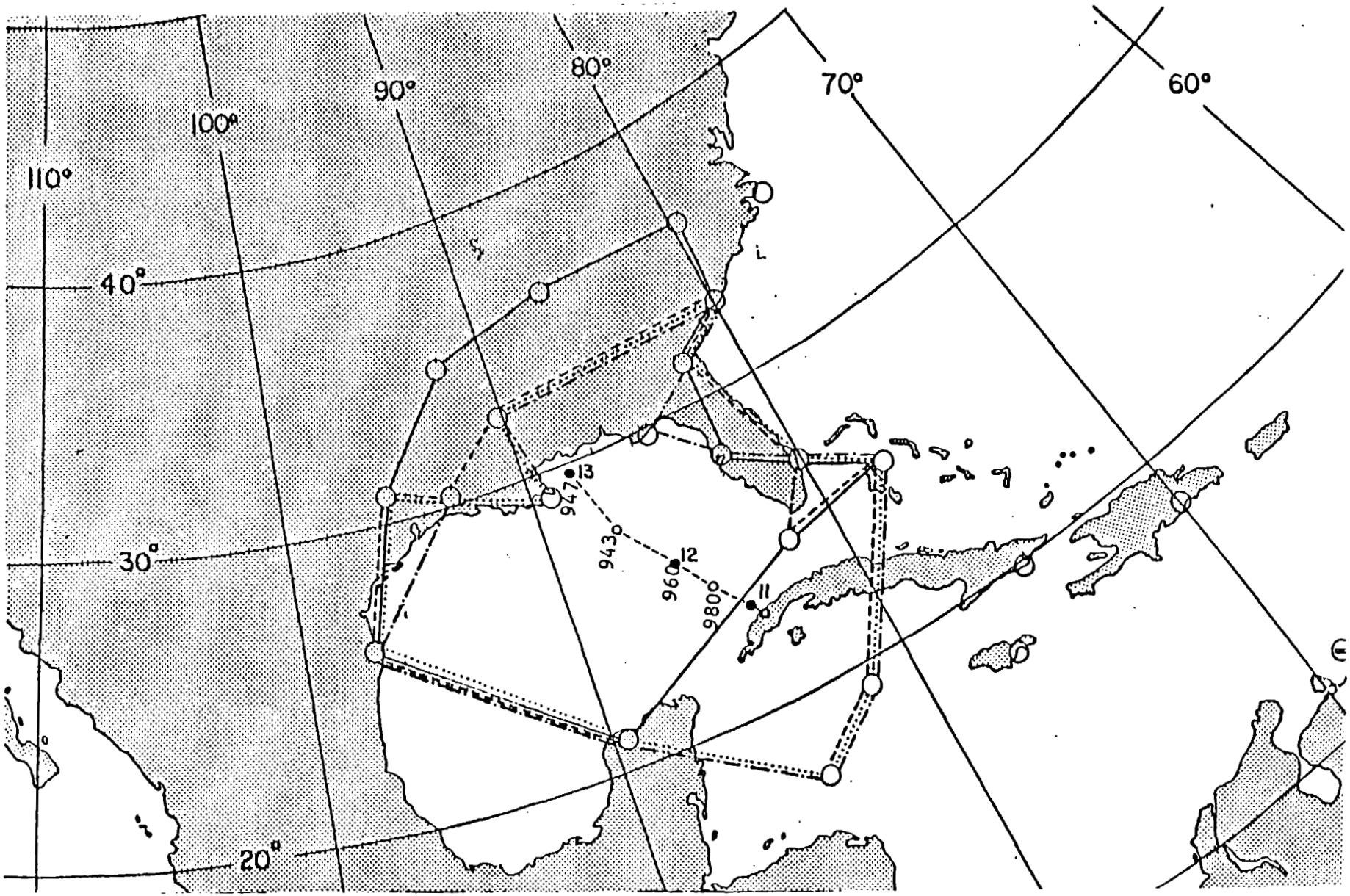

Figure 1 Positions and central pressures (mb) of Hurricane Frederick at 12 h intervals from 1200 GMT, 10 SEP 79 (open circle over Cuba) to 0000 GMT, 13 SEP 79. The large circles connected by lines show the network of rawinsonde stations.

TABLE 1. Reconnaissance flights in Hurricane Frederick.

(Frederick made landfall at 0300 GMT, 12 September 1979.)

Aircraft	Flight No.	Approximate altitude, m	Approximate times, GMT	Central surface pressure (hPa)
N42RF	790911H1	600	1120-1740	980
N6541C	790911F	6400	1130-1520	980
N42RF	790911H2	3140	1750-1820	968
N43RF	790911I	1500	2030-2120	
		500	2125-0125	960
		1500	0130-0340	
N42RF	790912H1	600	0540-0710	
		1700	0720-1245	943
N6541C	790912F	1550	1445-1820	950
N42RF	790912H2	500	2340-0015	946
		1500	0100-0250	

TABLE 2. Flight Data Parameters.

Parameter	Units	Approximate Accuracy
Time	1 s	1 s
Position	degrees lat./long.	0.9 n mi
Heading	degrees	0.1 deg
Track	degrees	0.1 deg
Radar Altitude	ft	8 ft or 1%
Pressure Altitude	ft	
Pressure	mb	0.2 mb
Wind Direction	degrees	0.1 deg
Wind Speed	kts	0.25 m/s
Vertical Wind Speed	$m\ s^{-1}$	0.25 m/s
Temperature	degrees C	0.2°C
Dew Point	degrees C	~ 0.6°C (10 s resolution)

heading per second. There were a total of 16 whole or partial legs at the 560 m level, 26 legs at 1600 m and 10 legs at 6400 m.

Each radial flux leg was divided into 10 km segments based on distance from the center. Center positions and the aircraft data tapes were supplied by David Jorgenson of NHRL. Values of each parameter were averaged for each 10 km segment. In addition, vertical fluxes of each parameter were obtained at 1 s intervals for each segment and averaged to give total segment fluxes.

The segment averages were assigned to the center point of each segment and were placed in bins of the compositing grid according to positions relative to the storm center. There were fifteen radial bands of 10 km extent divided into eight equal sectors in the azimuthal direction (120 total grid spaces). All values of a parameter falling in a grid space from the various flights were averaged together and assigned to the center of that space. Only 20 of the 120 spaces at 560 m and 2 of the spaces at 1600 m lacked data. These were linearly interpolated in the azimuthal direction. Composites were performed in both stationary and storm-relative coordinates. For the latter the mean storm motion vector over the compositing period was subtracted from all horizontal wind values.

The composited aircraft data were integrated into the larger scale analysis of the current study. The mean value of each parameter for each aircraft composite grid space was treated as an observation at that level. These observations were then combined with satellite wind vectors and rawinsonde observations as discussed in section 3.

3.2 Rawinsonde Data

Rawinsonde reports from the stations shown in Fig. 1 were obtained at

Figure 2 Low level satellite wind vectors for the 1600 GMT, 11 SEP 79 observation window.

Figure 3 As in Fig. 2 but for upper level winds.

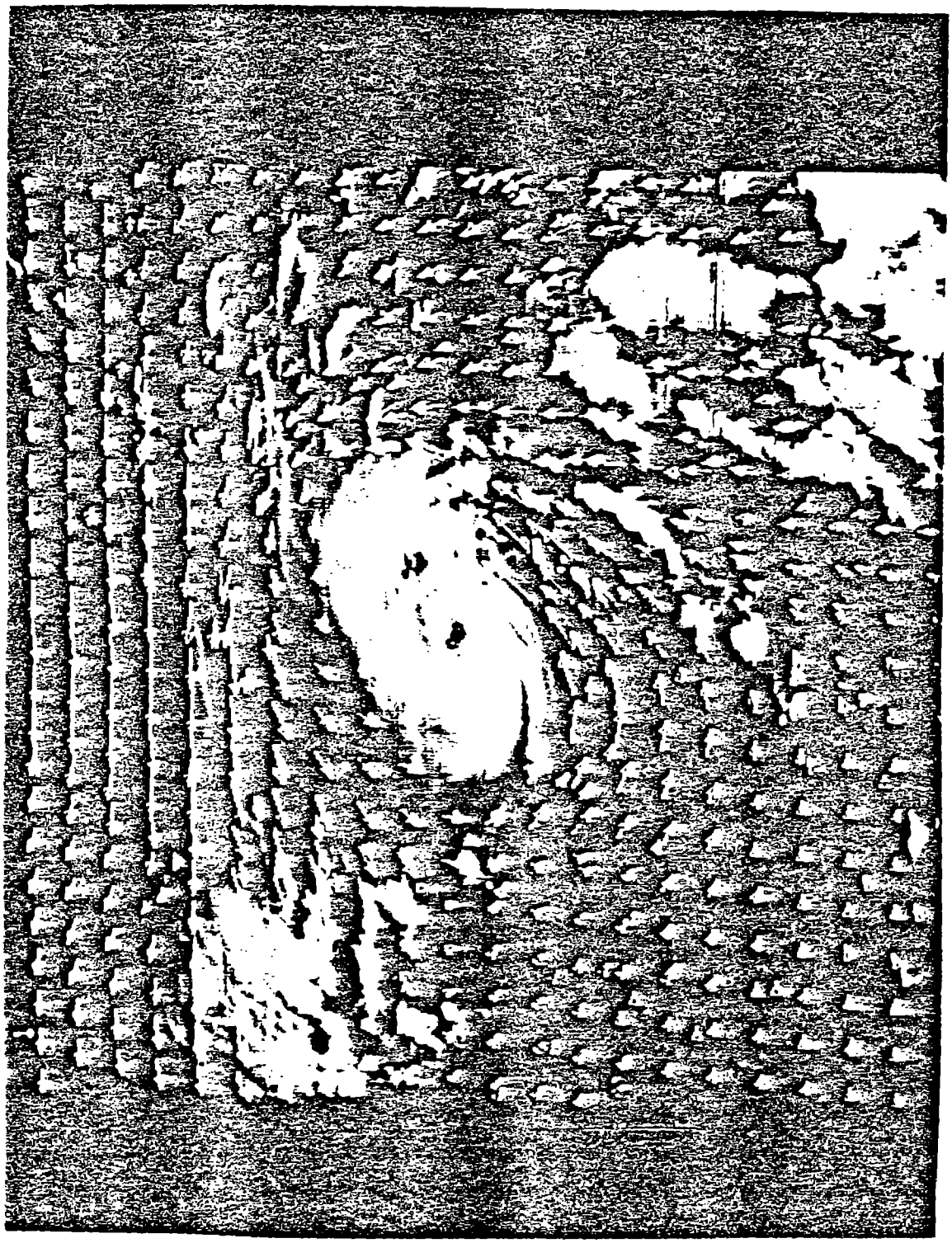

Figure 4 Objective analysis of low-level satellite winds, 1600 GMT, 11 SEP 79.

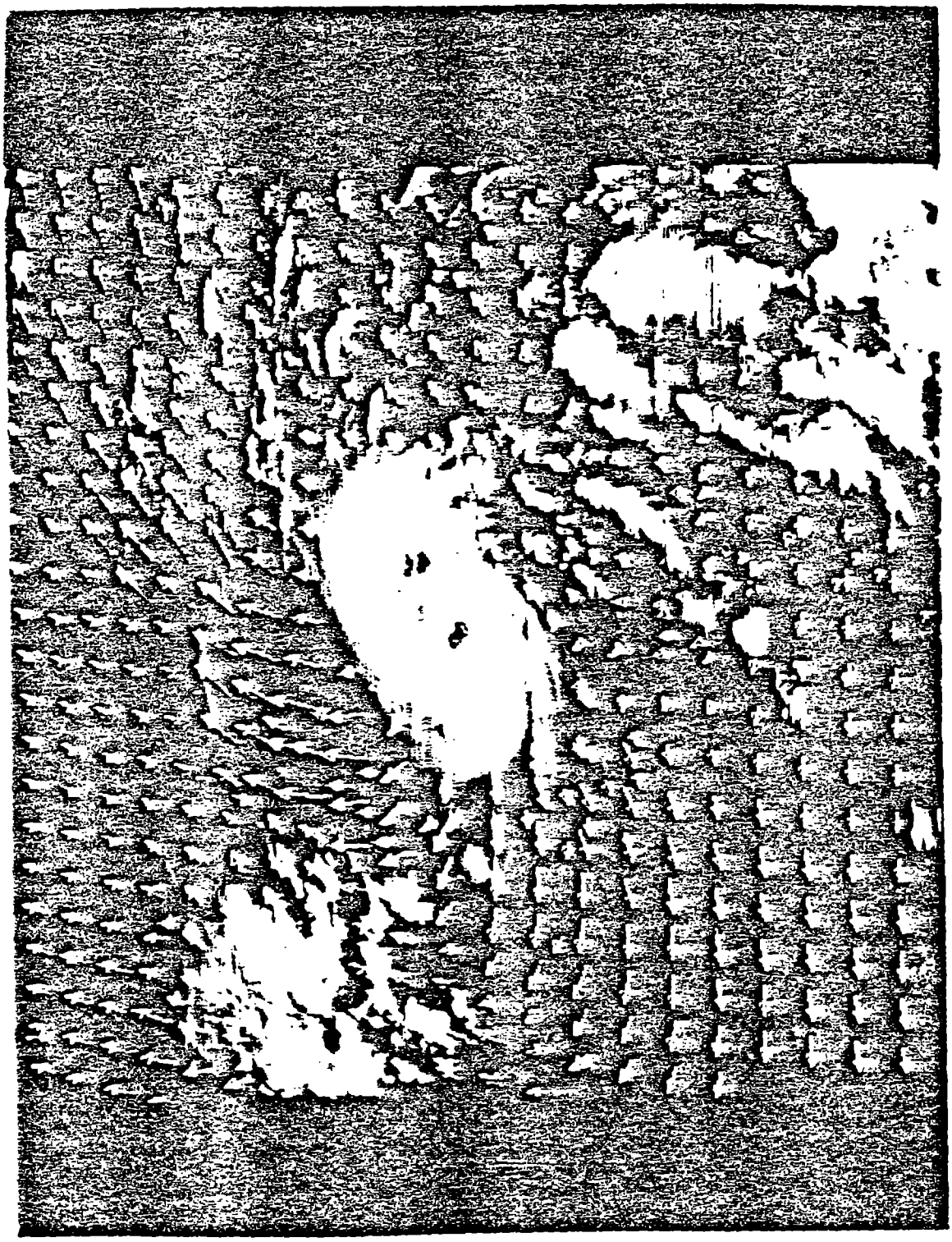

Figure 5 As in Fig. 4 but for upper level winds.

12 h intervals from 10 Sept. 1979 0000 GMT through 13 Sept. 1979 1200 GMT. At each 12 h observation time a subset of rawinsondes surrounding the storm was chosen (indicated by the lines connecting stations in Fig. 1). The winds were fitted linearly to a plane by least-squares regression analysis. The fitted data were used to compute area-averaged vertical profiles of divergence and relative vorticity. These profiles were smoothed vertically and then in time using a 1-2-1 weighting factor. Individual rawinsonde observations also were utilized in the composite analyses.

3.3 Satellite Data

Satellite winds were obtained at low levels and at the cirrus outflow level(s) for the 1600 and 1900 GMT times on 11 Sept. 1979 and for 1300, 1600 and 1900 GMT on 12 Sept. 1979. The winds were obtained using close-up (5° x 5° latitude) images at inner radii for optimum resolution, while larger (~ 10° x 10°) images were used for the outer radius areas. Rapid-scan visible images were available at 7.5 minute intervals at both levels. The wind vectors were determined by manual tracking of clouds using the AOIPS system at the NASA Goddard Space Flight Center. An example of low level satellite winds is shown in Fig. 2, while upper level winds at the same time are presented in Fig. 3. Figs. 4-5 show objective analyses of the winds in Fig. 2 and 3 respectively. The vectors were smoothed using a Lackman scheme (Rodgers and Gentry, 1981). Excessive smoothing and unrealistic flow patterns are clearly visible in regions where few wind vectors could be obtained (e.g. northwest of the storm) illustrating the need to include other data sources.

3.4 Integration of Aircraft, Rawinsonde and Satellite Data

A primary goal of this research program was to integrate data from the several available sources to produce plan-view analyses of the inflow layer and outflow layer winds. An eight-octant grid similar to that used in Frank's (1983) aircraft analysis was employed. Radial bands were 20 km wide between 10-150 km and 50 km wide between 150-800 km radius, while a single 0-10 km band was used near the center. Satellite wind vectors, rawinsonde observations and grid point data from the aircraft composite were assigned to the grid box in which they fell and were averaged to yield a grid box mean. The aircraft composite data were weighted as two observations each since they represented averages of large numbers of point measurements and were considered the most reliable observations.

In order to combine the three types of data it was necessary to match them as closely as possible in time and space. The aircraft composite covered the 36 h period from 1200 GMT 11 Sept. 1979 -0000 GMT 13 Sept. 1979 and thus lacked any time resolution. This was done primarily because the data distributions on either 11 Sept. or 12 Sept. alone were judged inadequate for obtaining smooth wind fields. The possibility of using winds separately from 11 and 12 Sept. is being studied during the continuation of this research. The satellite wind vectors were available only during the daylight hours. They were analyzed both separately for 11 Sept. 1979 and 12 Sept. 1979 and as a two-day mean containing all five observation windows.

The rawinsonde data were available at 12 h intervals. For 11 Sept. 1979 analyses the soundings at 1200 GMT 11 Sept. 1979 and 0000 GMT

12 Sept. 1979 were used, while 12 Sept. 1979 analyses included rawinsondes from 1200 GMT 12 Sept. 1979 and 0000 GMT 13 Sept. 1979. All four launch times were included in the 11-12 Sept. 1979 composites. Matching the vertical levels of the data sources was more difficult. The rawinsonde data were available at standard levels and contained the greatest vertical resolution. Since they were all launched from land stations, their data at the lowest levels are probably not representative of winds over water. The composited aircraft data were available only at the 560 m, 1600 m and 6400 m levels, and the latter level was not suitable for combination with satellite winds since there were few clouds at that level.

The satellite winds were available at upper (cirrus) and lower levels of indefinite height. In the current study the upper level composites were composed of the upper level satellite wind vectors and the 200 mb rawinsonde data. Assigning all of the upper level satellite winds to one level is not appealing, since significant variations in height of the cirrus have been documented from stereo imagery (Morris and Hasler, 1984). However, for the purposes of this paper, the cirrus-level wind vectors will be assumed to be indicative of the storm outflow layer. Inflow layer composites were performed using different combinations of 850 mb and 950 mb rawinsonde winds, low level satellite winds and the 560 m and 1600 m aircraft composites. Table 3 shows combinations of data used in the various composites. In some cases one or more of the three data sources were omitted to evaluate the importance of the individual data sources upon the final analyses. Of the low-level data combinations tried in this study, the most consistent results were obtained using the 560 m aircraft composite data, the 950 mb rawinsonde data and the low-level satellite

TABLE 3. Combinations of Wind Data and Levels Composited.

11-12 SEP Combined

	Aircraft (m)	Satellite (High /Low)	Rawinsonde (mb)
1.	---	High	200
2.	---	High	---
3.	---	Low	950
4.	1600	Low	850
5.	560	Low	950
6.	---	Low	---
7.	560	Low	---

11 SEP, 12 SEP Separately

	Aircraft (m)	Satellite (High /Low)	Rawinsonde (mb)
1.	560	Low	950
2.	---	Low	950
3.	---	High	200
4.	---	Low	850

winds. This combination was used for most of the analyses presented in this report. Radial and/or tangential smoothing of the composited wind fields was employed in some of the analyses using a 1-2-1 weighting factor. When used, smoothing is noted in the discussion of results.

The above method of integrating the satellite winds with aircraft and rawinsonde data is very crude, and a number of problems exist. While the aircraft data were all obtained over the waters of the Gulf of Mexico, all of the rawinsonde observations and many of the satellite winds north and east of the storm center were measured above land. Low-level winds tend to be weaker over land, and the effective heights of the small clouds tracked to obtain low-level winds are likely to differ systematically between over-land and over-water locations. Subjective evaluation of the composite wind analyses suggested that low-level wind speeds north of the storm, which were primarily obtained from satellite imagery, were significantly lower than aircraft winds measured over water at adjacent grid points. Point by point comparisons of satellite winds with nearby aircraft and rawinsonde measurements suggested that the low-level satellite winds should be assigned to different levels in different regions of the storm. Due to the strong vertical shear of the radial wind in the low-level inflow layer of hurricanes, relatively small inaccuracies in height assignments result in relatively large errors in the divergent component of the wind - a crucial parameter in most budget analyses. The continuation research project will attempt to obtain best estimates of the heights of each low-level satellite wind vector through comparative analysis of all available data sources including sterographic satellite imagery. In the current portion of the study, all low-level satellite winds were assumed to be at one level as discussed above.

There were also problems in determining the height of the cirrus used to measure upper-level winds. The cirrus tended to be significantly lower on the north side than on the south side (Morris and Hasler, 1984), probably due to increased vertical stability and shallower convection over the land.

As a result of these problems, only limited analyses of the combined data sets are possible. Plan view analyses showed considerable noise and are not presented here. Radial profiles of low-level parameters are presented as an eight-octant azimuthal average or as an average for octants 4, 5, and 6 (Fig. 7) which are on the southern side of the storm where both the aircraft and satellite winds are predominantly over water. All upper level analyses are 8-octant azimuthal averages.

Clearly, an optimum integration of the data will require very careful and detailed intercomparisons of all available data points to determine their true heights. It will also be necessary to separate low-level satellite winds into sets of those derived over water and over land due to the different stabilities and vertical wind shears in the those regions. These procedures are beyond the scope of the first phase of the Hurricane Frederick study discussed in this report. The remaining portion of the research will focus on the careful integration of all available data to perform a multiple-scale analysis of the storm inflow layer.

3.5 Radial Flux Computations

There are many measures of the intensity of a tropical cyclone. In addition to the usual core parameters, such as minimum central pressure and maximum observed wind speed, the area-averaged angular momentum and kinetic energy have often been used in diagnostic studies. The usual

procedure is to analyze budgets of these quanitites using forms of Eqs. 1 and 2:

$$\frac{\partial \overline{m}}{\partial t} = - \overline{\underset{\sim}{\nabla} \cdot m\underset{\sim}{v}} - \frac{\partial \overline{\omega m}}{\partial p} - \overline{frV_r} + \overline{F_r} \qquad (1)$$

$$\frac{\partial \overline{K}}{\partial t} = - \overline{\underset{\sim}{\nabla} \cdot \underset{\sim}{v}K} - \frac{\partial (\overline{\omega K})}{\partial p} = - \overline{\underset{\sim}{v} \cdot \underset{\sim}{\nabla}\phi} + \overline{\underset{\sim}{F} \cdot \underset{\sim}{V}} \qquad (2)$$

where $m = v_t r$ = relative angular momentum, K = kinetic energy, F_θ = tangential component of friction and the overbar denotes a time and space average. Eq. 1 states that the time rate of change of the area-averaged angular momentum results from the horizontal flux convergence, vertical flux convergence, spin-up due to the Coriolis torque acting on the radial wind and the frictional torque (terms 1-4, right side, respectively).

Frank (1977b), McBride (1981) and Holland (1983) have performed large-scale angular momentum budgets of tropical cyclones using composited rawinsonde data. Their studies all showed that on a scale of r ~ 600 km or greater, the lateral flux convergence of angular momentum was a major term, possibly related to storm intensity change. At larger radii, the import of angular momentum becomes increasingly concentrated in the upper troposphere and is increasingly due to sub-grid scale fluxes.

The role of lateral fluxes of angular momentum in tropical cyclone intensification is not well understood. Numerical simulations by Pfeffer (1981) suggest that sub-grid scale or "eddy" horizontal import of angular momentum is favorable for storm development. Rodgers and Gentry (1981)

analyzed lateral momentum fluxes in three hurricanes using satellite-wind vectors and concluded that increases in the net import of momentum at 3° radius appeared to precede intensification of the core. One goal of the current research is to examine lateral fluxes of relative angular at upper and lower levels and to relate these fluxes to the observed slow deepening of the core. At any radius, the net import of relative angular momentum is proportional to $- V_r \cdot V_t$ where V_r is the radial wind and V_t the tangential wind. Values of $V_r \cdot V_t$ were computed for each observation, and average values of $V_r V_t$ were then determined for each grid space.

Eq. 2 states that the time rate of change of the area-averaged kinetic energy (left side) equals the sum of the horizontal and vertical flux convergences of K, the generation by down gradient flow and the frictional dissipation, respectively (right side). Mature tropical cyclones tend to be net exporters of kinetic energy when viewed on the large scale (Frank, 1982). Most of the net outflow of K occurs in the upper troposphere, and it becomes increasingly dominated by sub-grid scale fluxes at larger radii (Black and Anthes, 1971; Frank, 1977b, 1982). Radial fluxes of kinetic energy were computed for each wind observation at both analysis levels and averaged in the manner described above for angular momentum fluxes. These fluxes were examined to determine whether they suggested relationships between the change in core intensity of an individual storm and its net export of kinetic energy.

Figure 6 Area-averaged divergence, approximately 7° radius, from rawinsonde data.

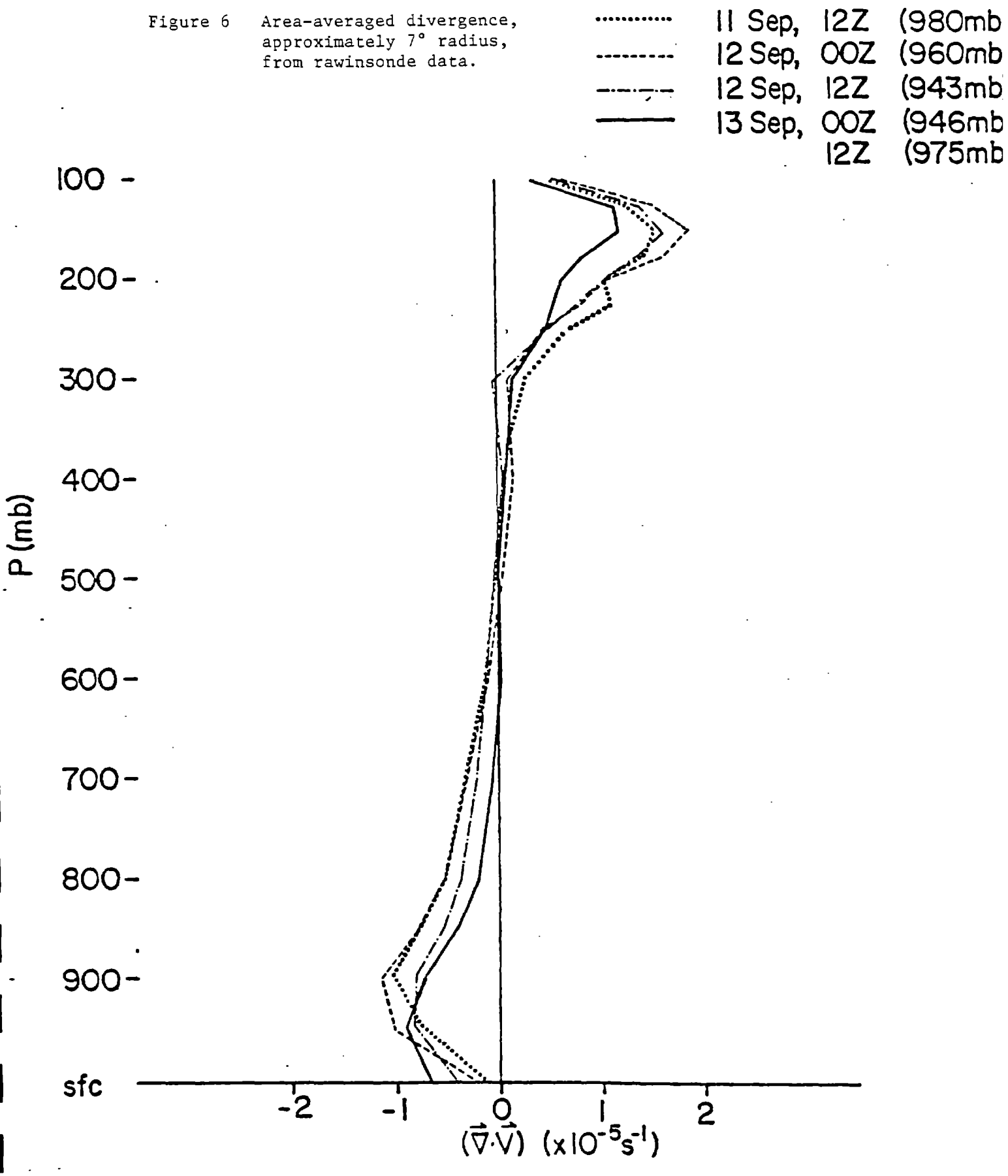

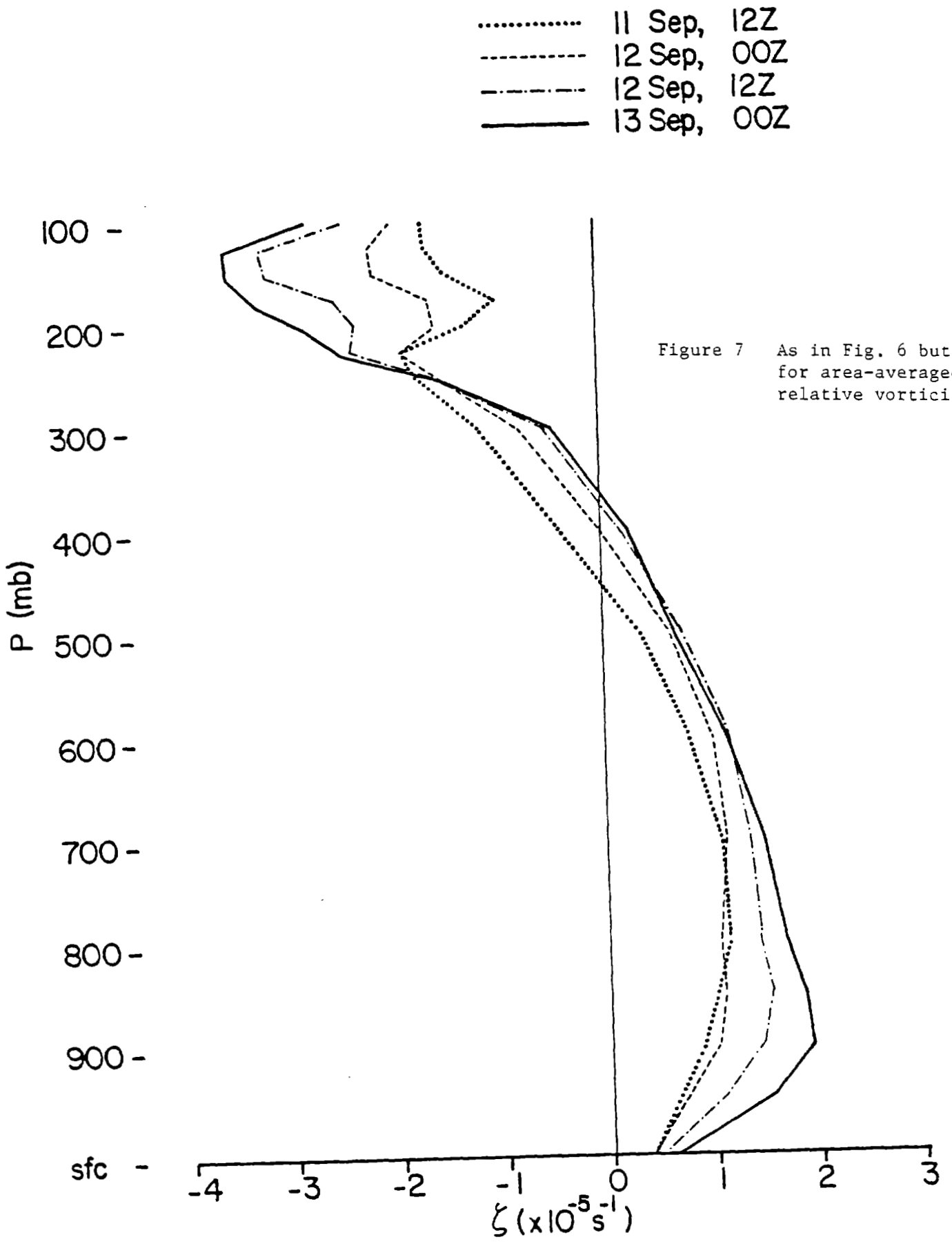

Figure 7 As in Fig. 6 but for area-averaged relative vorticity.

4. Results

4.1 Rawinsondes - Large Scale

Figs. 6-7 show the evolution of the area-averaged divergence and vorticity fields on 11-12 Sept. 1979. They represent an area with a radius of approximately 700 km. There was a distinct inflow layer below about 800 mb. The lower values of inflow at the surface relative to 950 mb are probably not representative of a hurricane over water, as they appear to result from the lower surface winds over land at the rawinsonde sites. Outflow is concentrated in a 200 mb thick layer (100-300 mb). Changes in the net large-scale mass flux through the storm were insignificant during the 36 h period shown. This is consistent with Frank's (1982) findings for composite storms that the radial wind perturbation associated with intensifying tropical cyclones is confined to the inner 6° radius. It is also interesting that the thickness of the outflow layer is very similar to that found for composites of many storms in the W. Pacific (Frank, 1977) and Atlantic (McBride, 1981; Frank, 1982). This suggests that storm outflow layers are consistently located in the upper 200 mb of the tropical troposphere, since individual storms with lower outflow layers should have resulted in deeper composite outflow layers.

The area-averaged vorticity behaves differently (Fig. 7). The cyclonic vortex strengthened steadily with time at all levels below about 250 mb, and strengthening of the upper level anticyclone was even more pronounced. These results agree with Frank's (1982) composite data which showed that the hurricanes rotational circulation tends to extend to radii in excess of 1000 km. Vertical shear of the tangential wind is small below 500 mb. The surface winds are presumed to be artifically low due to the land location of the rawinsonde stations. Powell (1982) noted

that surface winds in Frederick averaged 70% of the flight level (560 m) winds over water.

4.2 Two-day Average Properties (11-12 Sept.)

4.2.1 Radial and Tangential Winds

All results in this section are averages of the combined rawinsonde, aircraft and satellite data from 11-12 Sept. 1979 as described in section 3. Results are presented as radial profiles which are eight octant averages (all octants) unless noted as averages for octants 4-5-6 only (south side). The latter averaging method produces profiles where all data (except rawinsondes) are measured over water but suffers the significant drawback that the resulting averages are biased by the storm asymmetries.

Low-level radial winds (Fig. 8) are presented separately for the satellite winds and for the 560 m and 1600 m level aircraft composites of the core. Fig. 9 shows the tangential winds in the same format. Satellite radial winds are noisey, averaging about -2 ms^{-1}. It is unclear whether they are in better agreement with the 560 m or 1600 m aircraft values, and, as previously discussed, it is unlikely that they can all be assigned to a single level without serious degradation of the analysis. The satellite tangential winds vary smoothly with radius but appear to be lower in magnitude than either the 560 m or 1600 m aircraft winds. They agree best with the former level. Many of the satellite winds in Figs. 8-9 are over land where the low level winds are lower than would be expected over water.

Figs. 10-11 show the radial and tangential winds for octants 4-5-6 only (south side - over water). The solid curves in each figure are based on 560 m aircraft data, 950 mb rawinsonde data and the

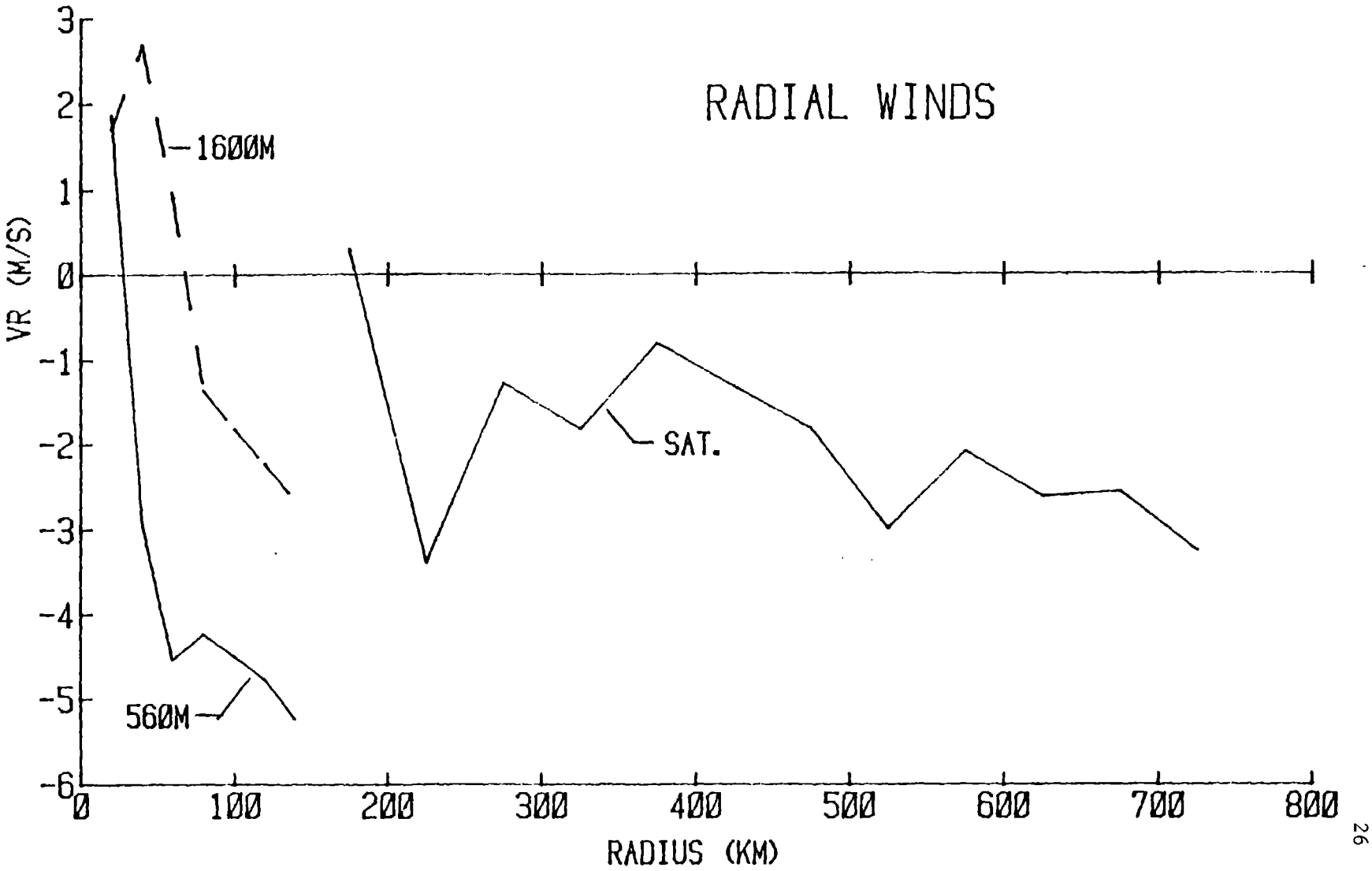

Figure 8 Low-level radial winds (ms^{-1}). From 0-150 km radius data are from aircraft composites at 560 m (solid) and 1600 m (dashed). From 175-725 km data are from low level satellite winds. All available data from 11-12 SEP 79 are used.

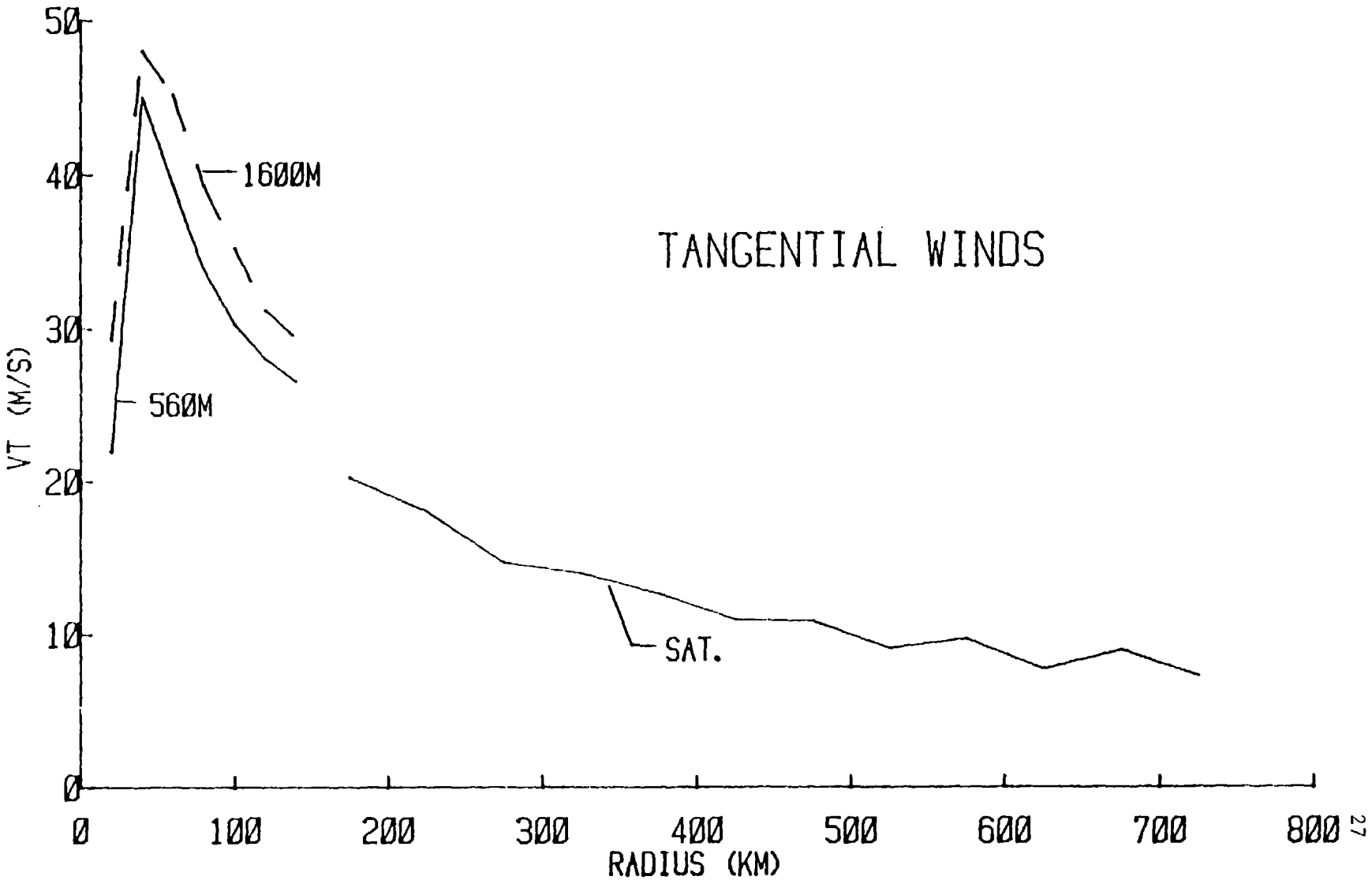

Figure 9 As in Fig. 8 but for tangential winds.

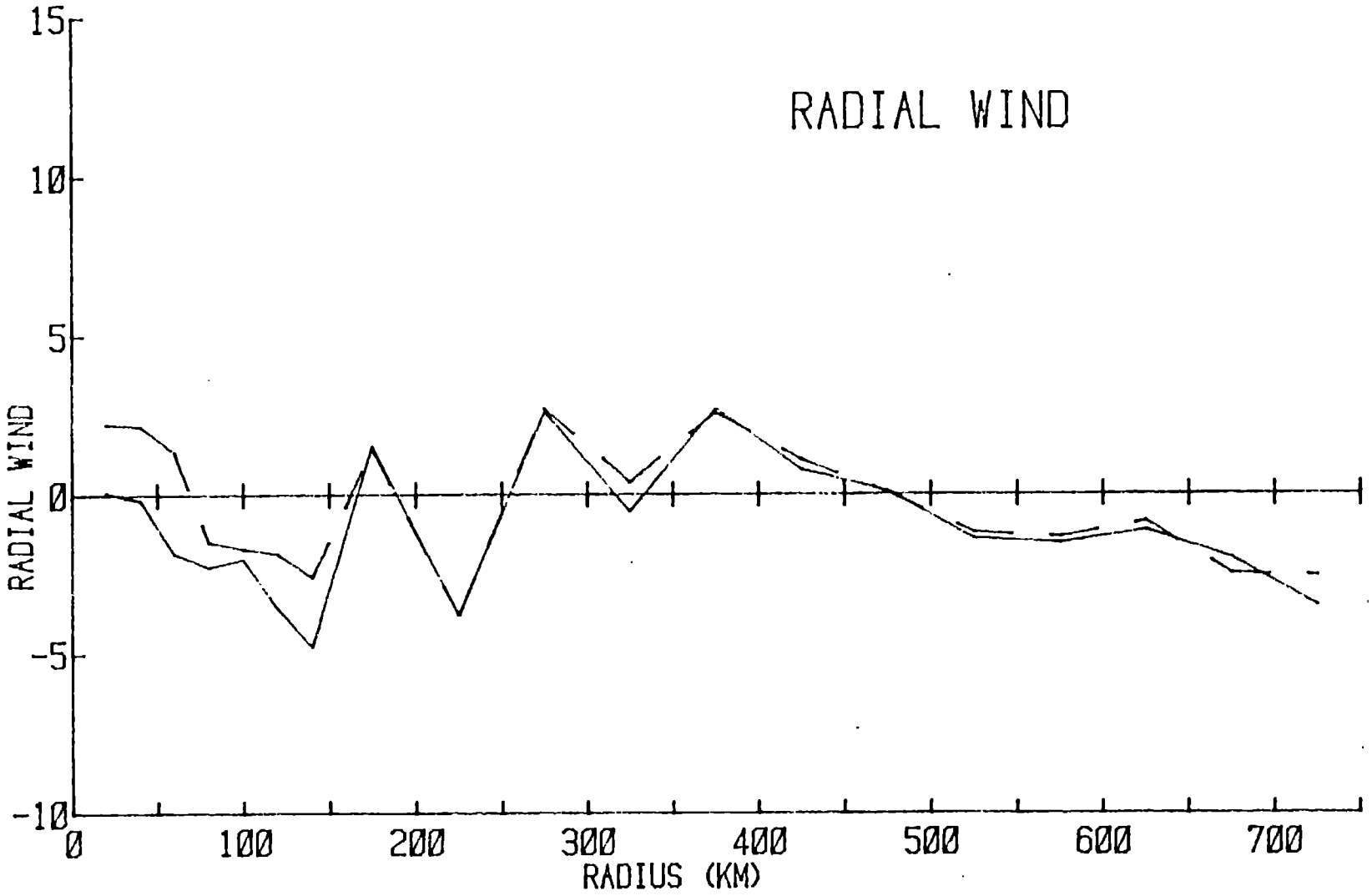

Figure 10 Radial winds (ms^{-1}) on the south side of the storm averaged for 11-12 Sept. using 950 mb rawinsonde, 560 m aircraft composite and low level satellite winds (solid) and 850 mb rawinsonde, 1600 m aircraft and low satellite winds (dashed).

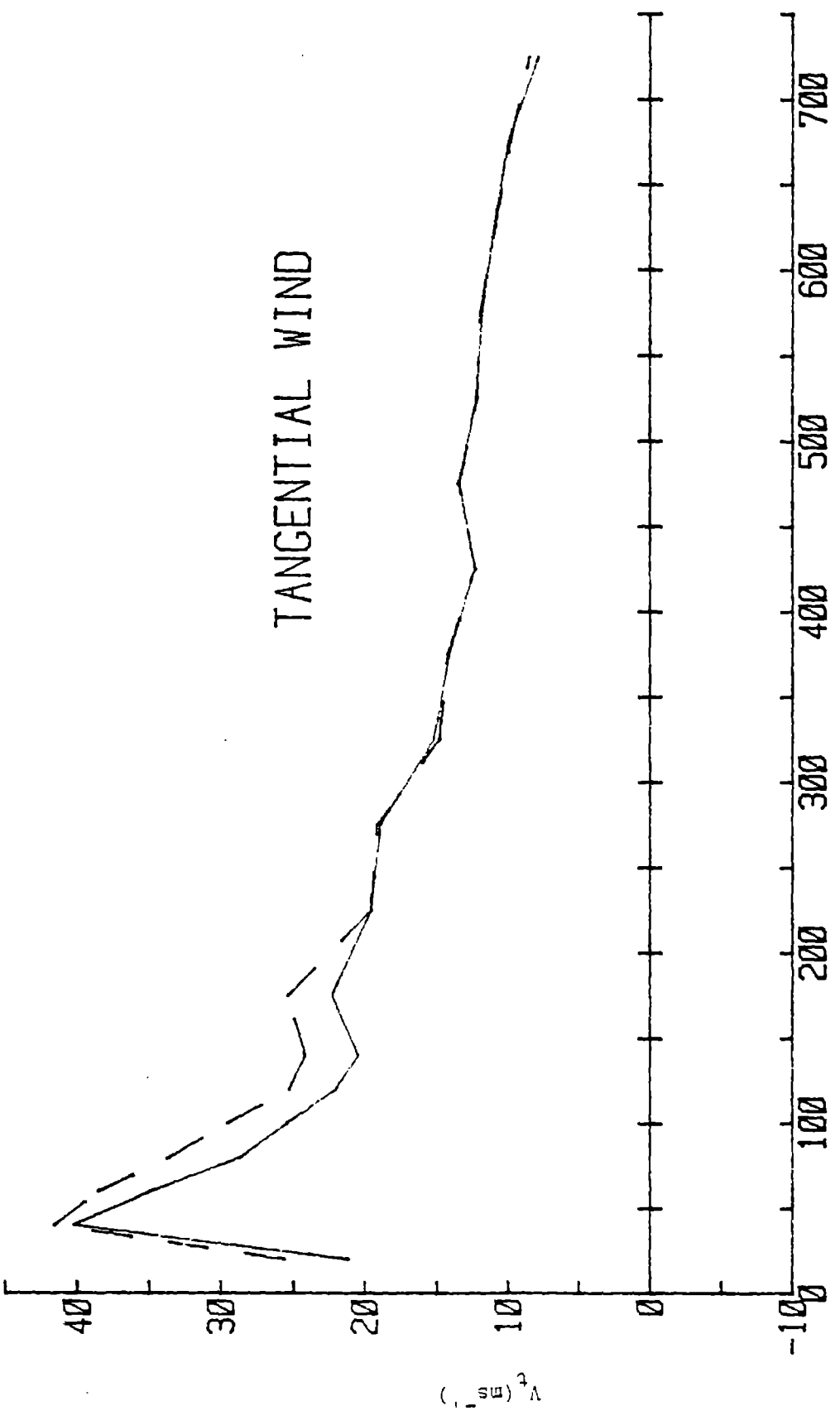

Figure 11 As in Fig. 10, but for tangential wind.

satellite winds. The dashed curves combine the satellite data with 1600 m aircraft and 850 mb rawinsonde data. The rawinsonde data has little effect on the profiles. Radial winds are erratic near the center and yield no useful information on whether the 560 m or 1600 m aircraft data is in better agreement with satellite winds. (All aircraft data is within 0-150 km radius). The tangential wind profiles of Fig. 11 suggest a better fit between the 1600 m aircraft data and the lower level satellite winds, but the differences are relatively small. In the present study, all subsequent profiles of low level parameters are for 8-octant means and are combinations of 950 mb rawinsonde, 560 m aircraft and satellite data with the exceptions of Figs. 13 and 14.

Upper level radial winds from satellite and 200 mb rawinsonde data (Fig. 12 -solid) show mean outflow of about 7-8 ms^{-1} with no with systematic variation with radius. The tangential wind profile in Fig. 12 shows anticyclonic flow at radii greater than 300 km which increases almost linearly with radius. All upper level profiles must be viewed with caution due to the uncertainty of the heights of the satellite winds.

4.2.2 Divergence and Vorticity

Figs. 13 and 14 show divergence and relative vorticity, respectively, plotted using the same convention as in Figs. 10-11. Once again, the rawinsondes have little impact, and the profiles are very similar at both levels outward of 150 km radius. Weak convergence occurs at all radii greater than 400 km with a maxium between 450-500 km. Both data levels indicate a sharp increase in convergence at r = 150 km, the limit of the aircraft data. It is not

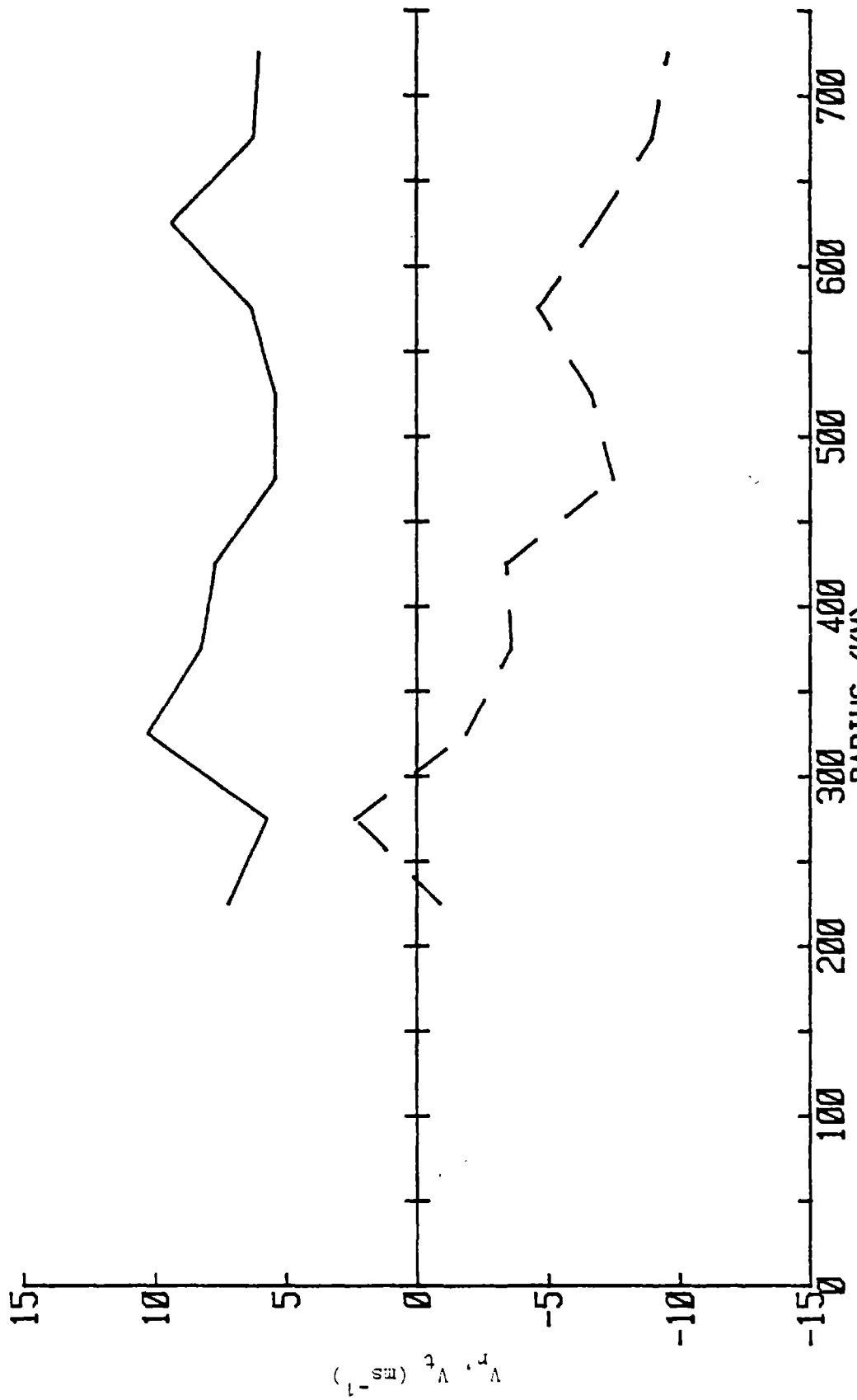

Figure 12 Radial (solid) and tangential (dashed) winds using high-level satellite winds and 200 mb rawinsonde data. Data are averaged for 11-12 Sept. 1979 and azimuthally.

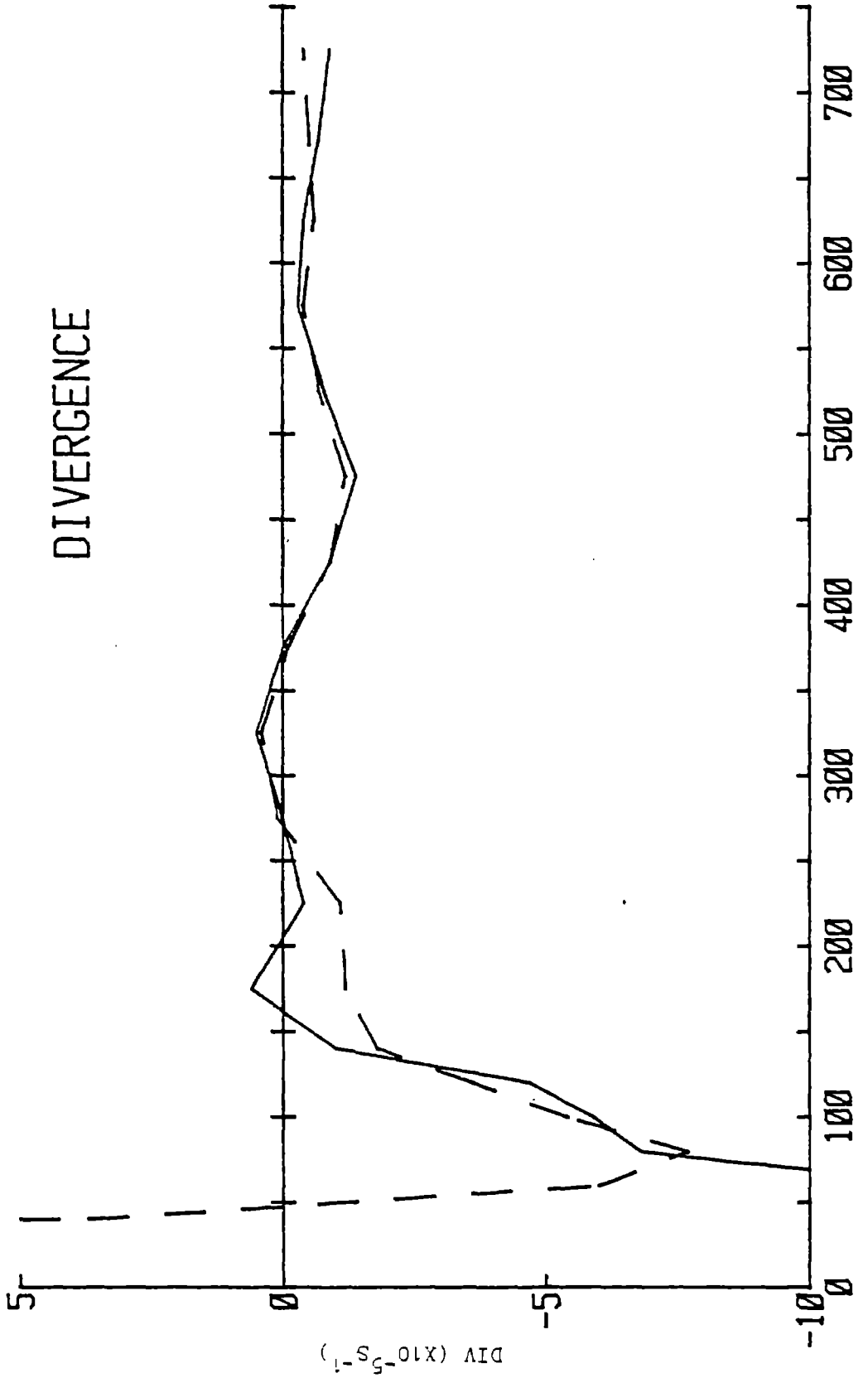

Figure 13 Divergence (x 10^{-5} s^{-1}) computed using 950 mb rawinsonde, 560 m aircraft and low satellite winds (solid) and using 850 mb rawinsonde, 1600 m aircraft and low satellite winds (dashed).

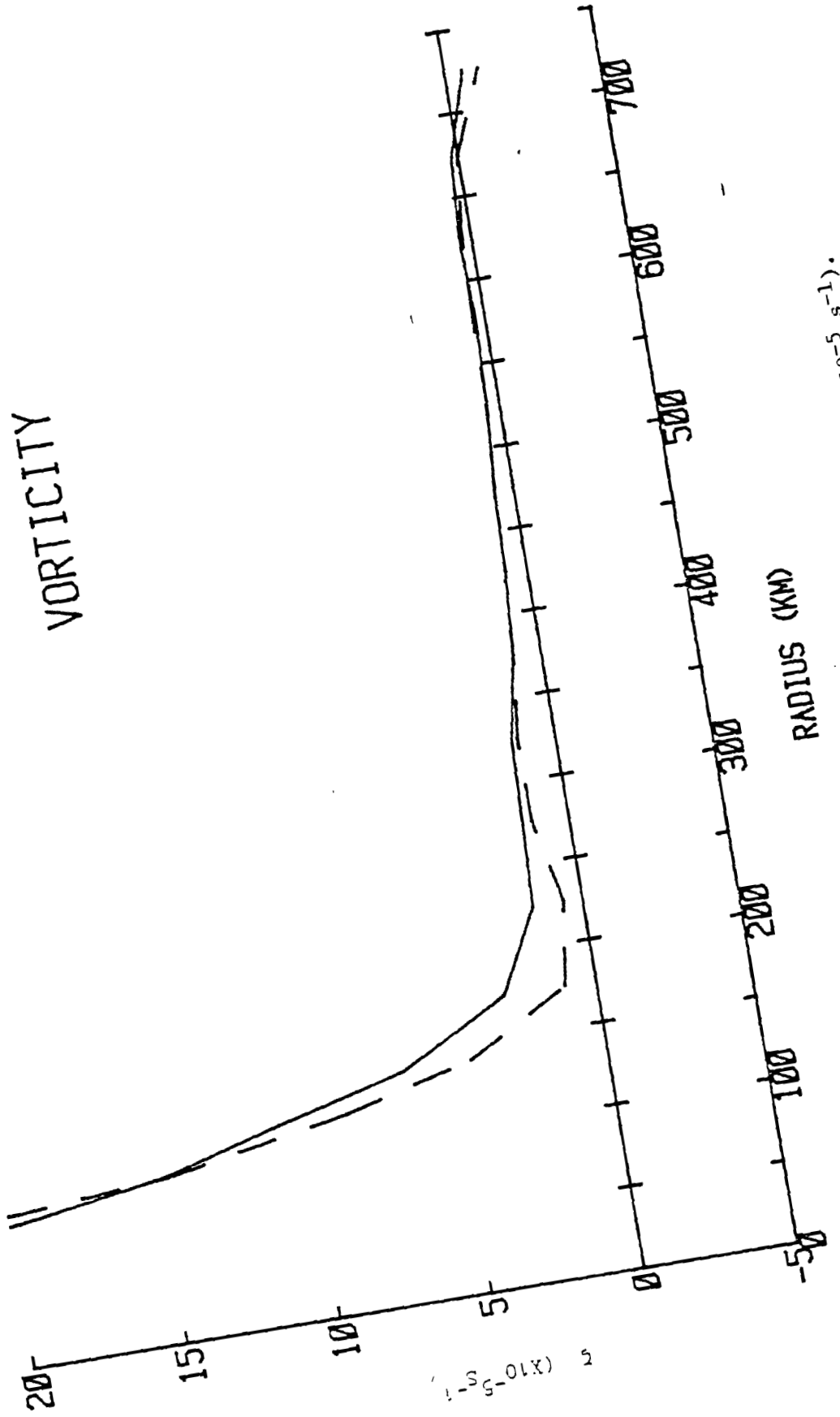

Figure 14 As in Fig. 13, but for relative vorticity (x 10^{-5} s^{-1}).

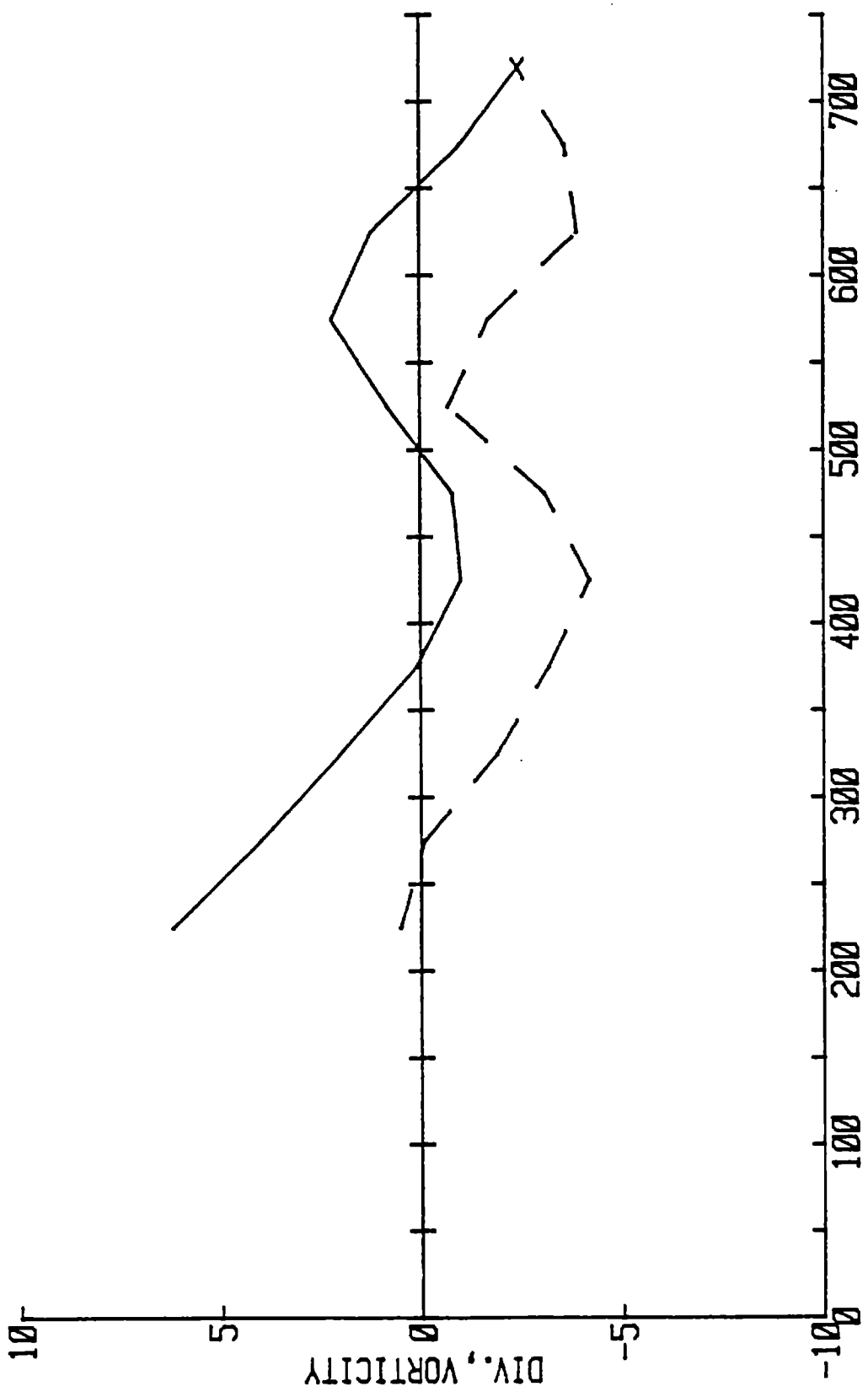

Figure 15 As in Fig. 12, but for divergence (solid) and relative vorticity (dashed) (x 10^{-5} s^{-1}).

clear whether this results from a problem with matching levels between the satellite and aircraft data or whether the pattern is real. The observation that the outer edge of the major convection and cirrus canopy is at approximately 150 km radius provides some support for the latter view.

Relative vorticity is weakly positive from 200-700 km radius. Inside 200 km the vorticity increases rapidly with decreasing radius. As with the divergence profile, there is some doubt as to whether this sudden change in slope is real. A significant wind discontinuity at 150 km radius due to data-level problems would be expected to produce a minimum in relative vorticity at r ~ 150 km. The dip in vorticity near 200 mb for the dashed curve (1600 m aircraft data) may reflect this matching problem (see Fig 9).

At the high level divergence oscillates about zero while relative vorticity is negative at radii greater than 250 km. No significance is attached to the variations with radius.

4.2.3 Radial Fluxes

Wind data were used to compute radial fluxes of the tangential wind ($V_r V_t$ -proportional to the angular momentum flux at each radius) and of kinetic energy ($V_r K$). Negative values denote inward fluxes. The low level angular momentum flux is inward at all radii, averaging about $-20\ m^2 s^{-2}$ at radii greater than 200 km (Fig. 16). The inward transport appears to increase rapidly inside 200 km as V_r becomes more negative and V_t becomes larger (Figs. 8, 9). The low-level kinetic energy flux is also inward at all radii, (Fig. 17) and the pattern is very similar to the momentum flux profile.

At the upper analysis level the angular momentum flux becomes

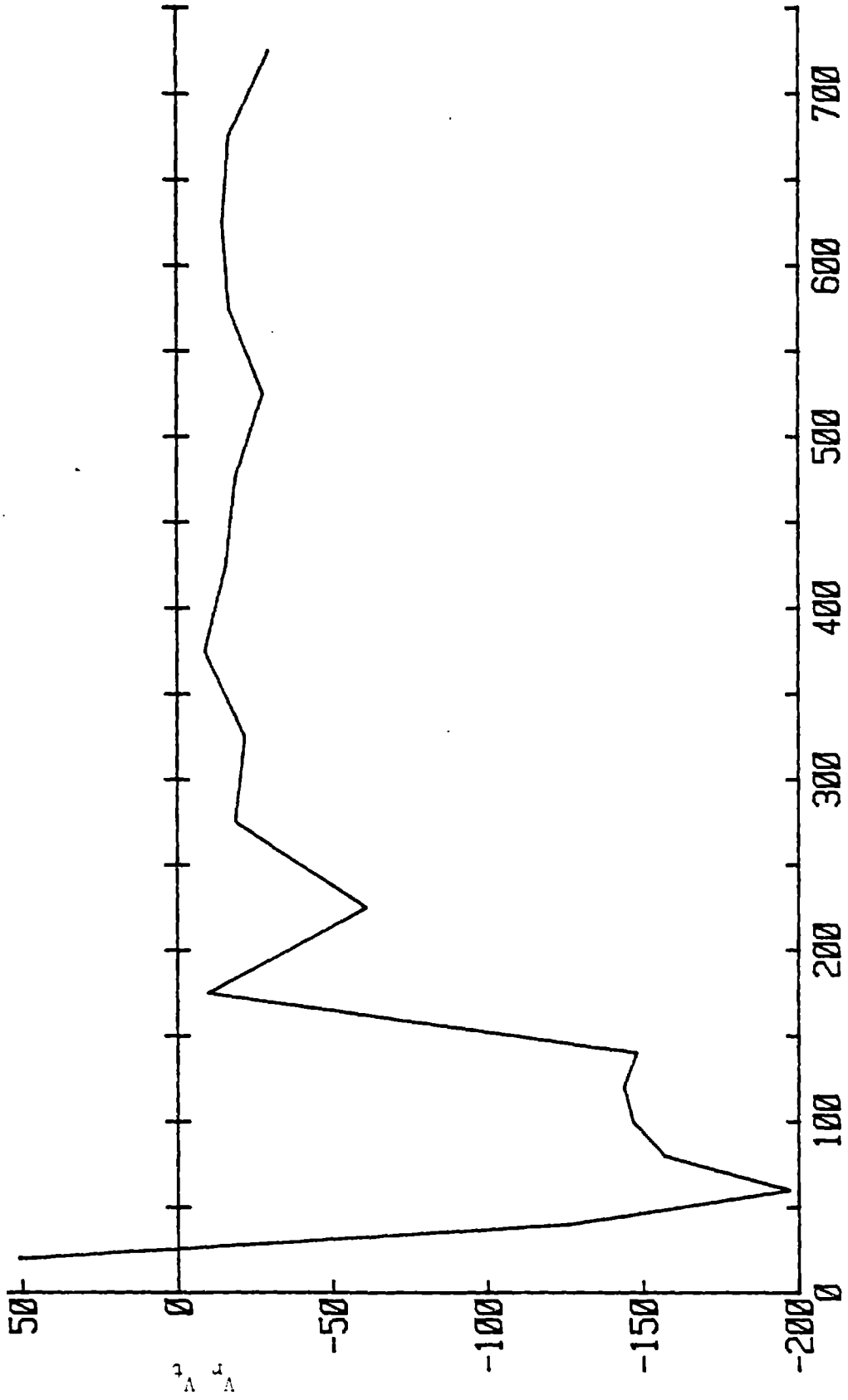

Figure 16 Radial times tangential wind ($m^2\ s^{-2}$) for 11-12 Sept. computed from 950 mb rawinsonde, 560 m aircraft and low-level satellite winds.

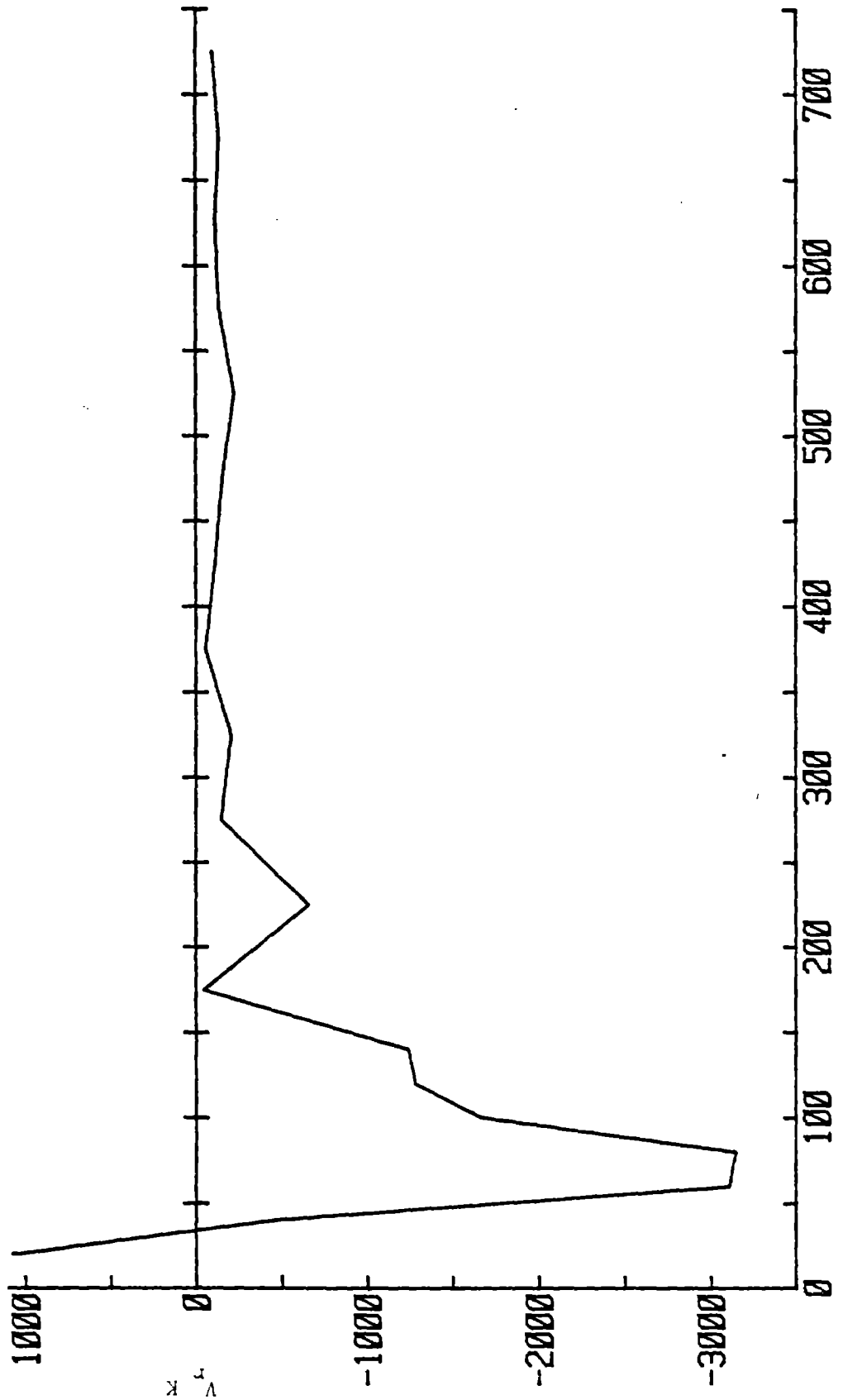

Figure 17 As in Fig. 16, but for radial wind times kinetic energy (K) (m^3 s^{-3}).

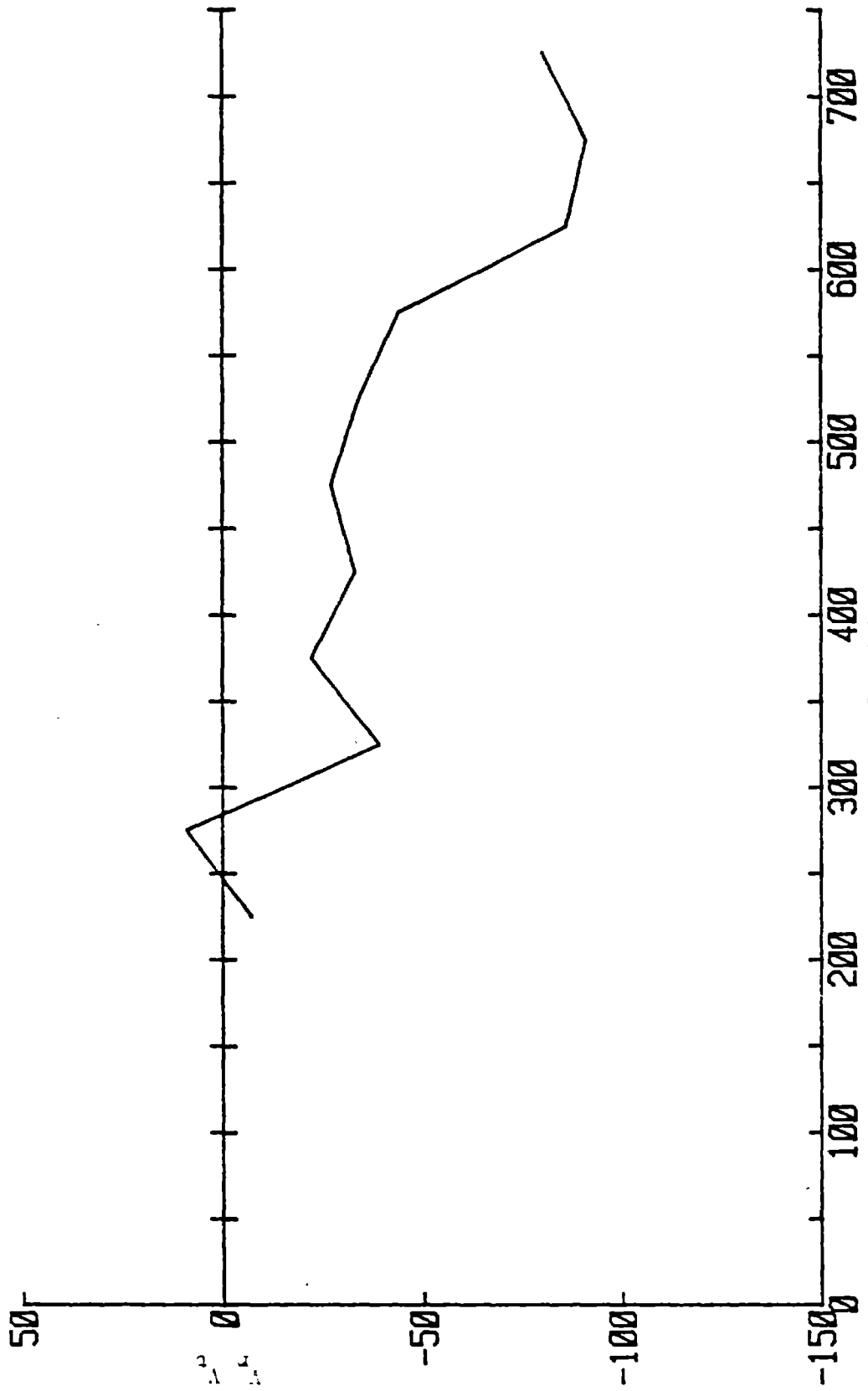

Figure 18 As in Fig. 16, but using high-level satellite and 200 mb rawinsonde winds.

increasingly inward (negative) with increasing radius (Fig. 18). This momentum import results from an export of anticyclonic momentum and has been shown to be largely dominated by sub-grid scale processes in analyses of other storms (Black and Anthes, 1971; Frank, 1977b). The upper-level flux of kinetic energy is outward at all observed radii and tends to increase with increasing radius. The mean profile of $V_r \cdot K$ is shown in section 4.3.3.

4.3 Individual Day Analysis

This section presents radial profiles of the same parameters discussed in section 4.2 but analyzed separately for 11 Sept. and 12 Sept. The purpose of this stratification of data is to document changes in the storm properties which may be related to the slow intensification which occurred through most of the analysis period. All low level analyses are combinations of 950 mb rawinsonde, 560 m aircraft and low level satellite data. The stratification of data into two subsets tends to reduce the number of grid spaces at each radius which contain observations. Table 4 lists the radial bands which contain data in fewer than five of the eight grid spaces for each of the composites. The analyses at these radii should be viewed with caution since they may be biased by asymmetries in storm structure. It should also be recalled that most of the data at radii less than 150 km are aircraft data which are averaged for both 11-12 Sept. They are included here only to give an estimate of radial continuity.

4.3.1 Radial and Tangential Winds

At radii between about 300-600 km, where both days had five or more grid spaces with data at the lower level, there was a small increase in radial inflow from 11 Sept. to 12 Sept. (Fig. 19). No increase was apparent outward of 600 km radius in agreement with the

TABLE 4. Regions with Sparse Data.

Date	Level	Radii with < 5 octants reporting data
11 Sept.	Low	150-300 km
12 Sept.	Low	150-200 km
11 Sept.	High	$\leq$ 300, 600-650 km
12 Sept.	High	$\leq$ 250 km

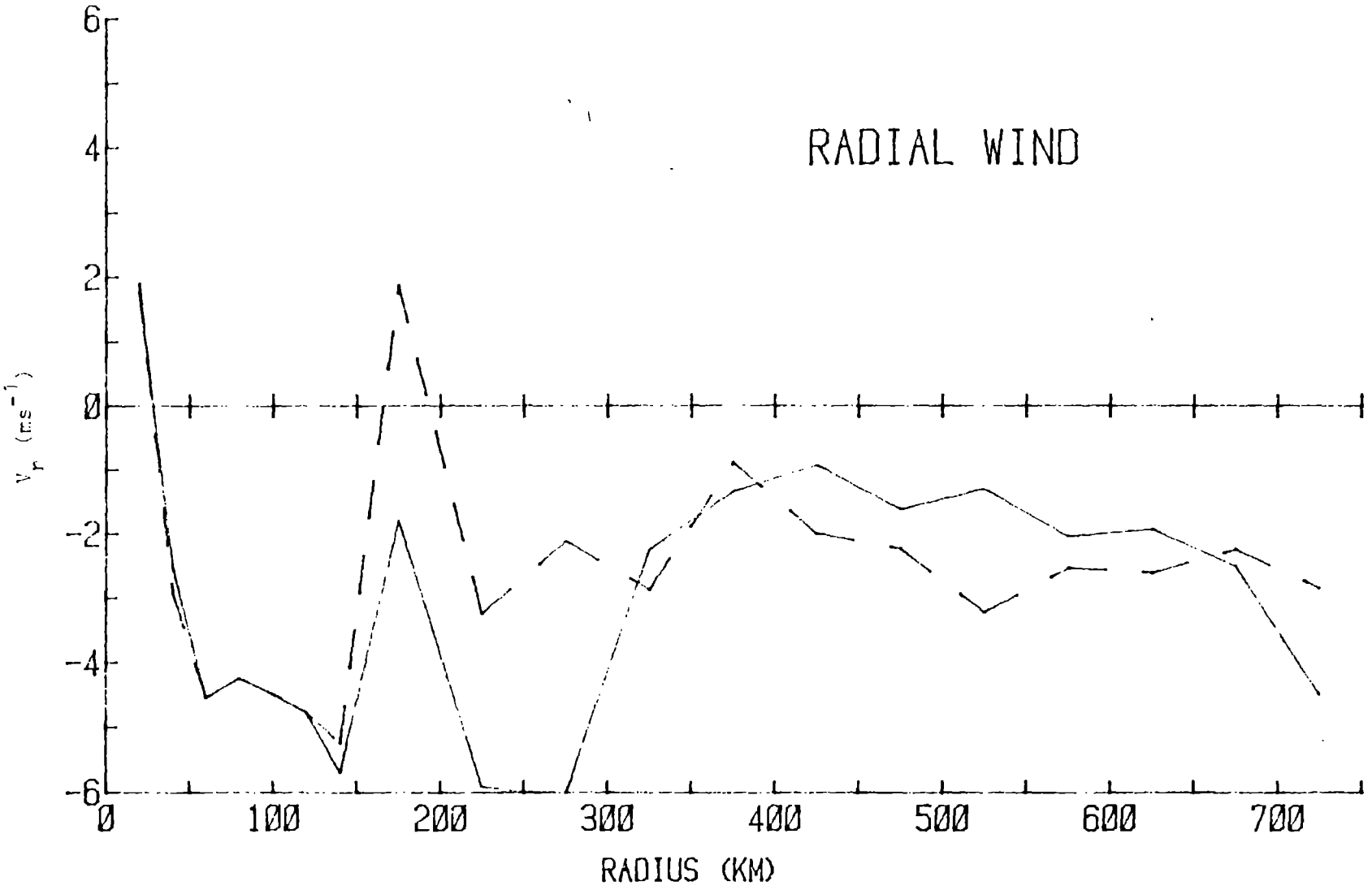

Figure 19 Radial winds (ms^{-1}) on 11 Sept. 1979 (solid) and 12 Sept. 1979 (dashed). Data from 0-150 km radius are predominantly 560 km aircraft data which are averages of both 11-12 Sept. 1979. Other data are low-level satellite and 950 mb rawinsonde winds.

typhoon and hurricane composites of Frank (1982). Tangential winds increased by about 1-5 ms^{-1} at all radii (Fig. 20) showing that the intensification of the rotational flow occured over a broad area. This suggests that satellite observations of the mean tangential winds at large radii (~ 200-800 km) may be used to monitor changes in the core strength. The central pressure dropped from 971 mb at 1600 GMT, 11 Sept. to a minimum observed value of 947 mb at 1600 GMT, 12 Sept. (Fig. 1) which is the approximate period covered by the satellite observations. The maximum winds increased from 48 ms^{-1} to 58 ms^{-1} over the same period (Powell, 1982).

At the high analysis level there was an increase in outflow at all radii from 11 Sept. to 12 Sept. (Fig. 21). This is in apparent contradiction with Fig. 19 which showed no increase in low-level inflow at radii greater than 600 km. The upper level anticyclone also strengthened at all radii (Fig. 22).

4.3.2 Divergence and Vorticity

There were no significant changes in the low level divergence profile between 11-12 Sept. (Fig. 23). Low-level relative vorticity increased from 11-12 Sept. at most radii (Fig. 24). At the high analysis level the data suggest increased upper level convergence at radii $\geq$ 400 km (Fig. 25) and a slight decrease in relative vorticity at most radii (Fig. 26)from 11 SEP to 12 SEP.

4.3.3 Radial Fluxes

The low-level analyses indicate increased inward transport of both angular momentum and kinetic energy at radii $\geq$ 400 km from 11-12 Sept. (Figs. 27 and 28, respectively). In both cases the transports approximately doubled. High-level import of angular

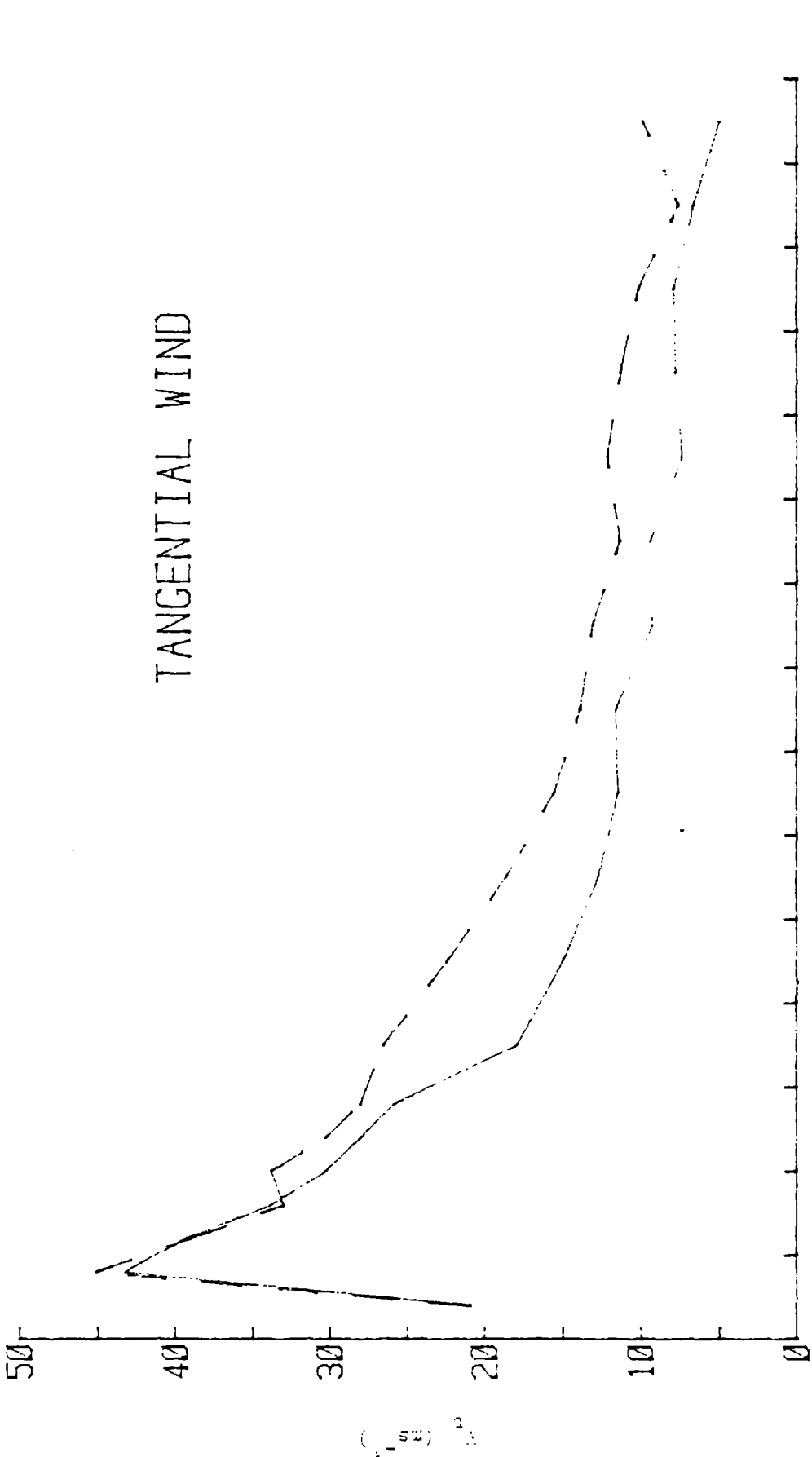

Figure 20 As in Fig. 19, but for tangential winds.

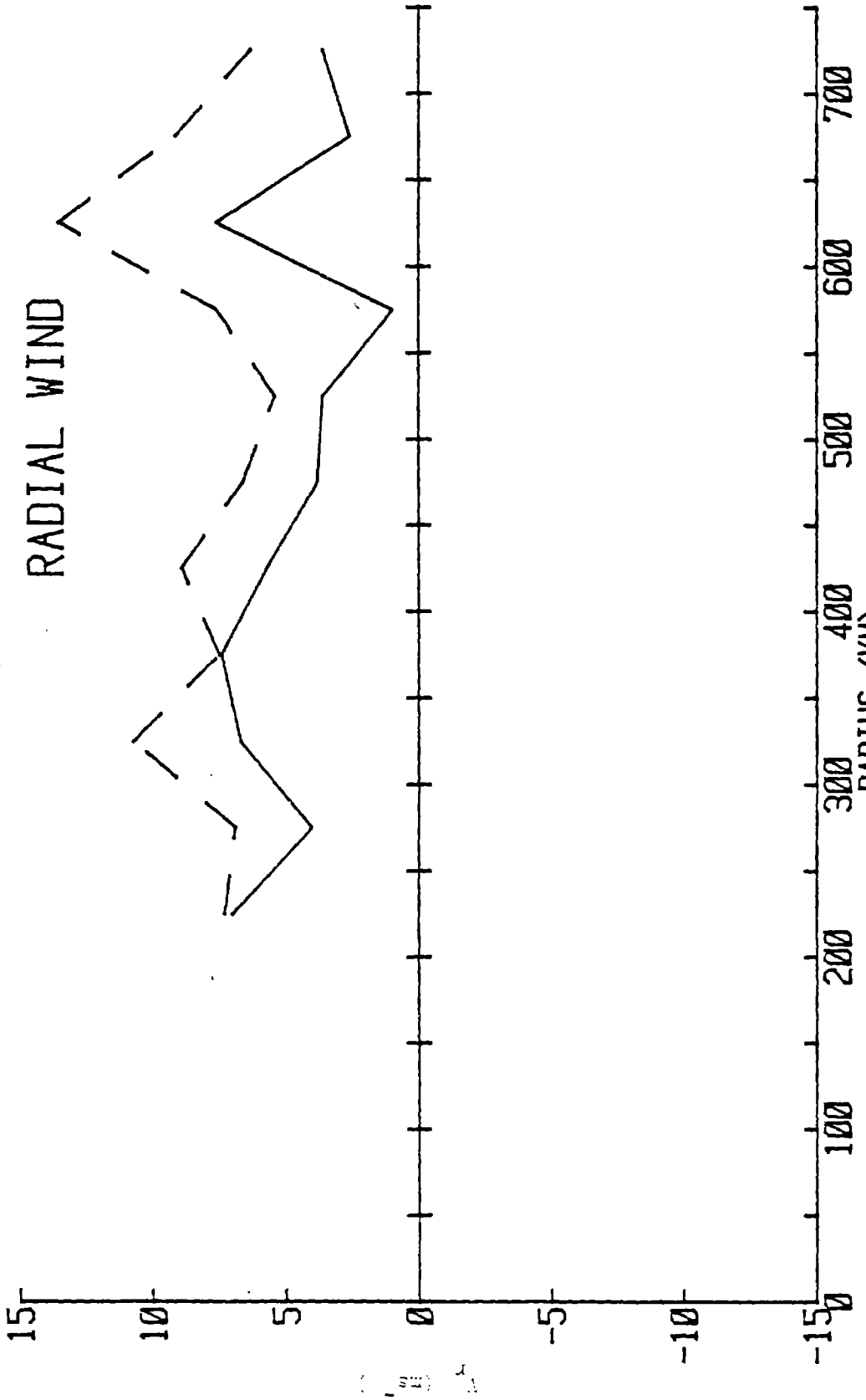

Figure 21 As in Fig. 19, but using only high-level satellite and 200 mb rawinsonde winds.

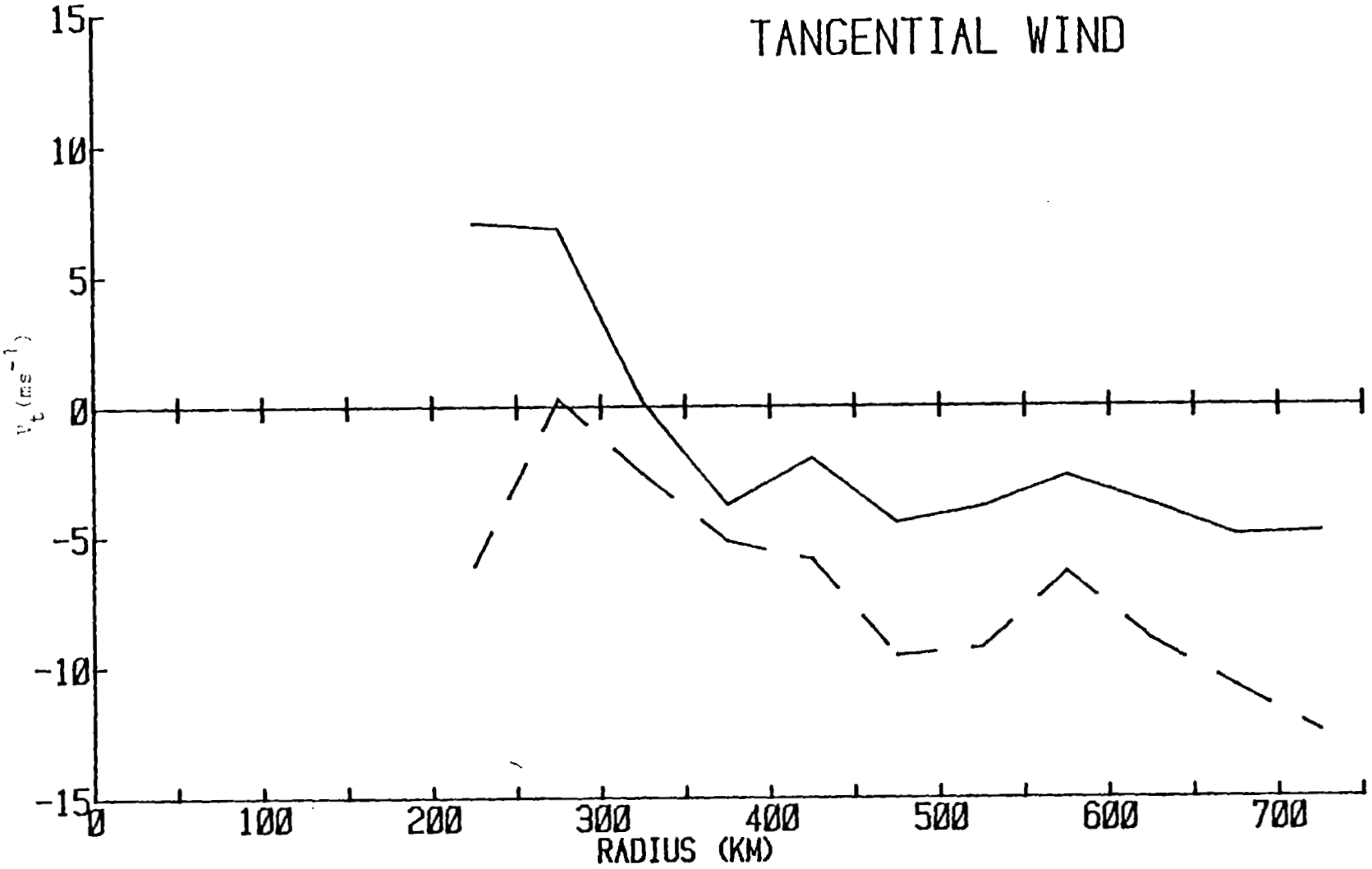

Figure 22 As in Fig. 21, but for tangential winds.

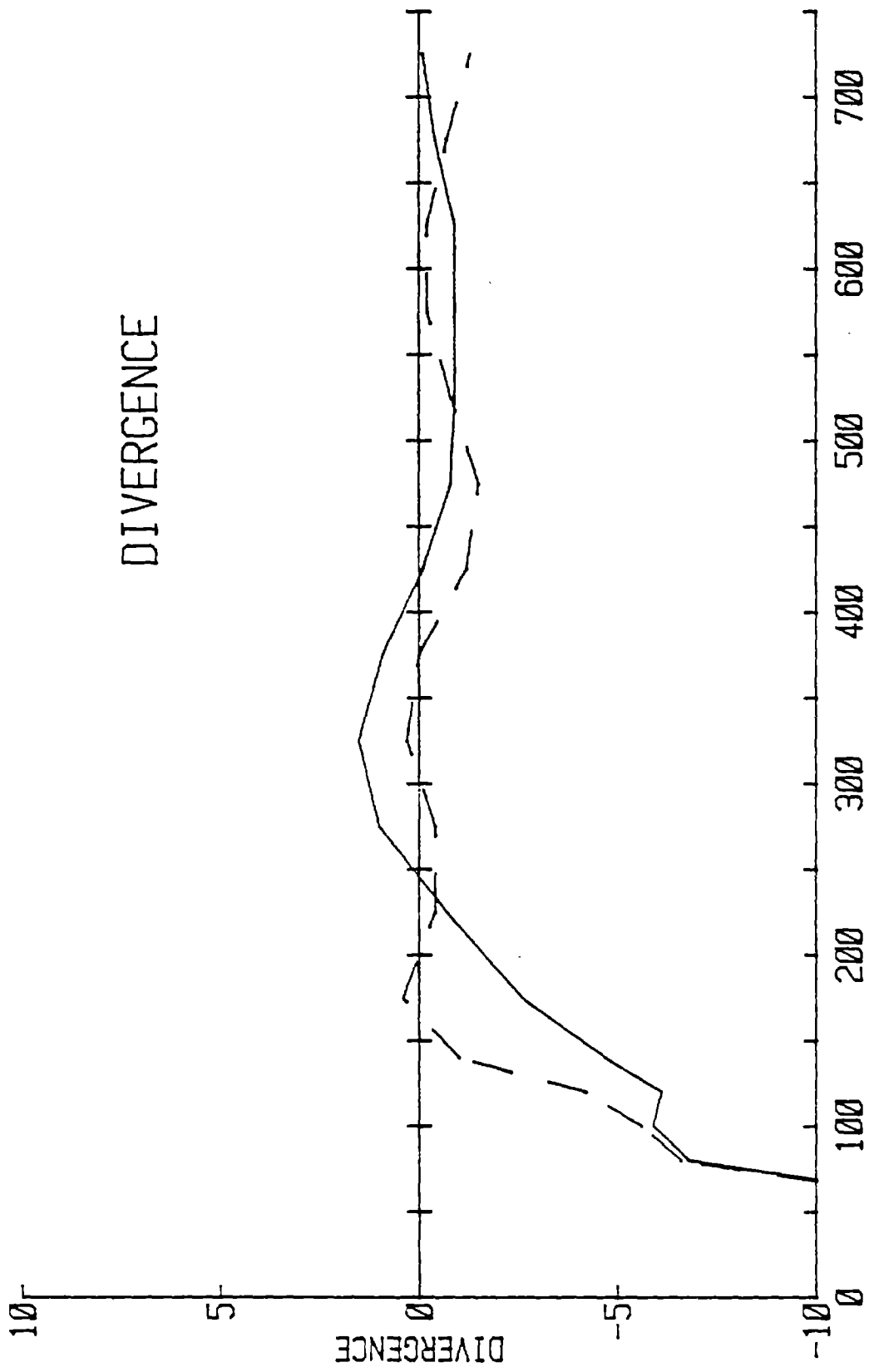

Figure 23 As in Fig. 19, but for divergence (x 10^{-5} s^{-1}).

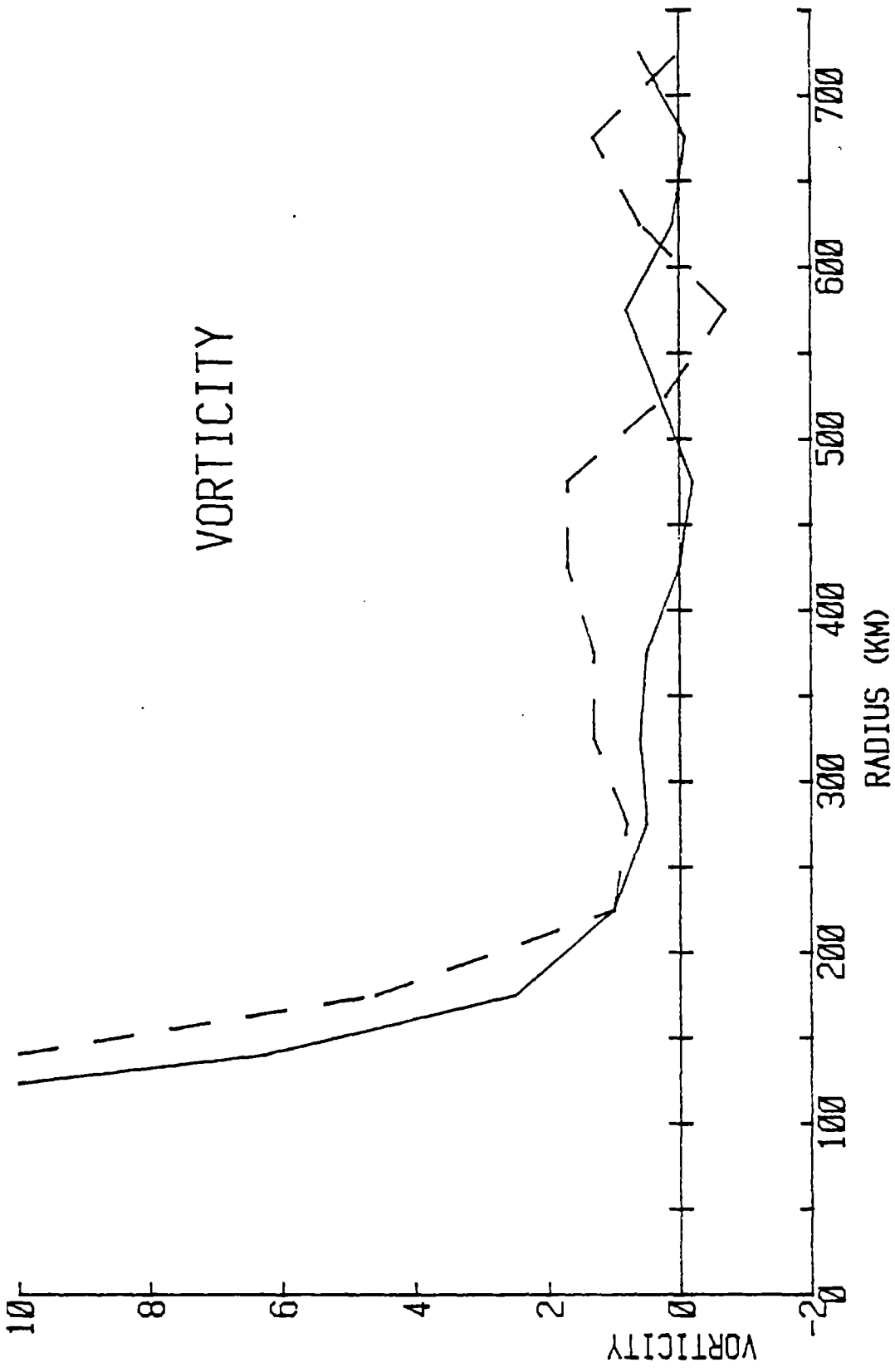

Figure 24 As in Fig. 19, but for relative vorticity (x 10^{-5} s^{-1}).

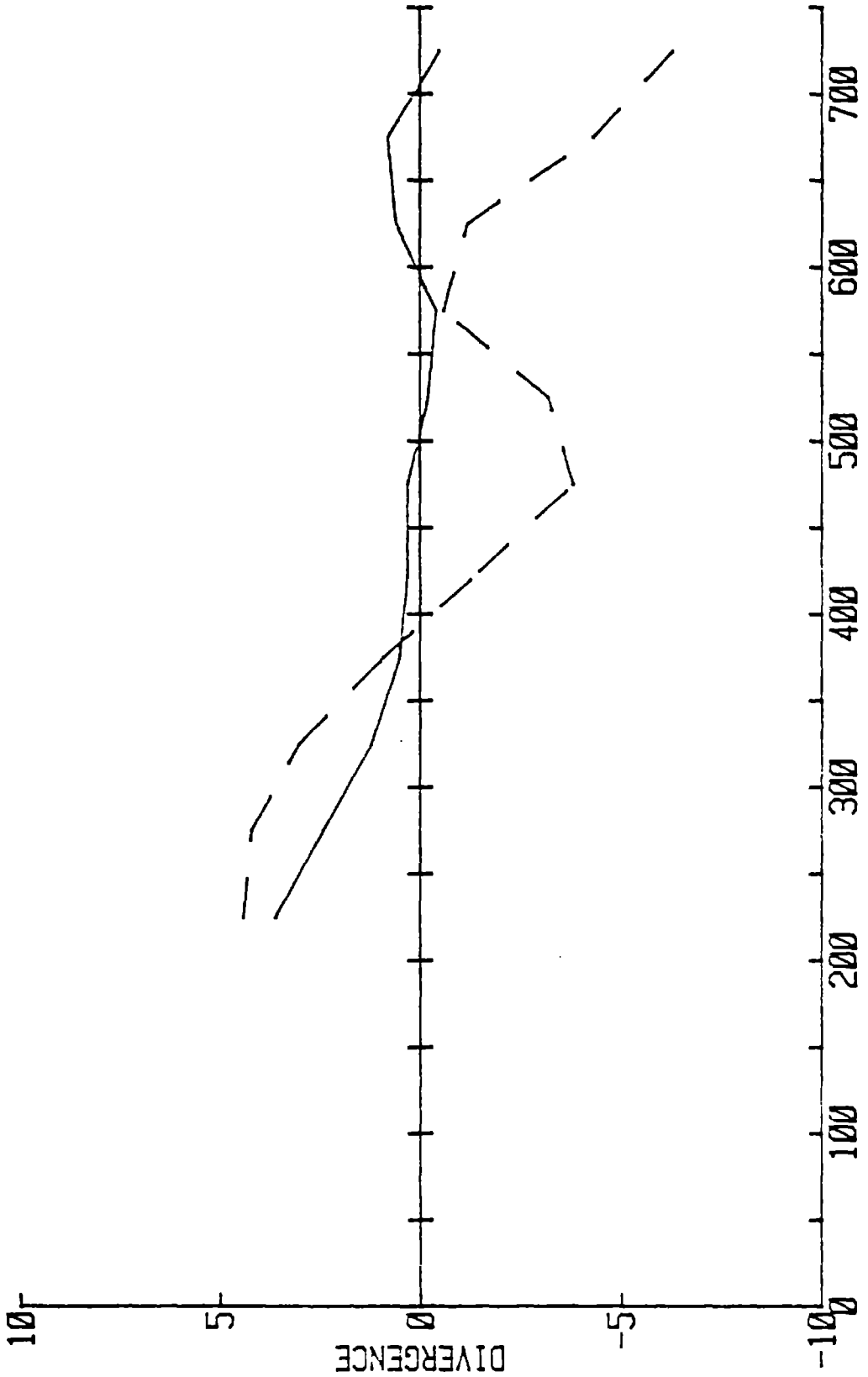

Figure 25 As in Figure 21, but for divergence (x 10^{-5} s^{-1}).

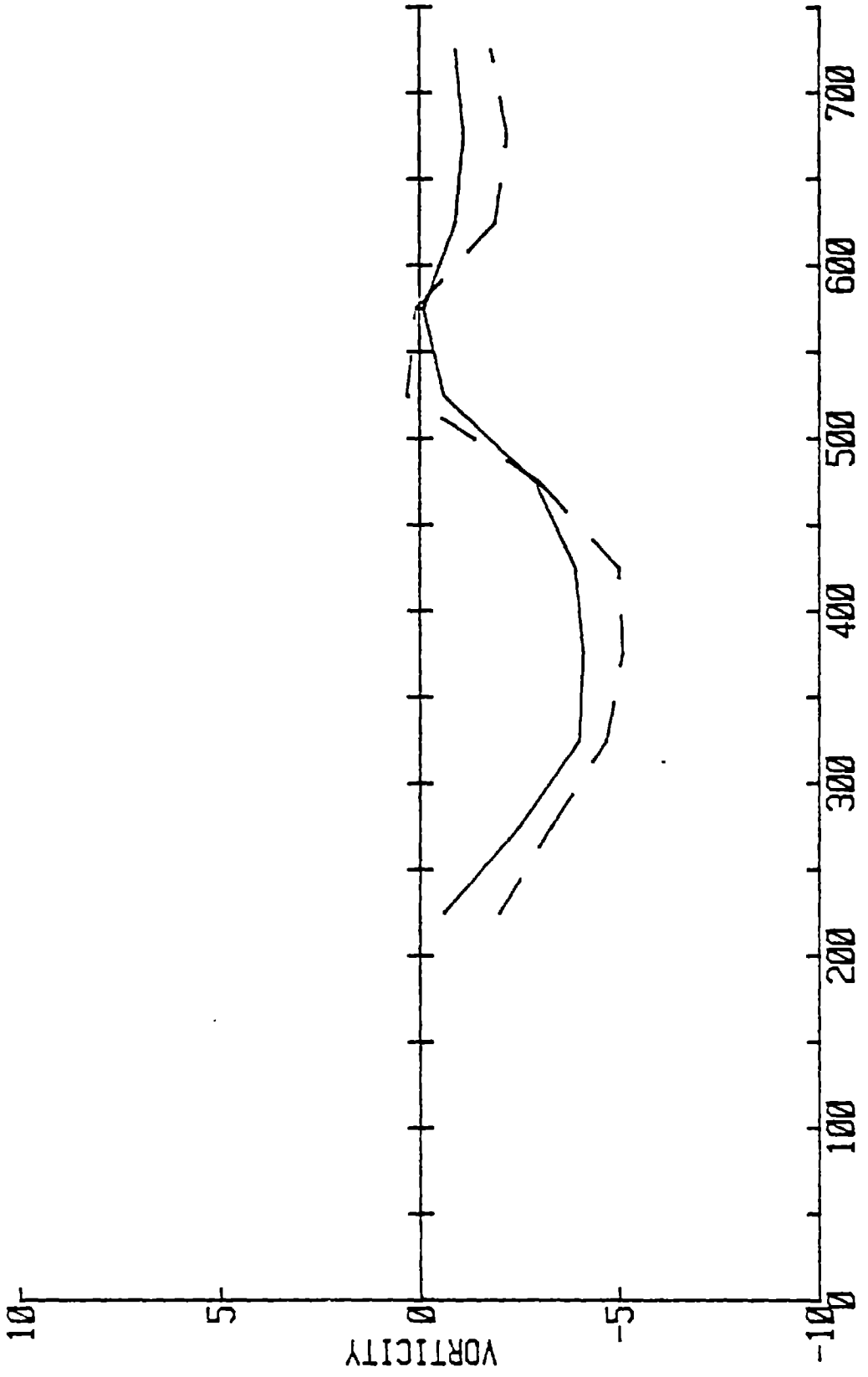

Figure 26 As in Fig. 21, but for relative vorticity (x 10^{-5} s^{-1}).

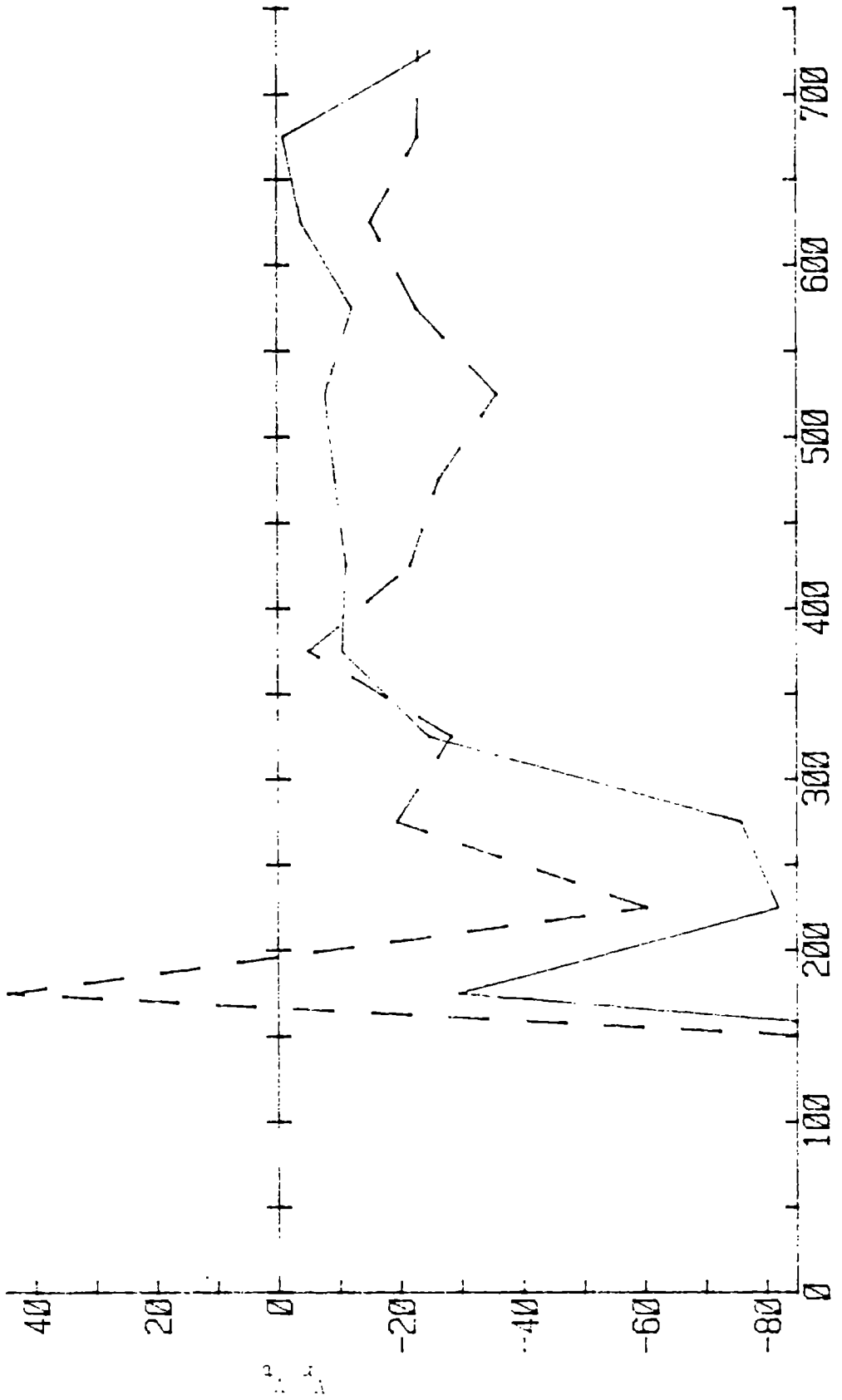

Figure 27 As in Fig. 19, but for radial wind times tangential wind ($m^2\ s^{-2}$).

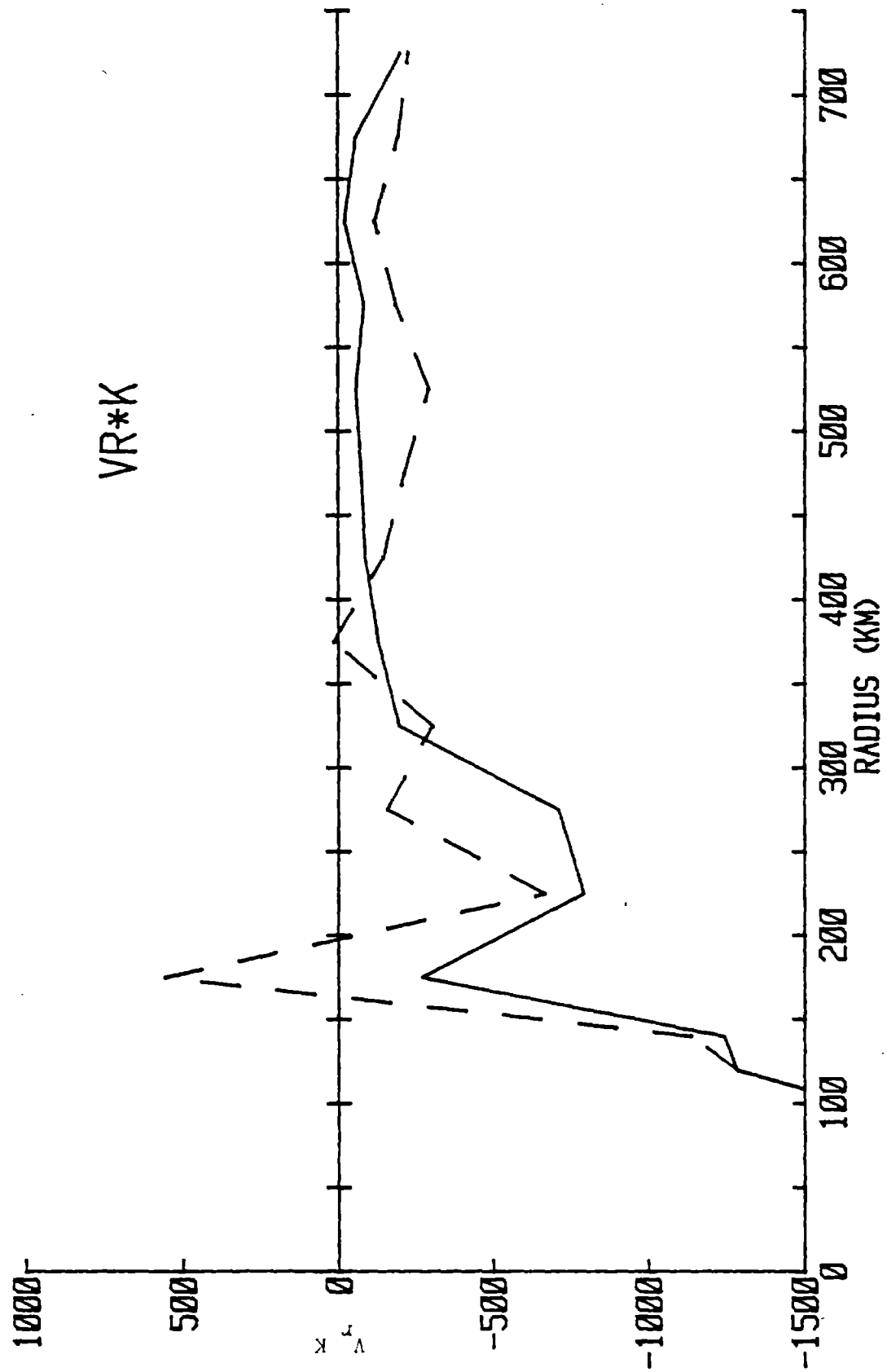

Figure 28 As in Fig. 19, but for radial wind times kinetic energy ($m^3\ s^{-3}$).

momentum and export of kinetic energy at radii $\geq$ 400 km increased even more dramatically over the same time interval (Figs. 29 and 30, respectively). The combined upper and lower level analyses suggest that the observed modest intensification of the core was accompanied by a net increase in import of angular momentum. The storm did not continue to intensify after 1600 GMT, 12 Sept. Therefore, with the limited time resolution of data available, it is not clear that changes in the momentum import or kinetic energy fluxes preceded changes in storm intensity as has been observed in some other hurricanes (Rodgers and Gentry, 1981). However, the changes in upper level radial fluxes of angular momentum and kinetic energy were sufficiently large to warrant their investigation as parameters for monitoring the core intensity using remote sensing.

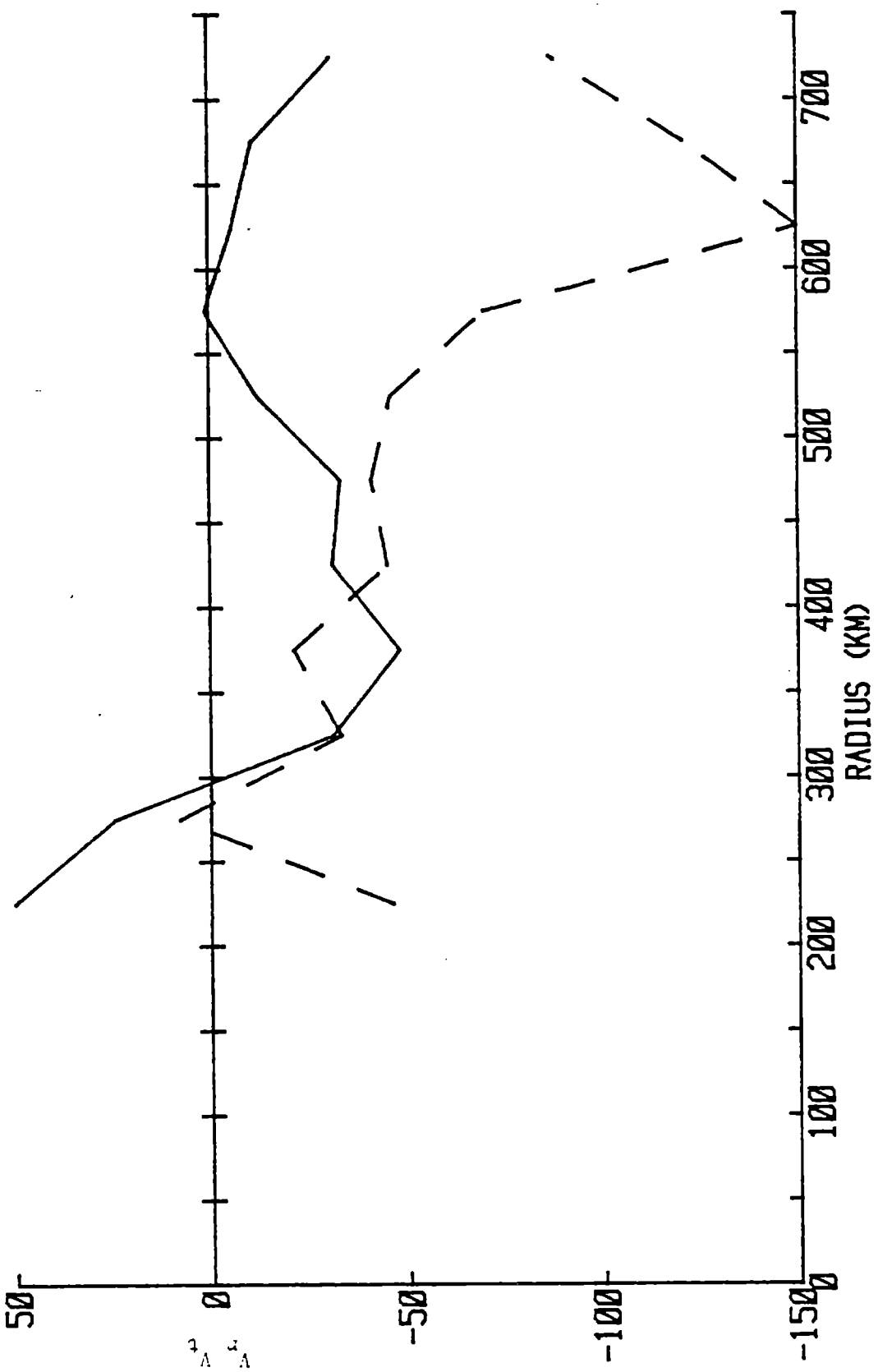

Figure 29 As in Fig. 21, but for $V_r \cdot V_t$ ($m^2\ s^{-2}$).

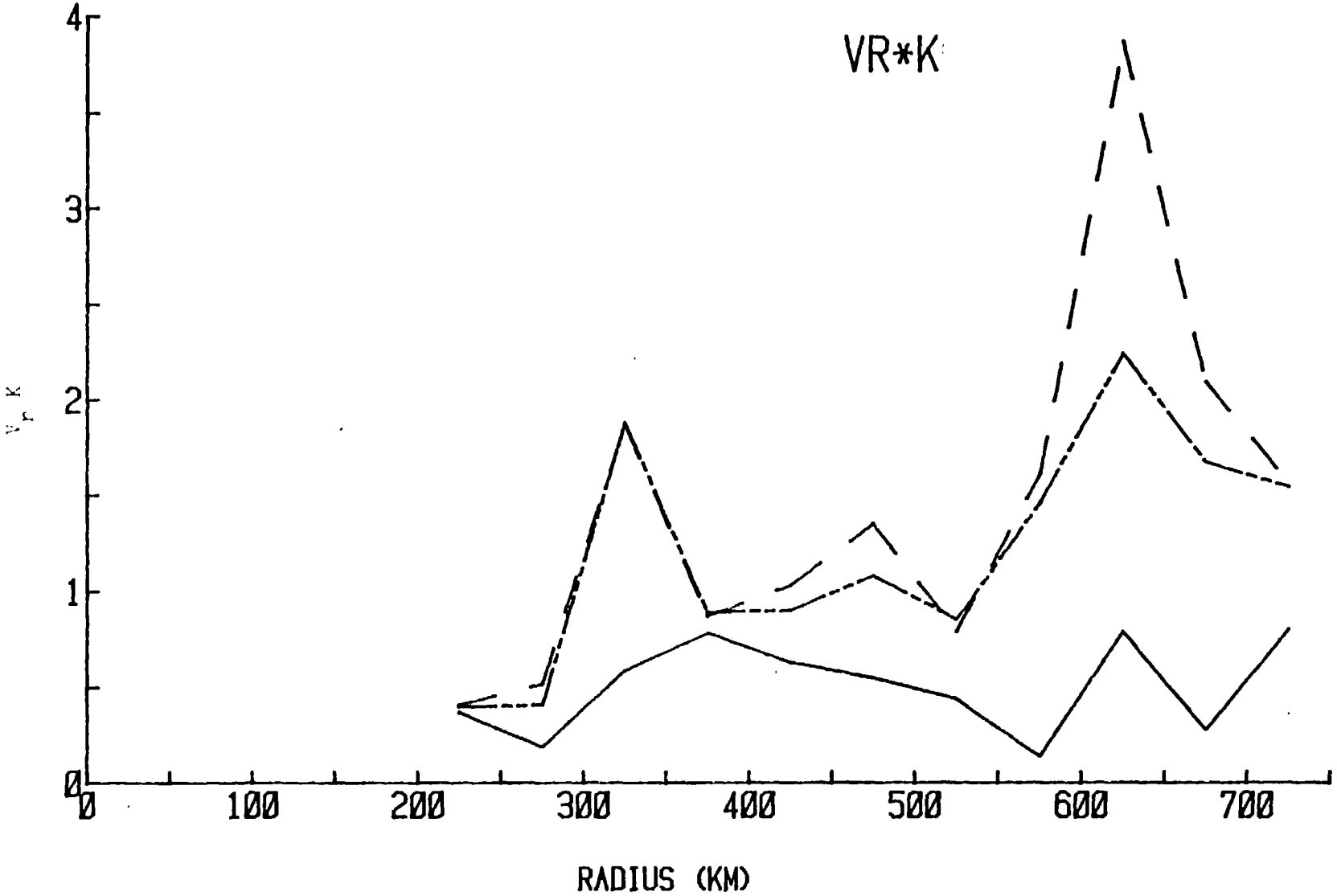

Figure 30 Radial transport of kinetic energy (x 10^3 m^3 s^{-3}) computed from high-level satellite and 200 mb rawinsonde winds, for 11 Sept. 1979 (solid) 12 Sept. 1979 (dashed) and averaged for 11-12 Sept. 1979 (dash-dot).

5. Summary and Conclusions

The major objective of this research was to analyze the structure of a mature tropical cyclone over a domain with a radius of 800 km by investigation of data from several sources. The ultimate goal was to evaluate properties of the hurricane circulation at radii $\geq$ 150 km which could be remotely sensed and used to monitor or forecast the properties of the intense inner core. The data were assembled and processed into fields of wind vectors. However, the level of integration of data achieved in this study was relatively crude. Results indicated that the major problem was determination of appropriate heights for the satellite derived winds. Nevertheless, by assigning all of the low-level satellite winds to the same level as the 560 m aircraft and 950 mb rawinsonde winds, radial profiles of inflow layer properties were analyzed to a first approximation. Assignment of all high-level satellite winds to the level of the 200 mb rawinsonde data yielded similar, though more tentative, profiles for the outflow layer.

The overall picture of storm structure which emerges is in good subjective agreement with earlier composite analyses such as Frank (1977a,b, 1982)and McBride (1981). The depths of the inflow and outflow layers of this individual storm at outer radii are close to those of composites of hundreds of storms. Within the limitations of the analysis, Hurricane Frederick exhibited strong low level convergence and vorticity only inside about 150-200 km radius. The storm imported angular momentum at the lower level and at radii $\geq$ 300 km at the upper level. Kinetic energy was imported at the lower level and exported aloft. These results are supportive of the earlier composite studies and are indicative that Hurricane Frederick was a rather typical tropical storm.

Changes in storm properties from 11 Sept. to 12 Sept. were examined to

find storm properties which might be related to the intensification of the core. At low levels the most dramatic change was the increase in the tangential wind at all radii. The 10 ms^{-1} increase in maximum winds in the core was accompanied by increases in V_t averaging 2.3 ms^{-1} over the 300-800 km radius area where many satellite winds were obtainable. At the upper analysis level both the radial outflow and the anticyclonic rotation increased by 4-5 ms^{-1} between 300-800 km radius. Despite the obvious variations in the radial and tangential wind fields, changes in the radial profiles of divergence and vorticity were small. However, there were substantial changes in radial fluxes of angular momentum and kinetic energy. At low levels the magnitude of the radial import of each quantity between 300-800 km radius doubled from 11 Sept. to 12 Sept. At the upper level the momentum import and kinetic energy export both appeared to increase by more that a factor of three (averaged over the same radii and time interval).

Without a longer time sequence of observations, it is not clear whether the noted changes in storm structure have predictive value as suggested by results of Rodgers and Gentry (1981). However, the analyses suggest that remote monitoring of storm intensity using satellite-derived winds at both upper and lower tropospheric levels deserves further exploration. In particular, changes in the azimuthally-averaged tangential winds and in the radial fluxes of angular momentum and kinetic energy appear to be large enough to be detectable from comparison of data between individual observation periods. It should be remembered that the current data series was only a single case study using special rapid-scan data. A number of additional case studies are needed, and the ability to acquire adequate wind data without rapid-scan imagery must be evaluated.

Research is continuing in an effort to overcome the data matching

problems of the current study. Through A careful subjective analysis of all available data, including Powell's (1982) surface winds and stereo imagery, the heights of the low-level satellite winds are being analyzed on a point-by-point basis. It is anticipated that by restricting these data to over-water measurements and by vertically interpolating each wind measurement to the analysis level, significant improvements in the analysis of the storm inflow layer will be achieved.

Acknowledgements

The authors thank Mrs. Nancy Warner for preparing the text and Mrs. Jackie Kunes for assisting with the figures. Mr. Robert Cochrell did much of the programing, and Mr. Joseph Steranka of NASA assisted with the data processing. The research was supported by NASA grant NAG5-102.

References

Black, P.G. and R.A. Anthes, 1971: On the asymmetric structure of the tropical cyclone outflow layer. J. Atmos. Sci., 281, 1348-1366.

Frank, W.M., 1983: Composite analysis of the core of Hurricane Frederick (1979), NOAA Report NOAANA80RAC00090, 89 pp., available from HRD, AOML, NOAA, Miami, FL.

Frank, W.M., 1982: Large scale characteristics of tropical cyclones. Mon. Wea. Rev., 110, 572-586.

Frank, W.M., 1977a: The structure and energetics of the tropical cyclone. Part I. Storm structure. Mon. Wea. Rev., 105, 1119-1135.

Frank, W.M., 1977b: The structure and energetics of the tropical cyclone. Part II. Dynamics and energetics. Mon. Wea. Rev., 105, 1136-1150.

Holland, G.J., 1983: Angular momentum transports in tropical cyclones. Quart. J. Roy. Meteor. Soc., 109, 187-209.

McBride, J.L., 1981: Observational analysis of tropical cyclone formation. Department of Atmospheric Science Research Report No. 308, Colorado State University, Fort Collins, CO 80523.

Morris, K.R. and A.F. Hasler, 1984: Hurricane Frederick cloud winds with heights from short interval stereoscopic GOES imagery. Postprints of the 15th AMS Technical Conference on Hurricanes and Tropical Meteorology, Miami, 9-13 January 1984.

Pfeffer, R.L., 1981: A numerical study of the role of eddy momentum flexes in the development of Atlantic hurricanes. J. Atmos. Sci., 38, 2393-2398.

Powell, M.D., 1982: The transition of the Hurricane Frederick boundary-layer wind-field from the open Gulf of Mexico to landfall. Mon. Wea. Rev., 12, 1912-1932.

Rodgers, E.B. and R.C. Gentry, 1981: Monitoring tropical cyclone intensity using wind fields derived from short-interval satellite images. NASA Technical Memorandum 82162, Goddard Space Flight Center, Greenbelt, MD 20771.

Rodgers, E.B., R.C. Gentry, W.E. Shenk and V. Oliver, 1979: The benefit of using short-interval satellite images to derive winds for tropical cyclones. Mon. Wea. Rev., 109, 506-521.

Shapiro, L.J., 1983: The asymmetric boundary layer flow under a translating hurricane. J. Atmos. Sci., 40, 1984-1998.

Appendix A

Core Structure of Hurricane Frederick, from Frank (1983)

a. Introduction

Frank (1983) analyzed the core of Hurricane Frederick using aircraft data from a 40 h period on 11-12 Sep 79. The data were combined with the inflow layer analyses of Powell (1982) resulting in an analysis of the mean wind and thermodynamic fields from the surface to the 1600 m level and from the center to about 150 km radius. Some examples of the results are discussed below. In general, the quality of the composite wind fields appears to be quite good. Plan view analyses of divergence and kinematically-determined vertical velocity agreed well with independent measurements of cloud water and radar echo patterns. Asymmetries in the flow were well resolved.

In addition to the above, Frank (1983) used the wind fields to perform preliminary budget analyses of sensible heat and angular momentum for the subcloud layer (surface to ~ 560 m). Angular momentum budgets were also performed through the estimated depth of the inflow layer in the core areas. The results of these analyses suggested that net fluxes of sensible heat from the sea surface to the air were relatively small in the core and that surface drag coefficients did not appear to increase with increasing wind speed. Both of these findings are in conflict with several earlier studies, although Anthes and Chang (1978) hypothesized that surface sensible heat fluxes are generally small in hurricanes. Frank (1983) concluded that refinement of the analyses is needed including a more comprehensive integration of Powell's (1982) data, incorporation of Black's (1983) sea surface temperatures, and extension of the domain to much larger radii by incorporating the available satellite wind vectors and rawinsonde data.

b. Axisymmetric Structure

Azimuthally-averaged radial profiles of kinematically derived radial winds (V_r), divergence (DIV), vertical velocity ($\bar{w}$), cloud water (JW), tangential winds (V_t), relative vorticity (ζ), pressure (p), potential temperature (θ) and specific humidity are shown in Figs. A1-A9, respectively. Values at z = 560 m are shows as solid lines, while z = 1600 m values are dashed.

The radial inflow at 560 m was almost constant with radius from 60 km radius outward (Fig. A1). Inward of that radius the inflow dropped sharply, and outflow was found inward of 30 km. At 1600 m the inflow at larger radii was weaker, and the radius of zero inflow was about 70 km. The resulting divergence profiles for the two lower layers are shown in Fig. A2. Maximum convergence at 560 m occurred at 35 km radius, while the maximum at 1600 m was near 65 km. The lower level peak was located at the radius of maximum cloud water, while the smaller peak at 1600 m was near the outer edge of the cloud water maximum. At outer radii divergence values on the order of -5×10^{-5} s^{-1} were found at both levels.

Upward vertical velocities were computed at all radii greater than about 15-20 km at 560 m and 1600 m (Fig. A3). There were significant upward anomalies between about 20-60 km radius at 560 m (maximum = 0.17 m s^{-1} at 35 km) and between 20-70 km at 1600 m (maximum = 0.32 m s^{-1} at 35 km) corresponding to the eyewall cloud. Subsidence was indicated in the eye at both levels, although values at small radii must be viewed with caution done to the large effects of storm positioning errors on V_r. Upward motions were stronger at 1600 m than at 560 m at all radii outward of 25 km.

The profiles of cloud water (JW, Fig. A4) were in close agreement with

the vertical motion profiles. Strong maxima at 560 m and 1600 m were found between about 20-60 km. Since the Johnson-Williams measurements indicate primarily active cloud (rather than rainfall), the close agreement between vertical velocity and cloud water was expected.

Tangential winds showed relatively blunt peaks at about 35-45 km radius (Fig. A5). There was some suggestion of a slightly greater radius of maximum winds (RMW) at 1600 m. Total wind speeds were about 1 m s^{-1} greater than the tangential winds at most radii and are not shown separately. Wind speeds at 1600 m were stronger than 560 m winds at all radii.

Relative vorticity profiles computed from V_t showed nearly constant values of about 1-2 x 10^{-4} s^{-1} at radii greater than 60 km (Fig. A6). Values increased rapidly with decreasing radius, reaching maxima of 29 x 10^{-4} s^{-1} near 25 km radius at both levels. At 1600 m the vorticity remained nearly constant at radii less than 25 km, while at 560 m ζ decreased to 19 x 10^{-4} s^{-1} at 5 km radius.

The mean pressure profile (corrected to the 560 m level) is shown in Fig. A7. At both 560 m and 1600 m (not shown) the maximum gradients were found between 25-35 km, slightly inside the radii of maximum winds. The pressure drop from 135 km radius to 5 km radius was 34 mb at 560 m.

Radial profiles of potential temperature showed gradually increasing θ values with decreasing radius at both 560 m and 1600 m (Fig. A8). At the lower level the gradient became stronger inward of 50 km radius, and values were maximum near the center. At 1600 m the strongest gradient was between 15-60 km.

Specific humidity increased monotonically with decreasing radius Fig. A9).

c. Height of the Inflow Layer

The depth of the hurricane inflow layer has been difficult to ascertain in the core region due to difficulties in obtaining representative radial wind values at multiple levels. Fig. A10 shows a vertical cross-section analysis of the radial winds based on data from the surface, 560 m and 1600 m. The V_r = 0 contour at radii outward of 65 km was obtained from linear extrapolation, and the zero contour line shown is based on exact linear interpolation/ extrapolation followed by 1-2-1 radial smoothing. (Other contours were subjectively analyzed). As expected, inflow as maximum near the surface. From 95-135 km radius the top of the inflow layer was nearly constant at approximately z = 2.2 km. Interestingly, this is nearly the same height as was found at r = 222 km in the mean W. Pacific typhoon composites of Frank (1977a) and at about r = 7° radius for Hurricane Frederick (Fig. 6, this report).

The top of the inflow layer decreased almost linearly with decreasing radius inward of 95 km. It must be remembered that surface data in the eye/ eyewall region were very limited. It is also worth noting that the inflow was quite asymmetrical so that the concept of a top of the inflow layer is only strictly applicable to axisymmetric analyses.

d. The Asymmetric Storm

Plan view analyses of parameters were prepared at the surface, 560 m and 1600 m levels to examine asymmetric properties of Hurricane Frederick. Some of the results are presented in Figs. A11-A21. Wind data are presented in stationary coordinates unless noted as "relative" (which indicates that the mean storm motion vector has been subtracted from all winds). Some data were subjected to a 1-2-1 radial smoothing prior to the subjective analysis, and these cases are noted as radially smoothed in the text or figure captions.

Surface wind speeds (Fig. A11) were strongest ahead and to the right of

the storm's track (looking downstream). At 560 m (Fig. A12) the pattern was similar with maximum winds greater than 56 m s^{-1} found at 35 km radius. When the storm's motion was subtracted, the winds were nearly symmetrical to the left and right of the track (not shown). However, a front to back asymmetry remained with winds ahead of the storm at the RMW exceeding those behind the storm by about 12 m s^{-1}. The pattern is in good qualitative agreement with the surface winds in Shapiro's (1983) analysis of Frederick based on Powell's (1982) data.

The surface radial wind analysis relative to the moving storm (Fig. A13) shows that inflow was concentrated heavily in the north and northeast portions of the storm, while weak outflow occurred to the southwest. Radial inflow of greater than 15 m s^{-1} extended inward to within 65 km radius on the north side. At 560 m the relative radial winds displayed a similar pattern (Fig. A14) except that the outflow region on the southwest side was stronger (maximum > 6 m s^{-1}) and more extensive. At 1600 m (not shown) the northeast quadrant inflow and southwest quadrant outflow were of approximately equal magnitude (about ± 10 m s^{-1}). Despite significant changes in the mean inflow with height from the surface to 1600 m, the asymmetries in the radial wind fields were comparable at all three levels. It is interesting that all three levels showed outflow in the southwest quadrant at all radii, including the radius of maximum winds and the mean eyewall cloud radius.

Surface inflow angles (α_o - Fig. A15) are shown in stationary coordinates. The angles were highly asymmetrical with values of 40°-50° in the right rear quadrant and weak outflow on the left side of the storm. The veering angles between the surface (based on Powell's data) and 560 m (based solely on aircraft data) are shown in Fig. A16. Strong veering was observed in the soutwest quadrant (right rear) with surface inflow angles exceeding

inflow at 560 m by as much as 40°. Elsewhere the veering angles were on the order of 10° with some weak backing observed in the southwest quadrant at radii greater than 100 km.

Relative vorticity at 560 m (Fig. A17, radially smoothed) was nearly symmetrical with maximum values exceeding 25 x 10^{-4} s^{-1}. At 560 m a band of convergence with magnitudes greater than 2 x 10^{-4} s^{-1} was found between about 25-65 km radius and extending from the southeast quadrant cyclonically through the west quadrant (Fig. A18). A secondary maximum of convergence was found north and northeast of the center at about 100-130 km radius. Divergence was found in the eye extending outward through the mean eyewall radius on the south and southwest sides. These divergence patterns were in subjective agreement with radar echo composites. Regions of convergence corresponded roughly to regions of high rainfall, although the rainband near 100 km radius on the northeast side was not distinct in the radar composites.

Upward vertical velocity at 560 m (Fig. A19) was concentrated in a band extending from the southeast cyclonically to the west. Maximum values exceeded 0.3 m s^{-1} (east side, 35 km radius). A weaker band occurred at about 100 km radius to the north and northeast. Subsidence occurred to the northwest and west at outer radii. Strong subsidence was found in the eye extending outward to about 40 km radius in the southwest quadrant. Agreement between the kinematic vertical velocities and the radar echo composites was good.

Cloud water at 560 m (Fig. A20) confirms the kinematic vertical velocity patterns in the eyewall region, since the presence of cloud (as opposed to rain) water indicates regions of active convection. There was an indication of a weak cloud water maximum in the northeast quadrant near 100 km radius, the approximate location of the outer vertical velocity band.

Fig. A21 shows the percentages of the 1 s interval observations at which liquid water was detected at 560 m. This may be interpreted as a rough indicator of the fraction of the total area covered by active clouds (i.e., clouds with significant condensation occurring). The pattern in the eyewall-RMW region was similar to that of the total liquid water amount. Values of 100% occurred 35-45 km north and northeast of the center, while less than 20% of the samples southwest of the center measured cloud water. Values of 20-40% occurred over most of the grid, and zero values were found near the northeast and southwest edges.

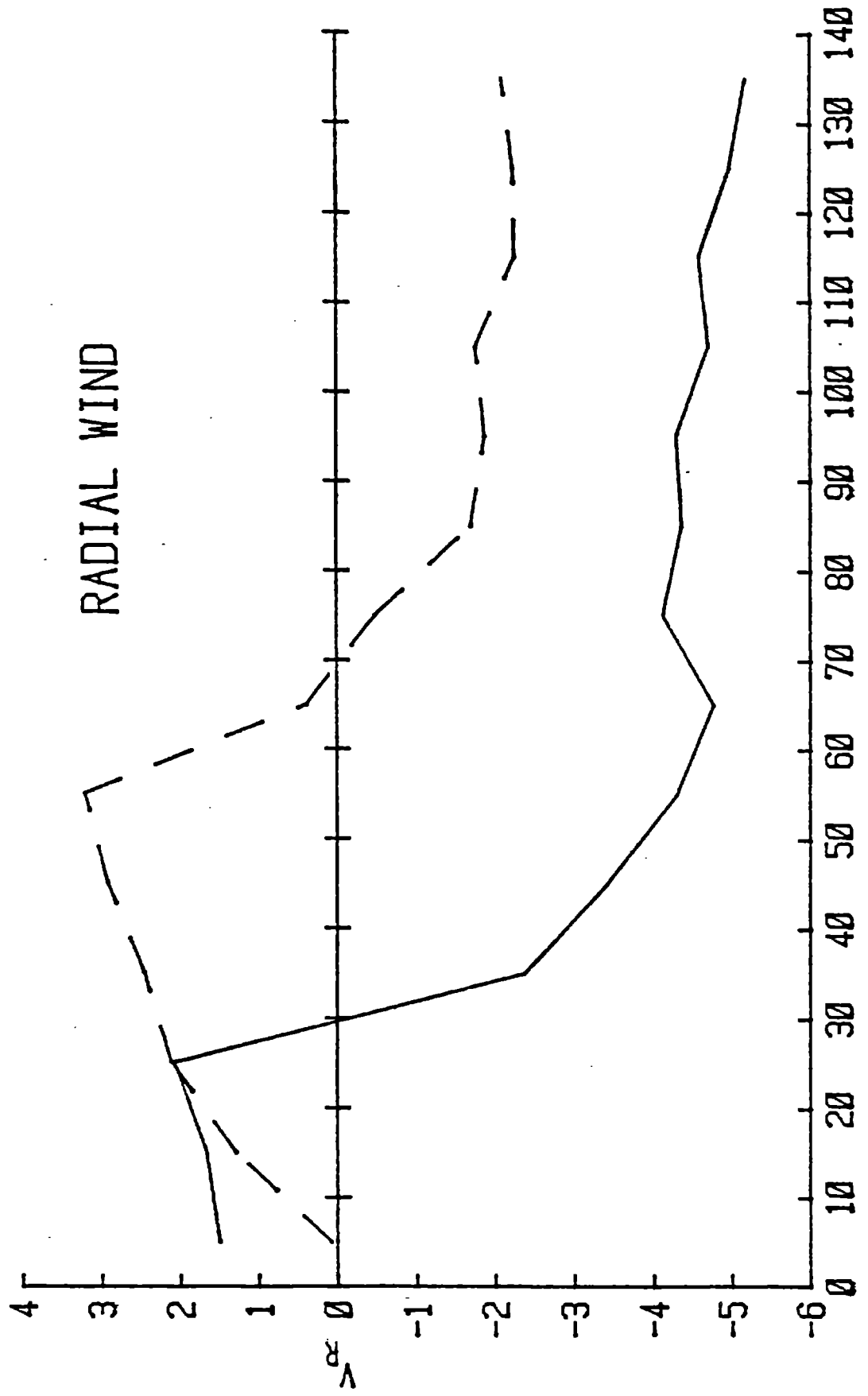

Figure A1. Radial winds at z = 560 mb (solid) and z = 1600 m (dashed) (m s^{-1}).

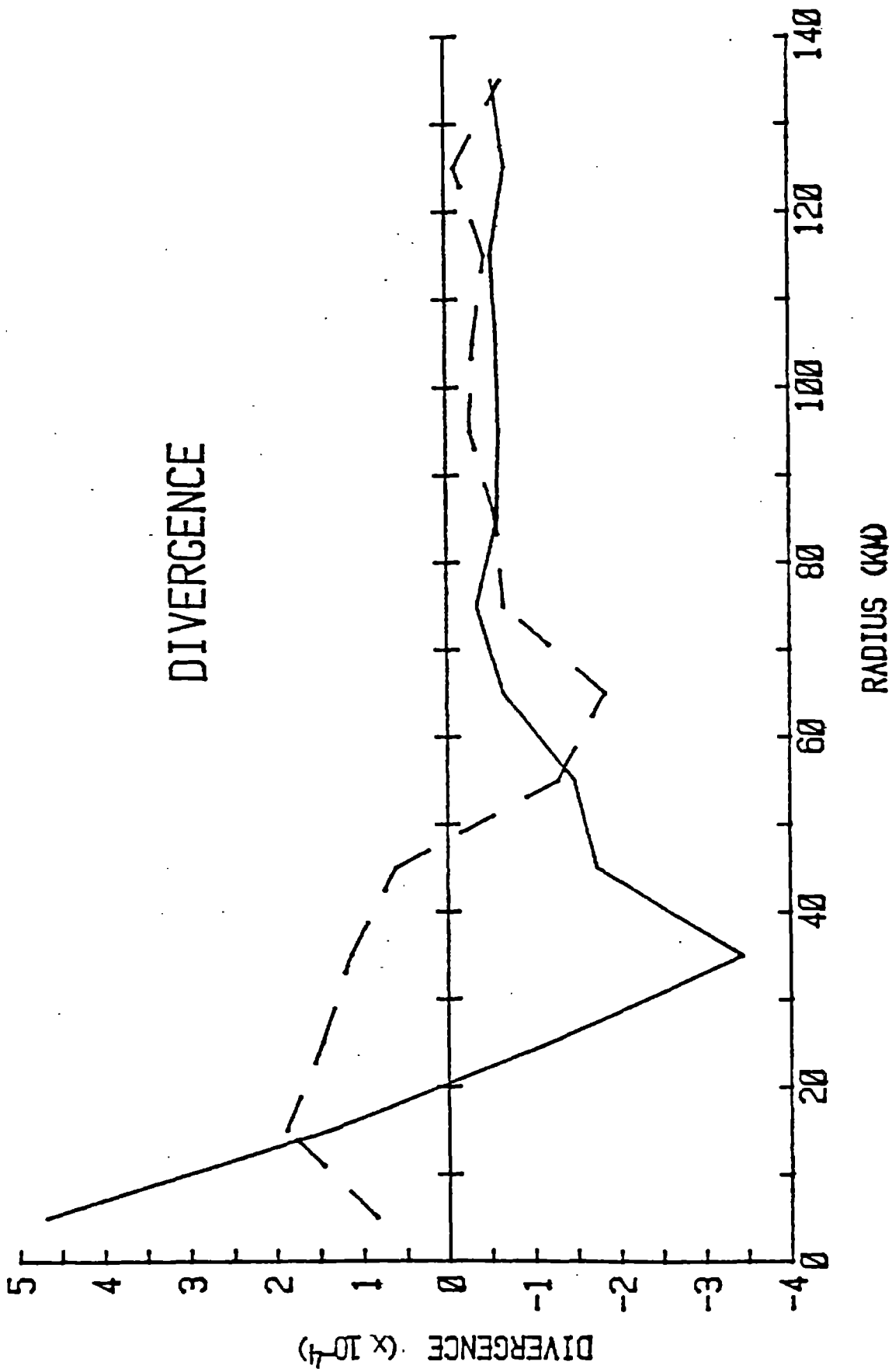

Figure A2. As in Fig. A1. but for divergence (x 10^{-4} s^{-1}).

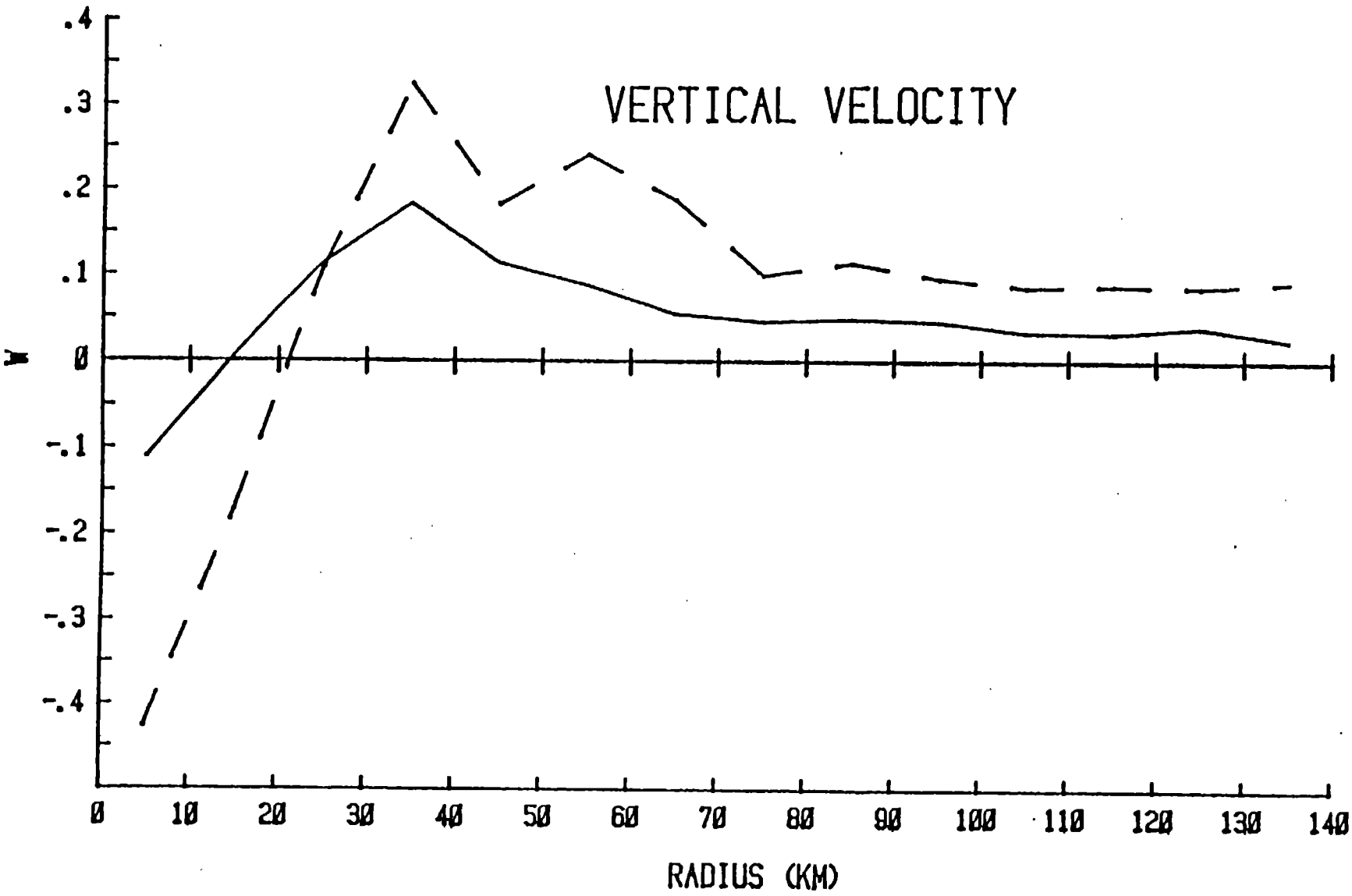

Figure A3. As in Fig. A1. but for vertical velocity (m s^{-1}).

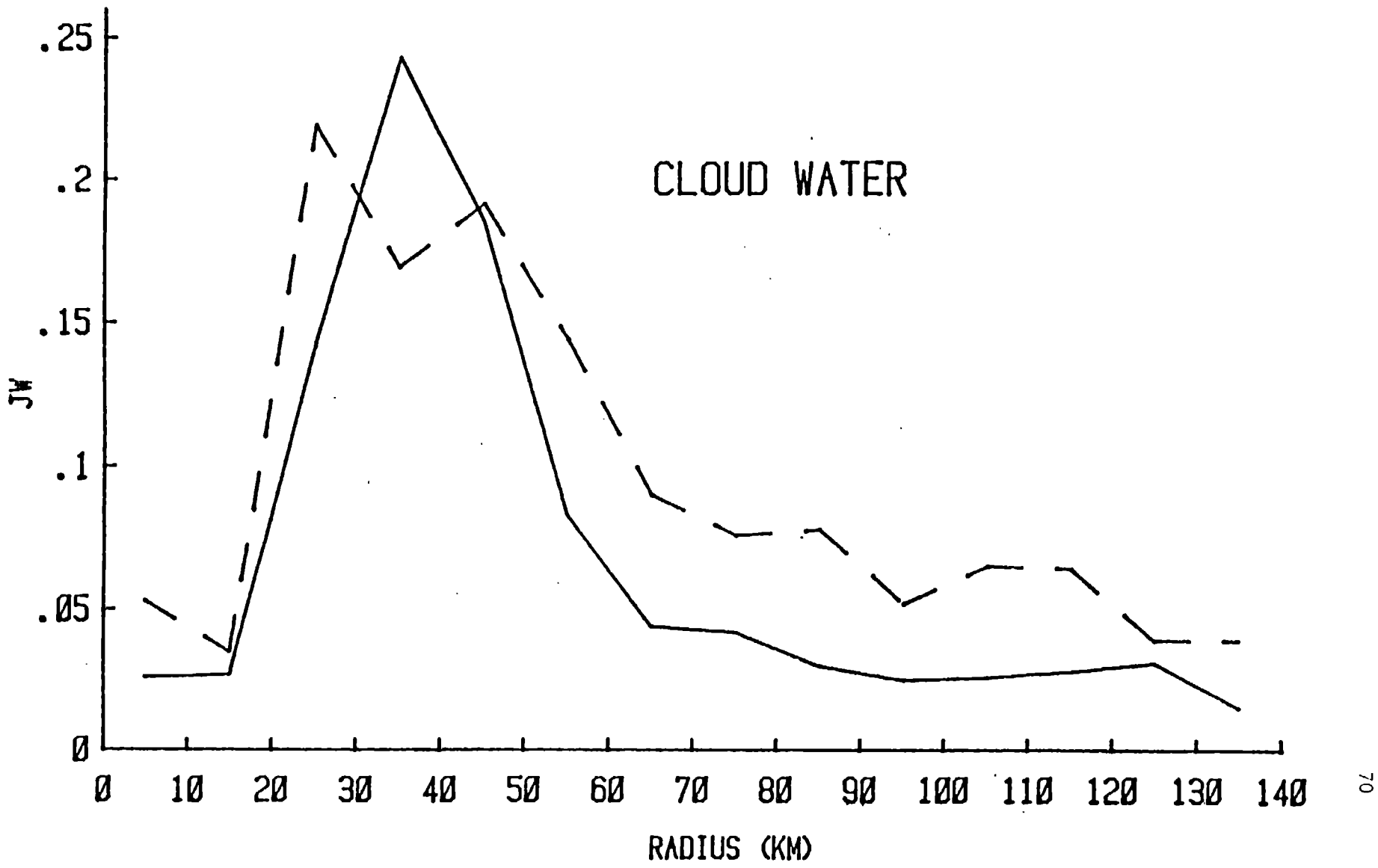

Figure A4. As in Fig. A1 but for cloud water (JW - g m^{-3}).

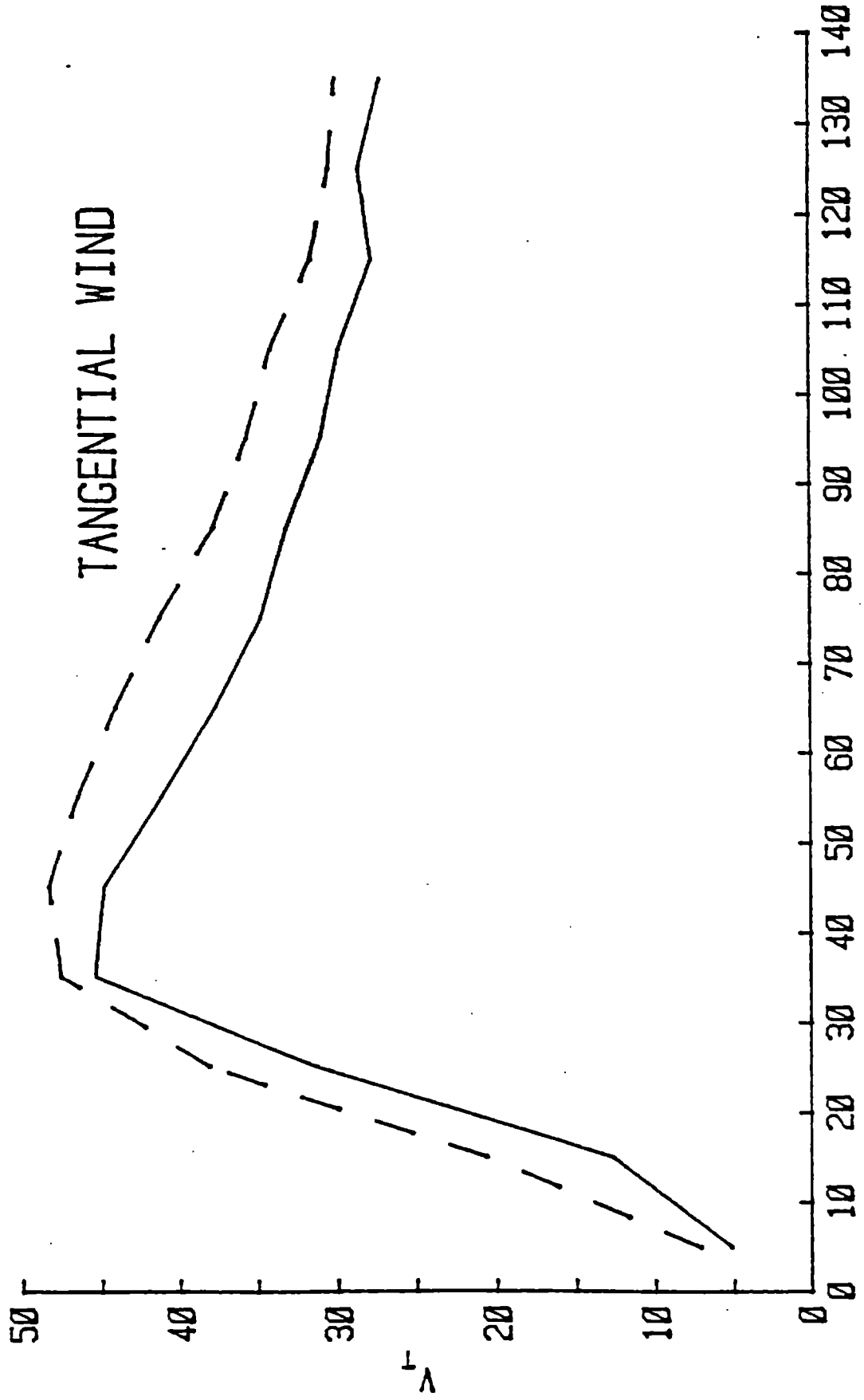

Figure A5. As in Fig. A1 but for tangential winds ($m\ s^{-1}$).

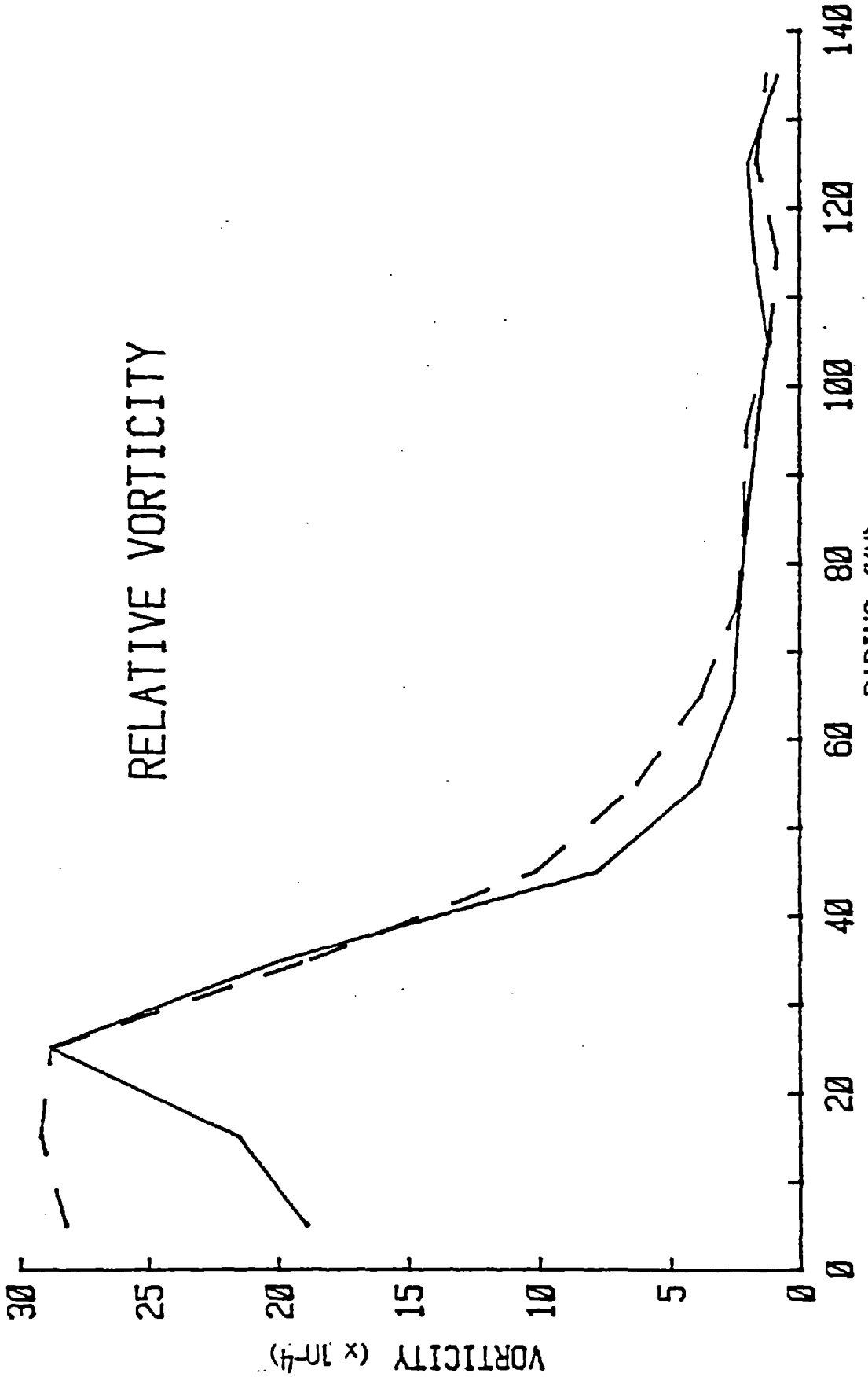

Figure A6. As in Fig. A1 but for relative vorticity (x 10^{-4} s^{-1}).

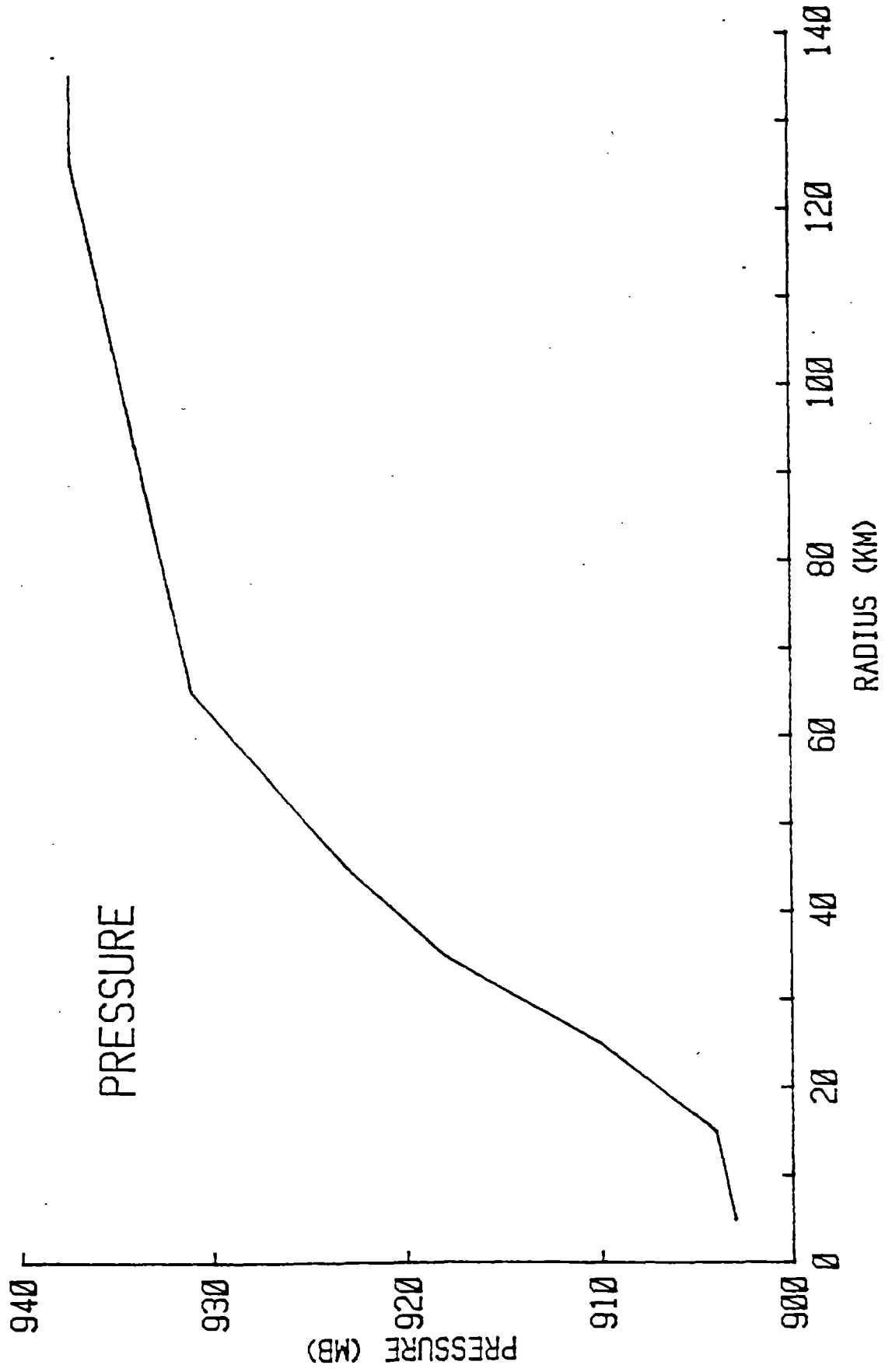

Figure A7. Pressure at z = 560 m (mb).

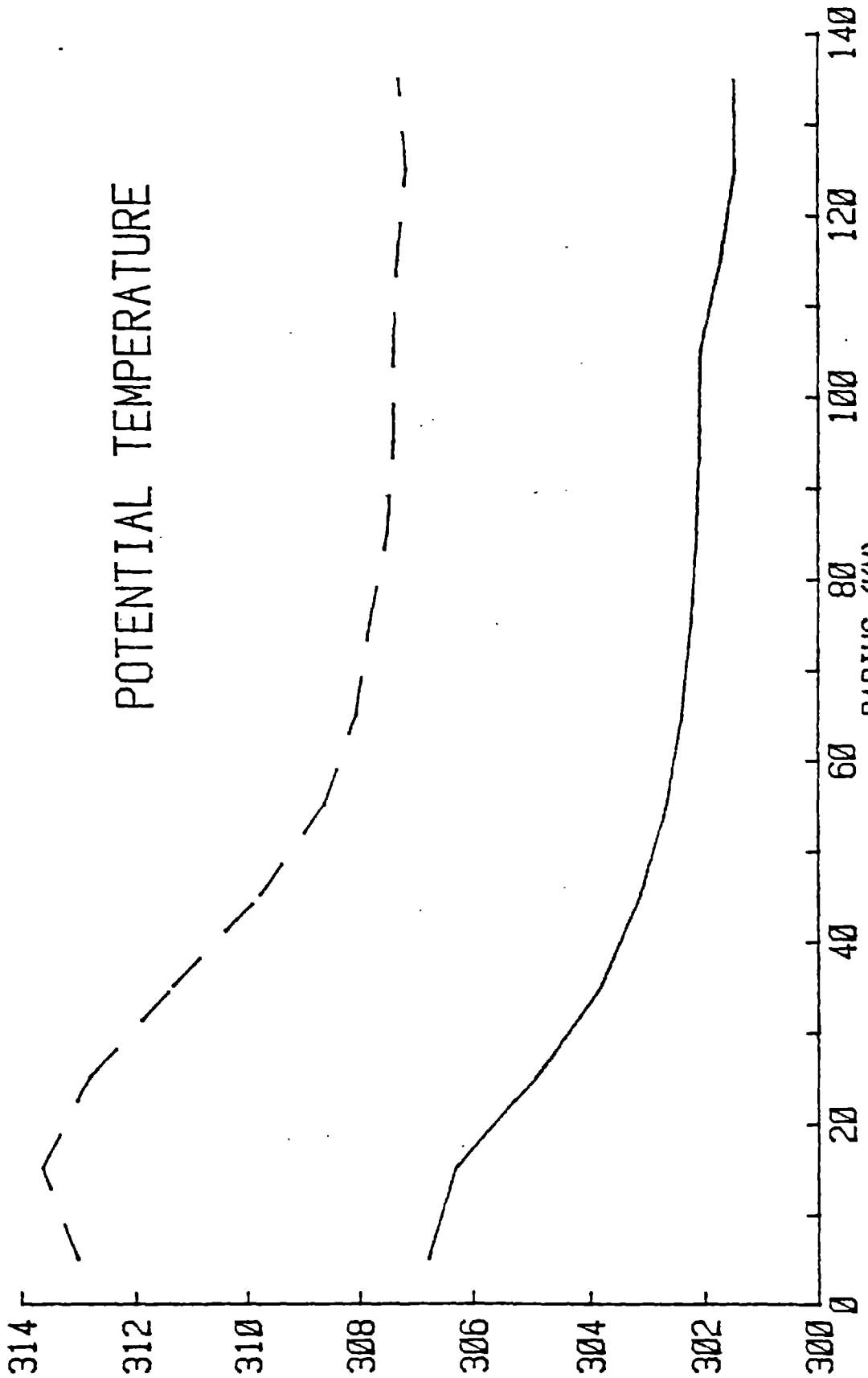

Figure A8. As in Fig. A1 but for potential temperature (θ -°K).

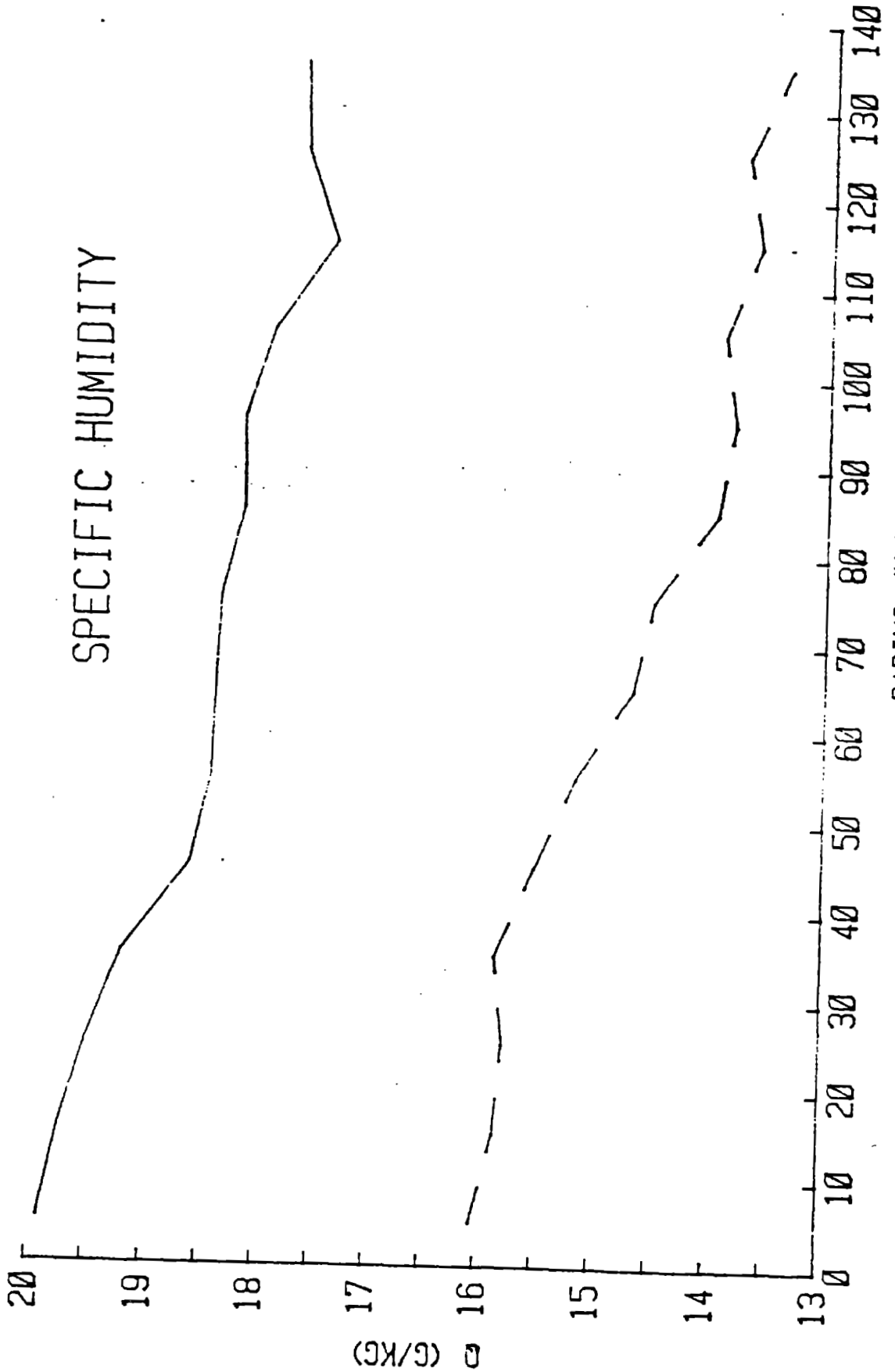

Figure A9. As in Fig. A1 but for specific humidity (q - g Kg^{-1}).

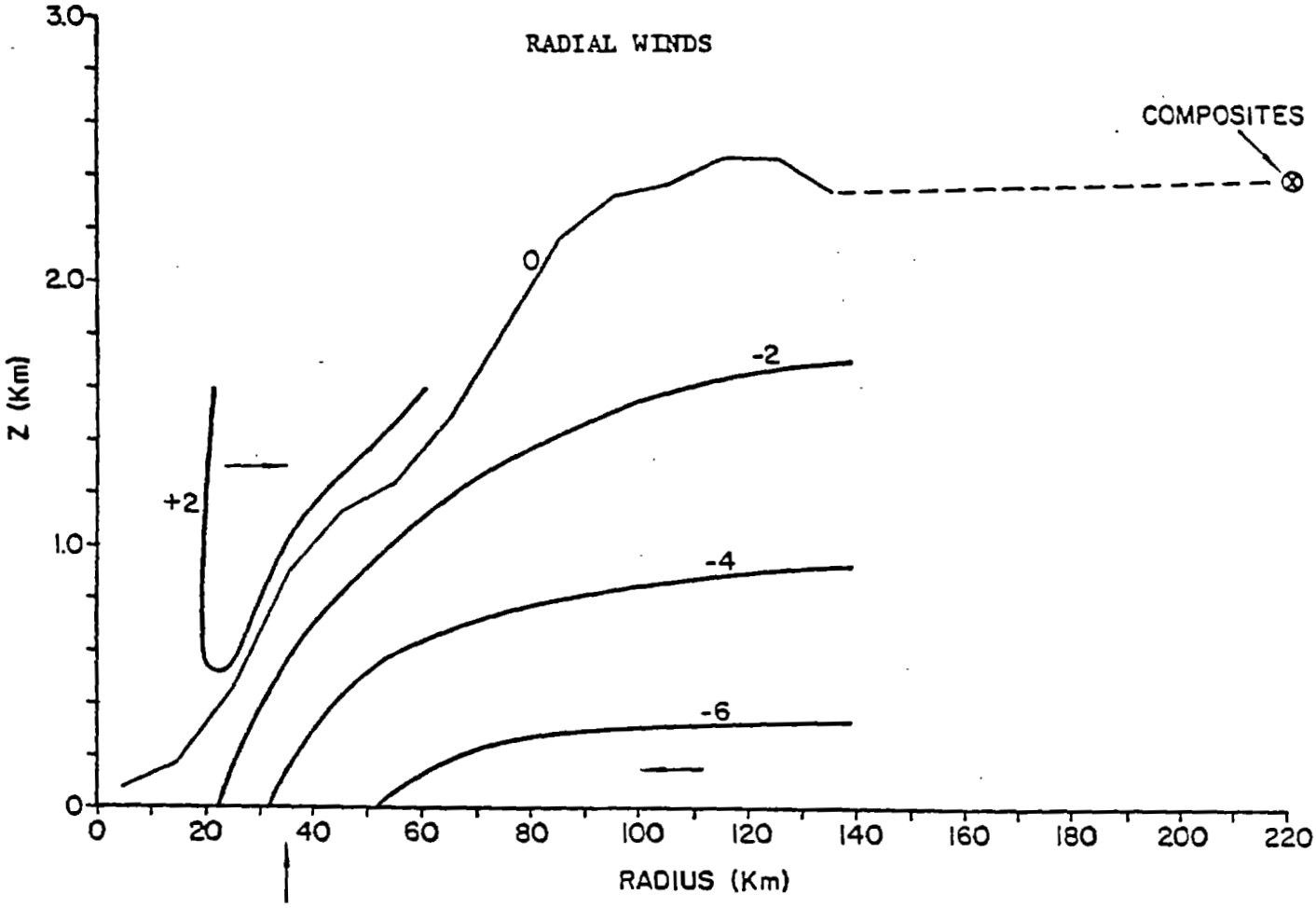

Figure A10. Vertical cross-section of the mean radial wind (m s^{-1}). The zero contour (vertically interpolated, then radially smoothed) corresponds to the top of the inflow layer. Other contours were drawn subjectively. Also shown is the V_R = 0 level at R = 2° (222 km) from Frank's (1977b) composite analysis of typhoons.

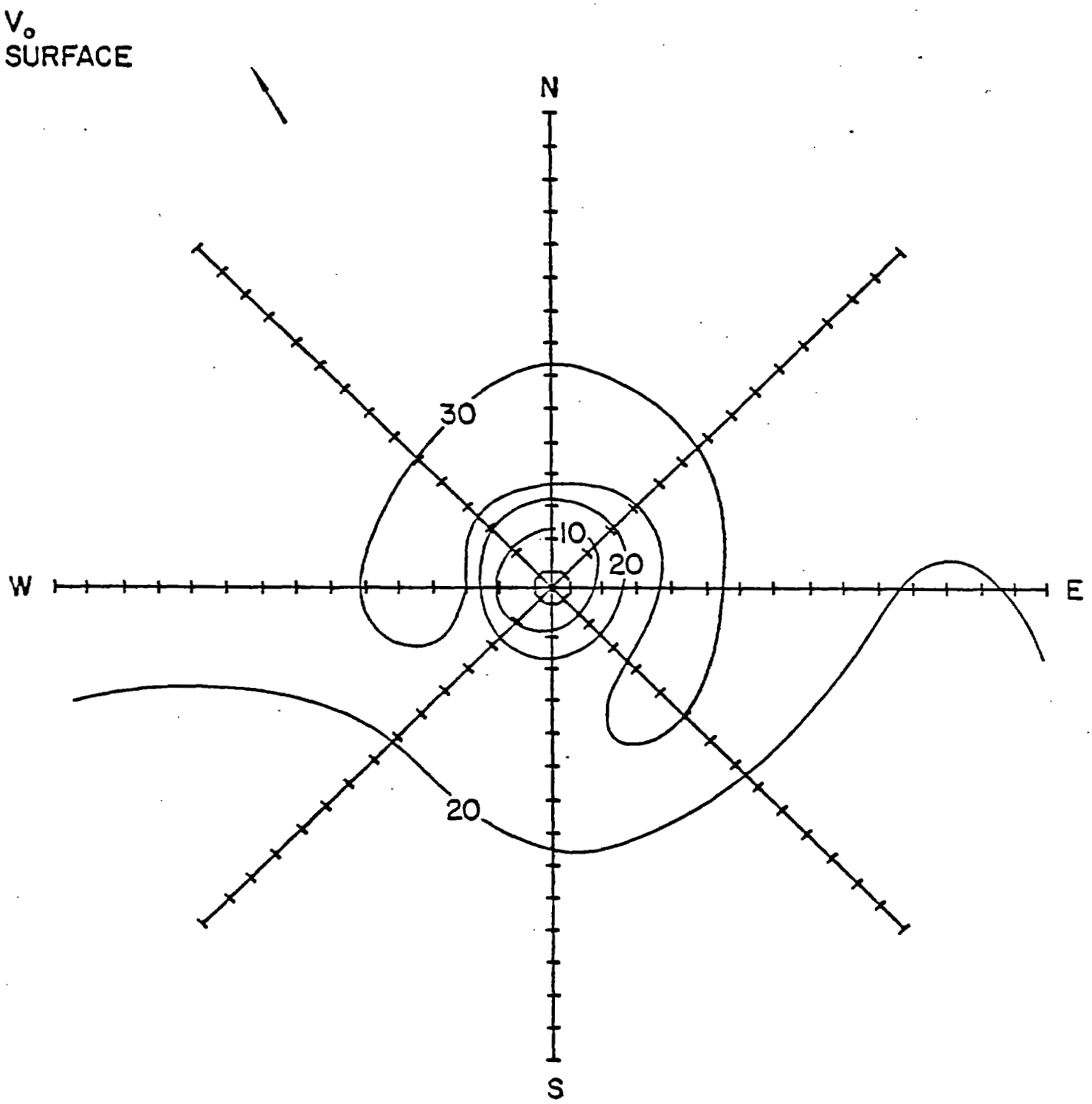

Figure A11. Surface wind speeds (V_o - m s^{-1}) in stationary coordinates based on corrections to 560 m winds suggested by Powell (1982 and personal communication). The grid tic marks are at 10 km radial intervals from 5-145 km radius. The

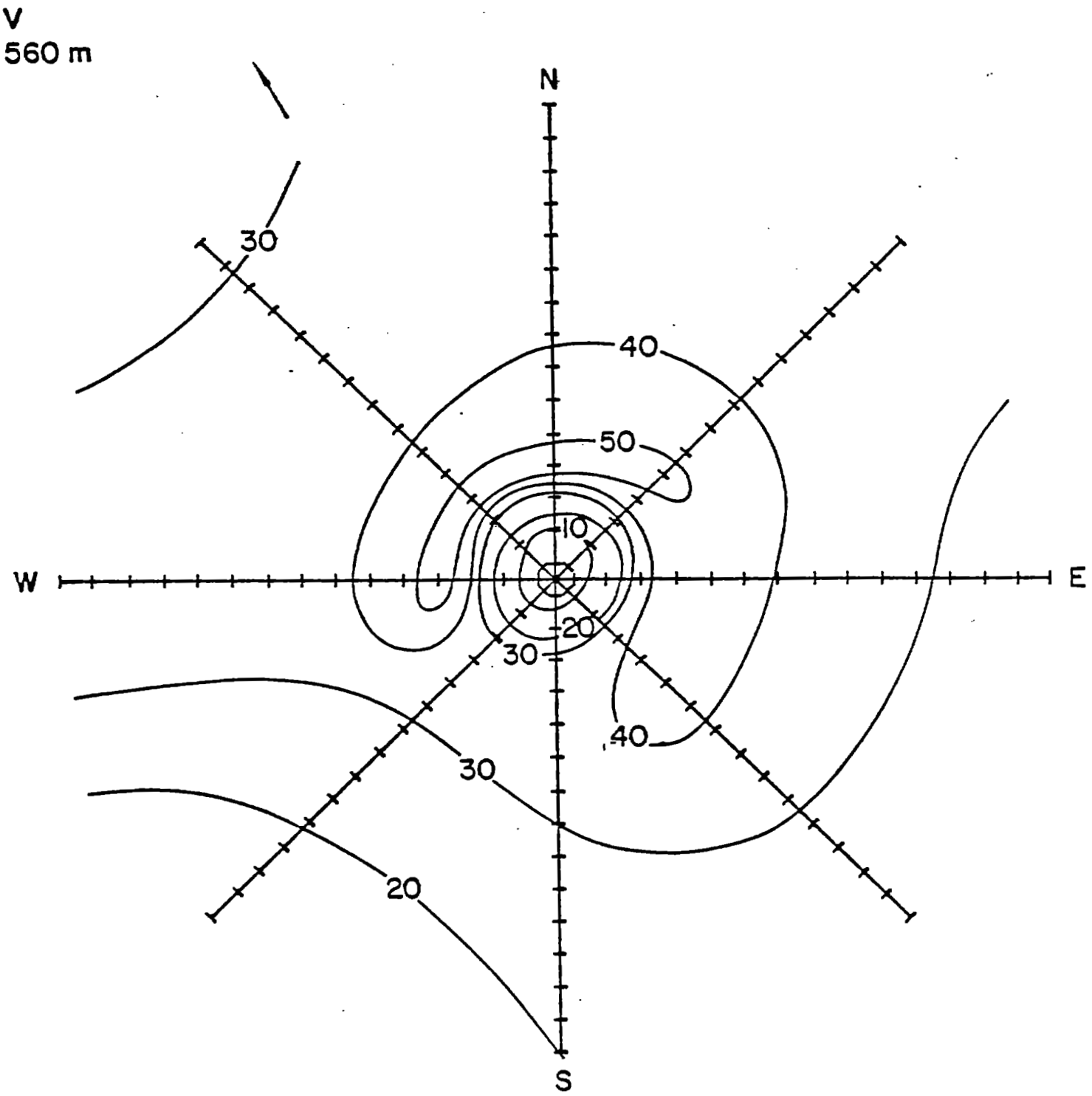

Figure A12. Wind speeds at 560 m in stationary coordinates (m s^{-1}).

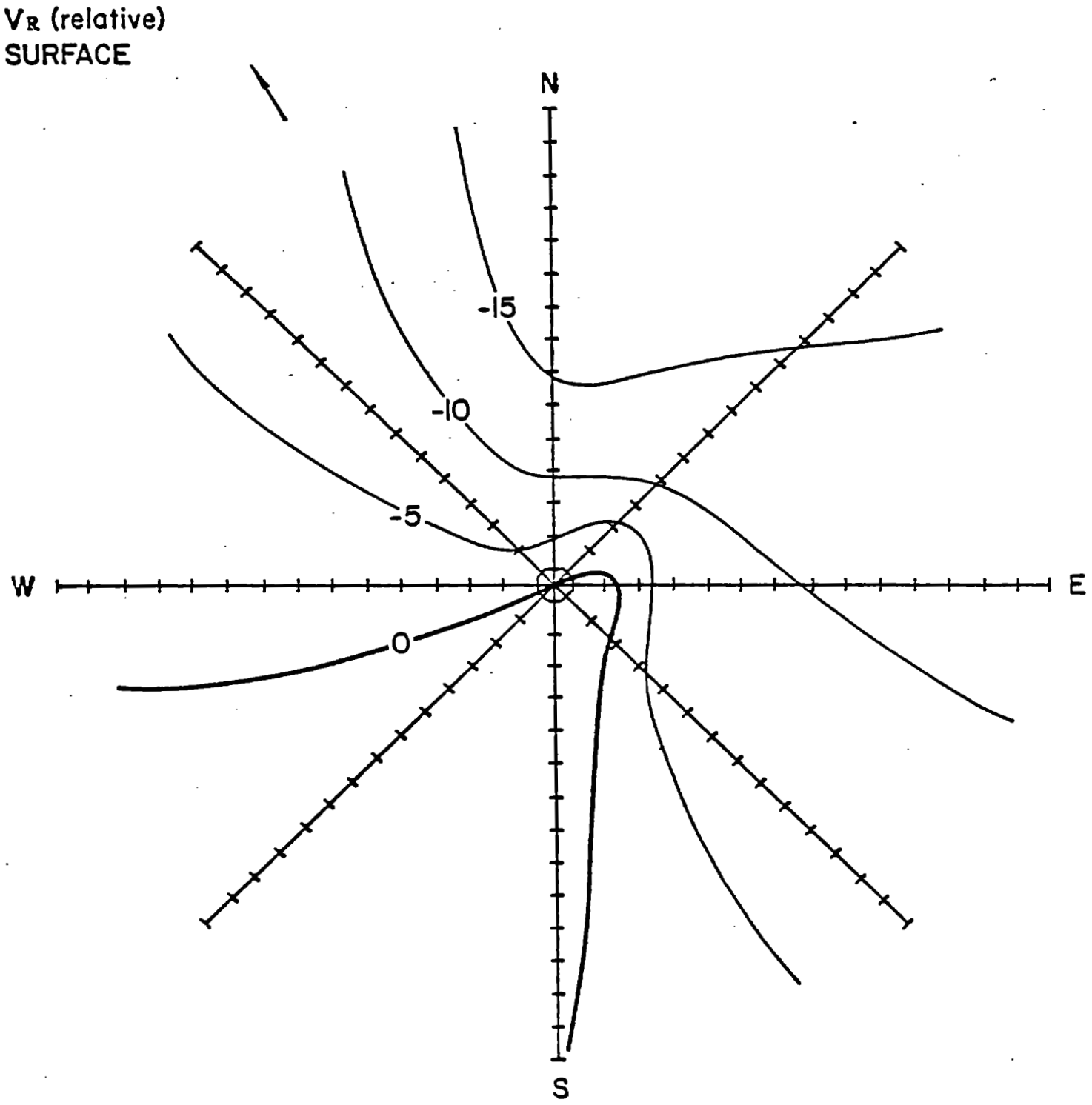

Figure A13. Radial winds (V_R - m s^{-1}) at the surface in storm-relative coordinates.

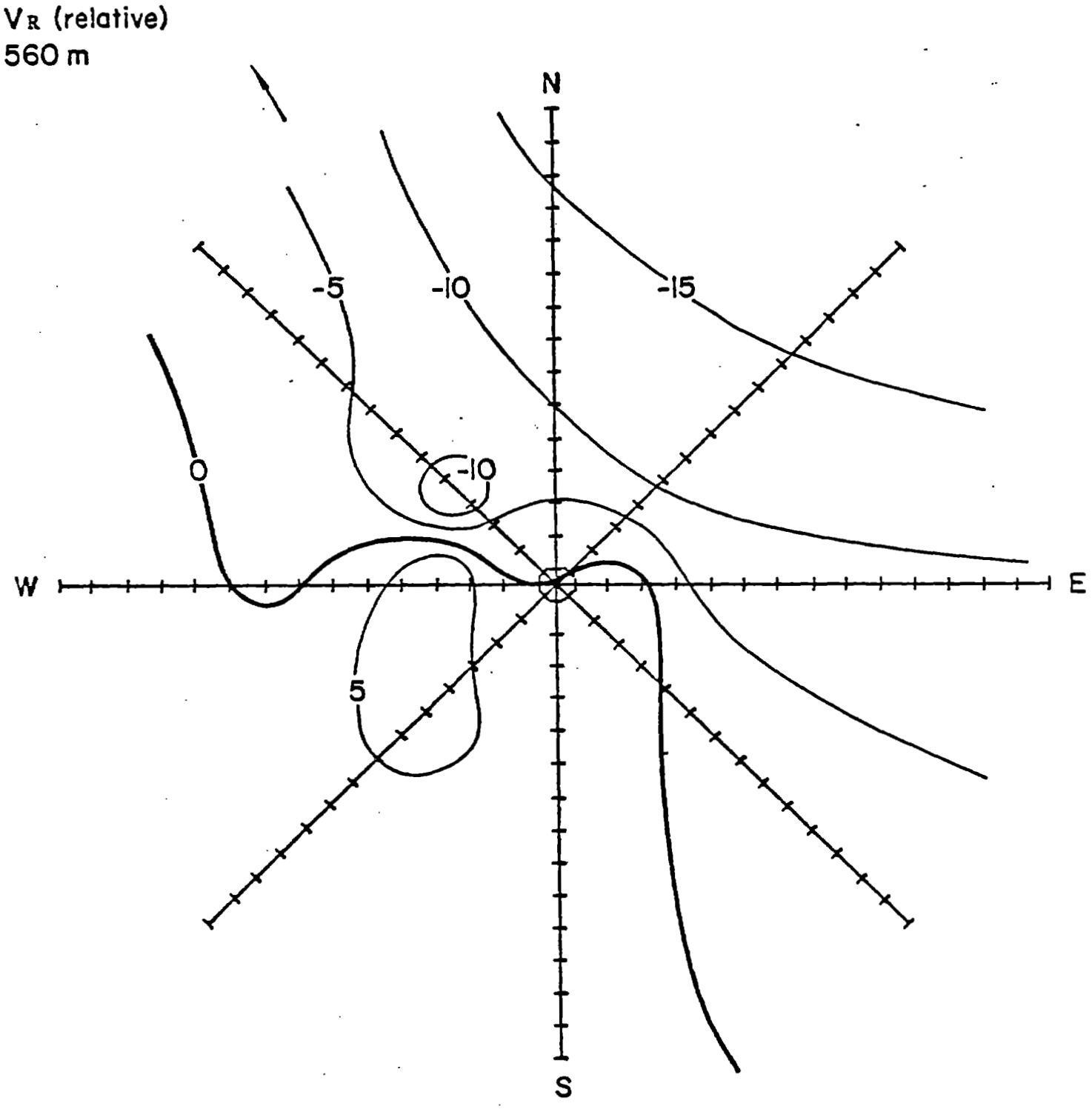

Figure A14. As in Fig. A 13 but at z = 560 m.

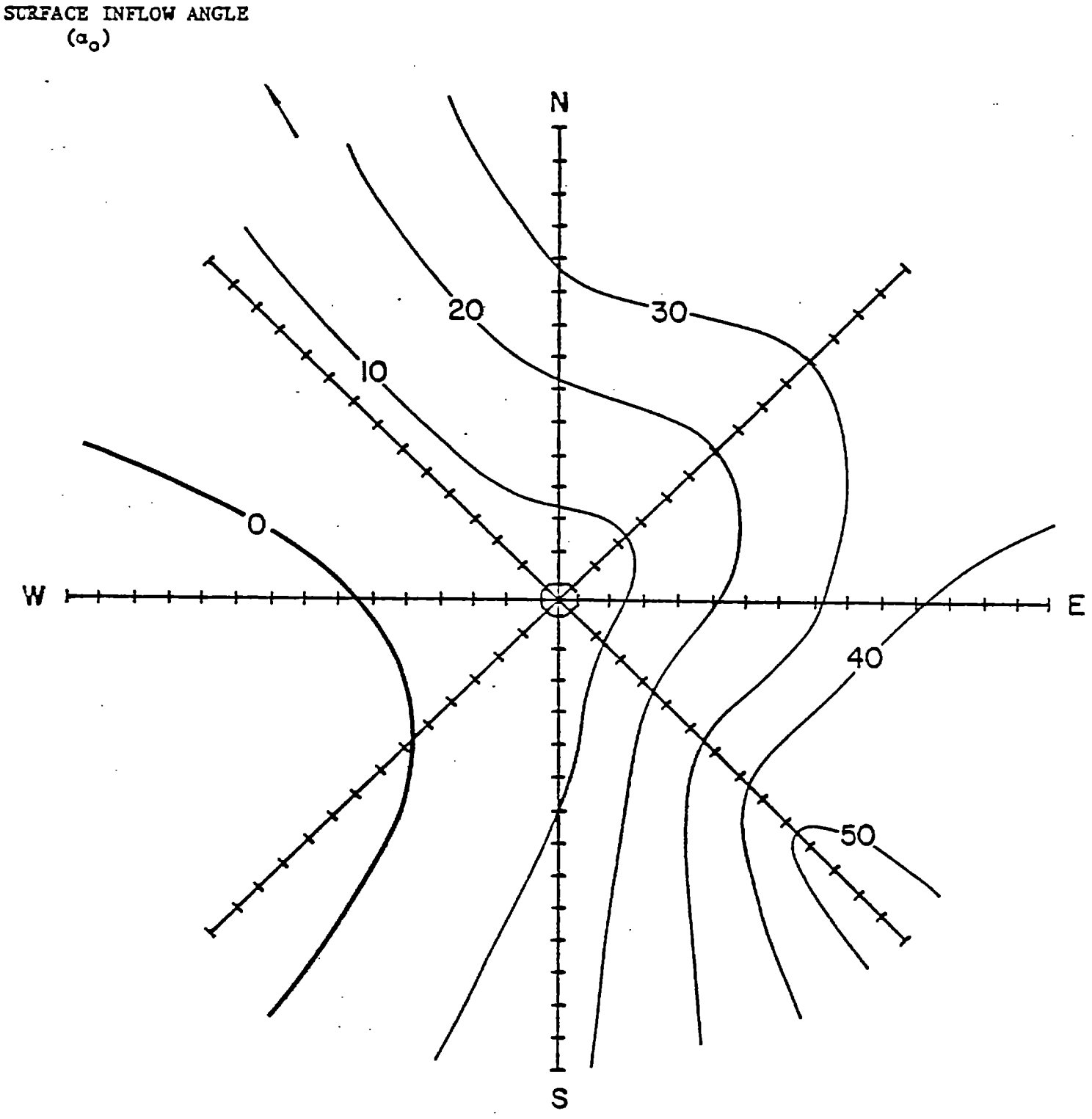

Figure A15. Surface inflow angles (degrees - positive for inflow) in stationary coordinates.

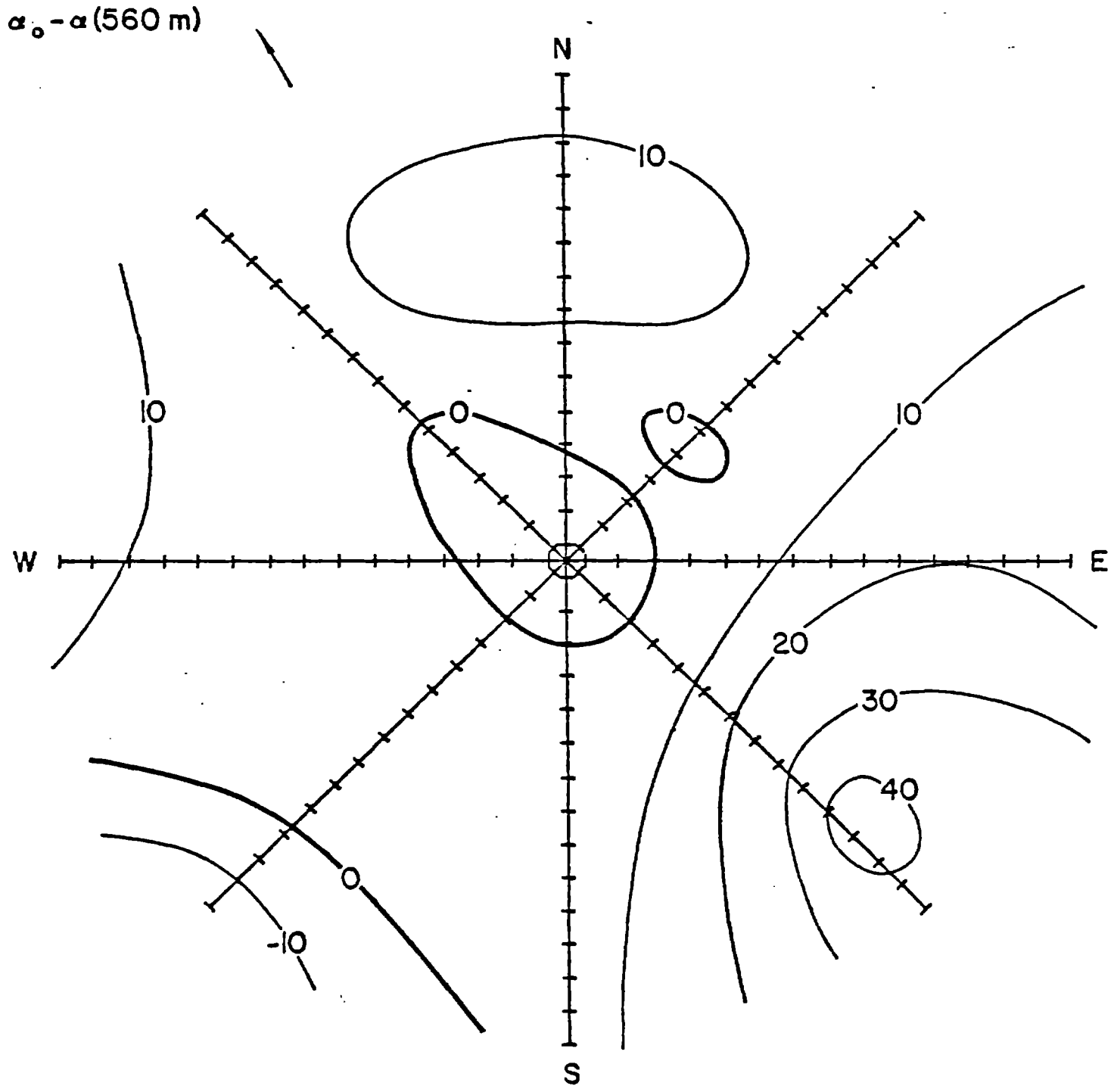

Figure A16. Inflow veering (surface inflow angle minus the inflow angle at z = 560 m) in stationary coordinates.

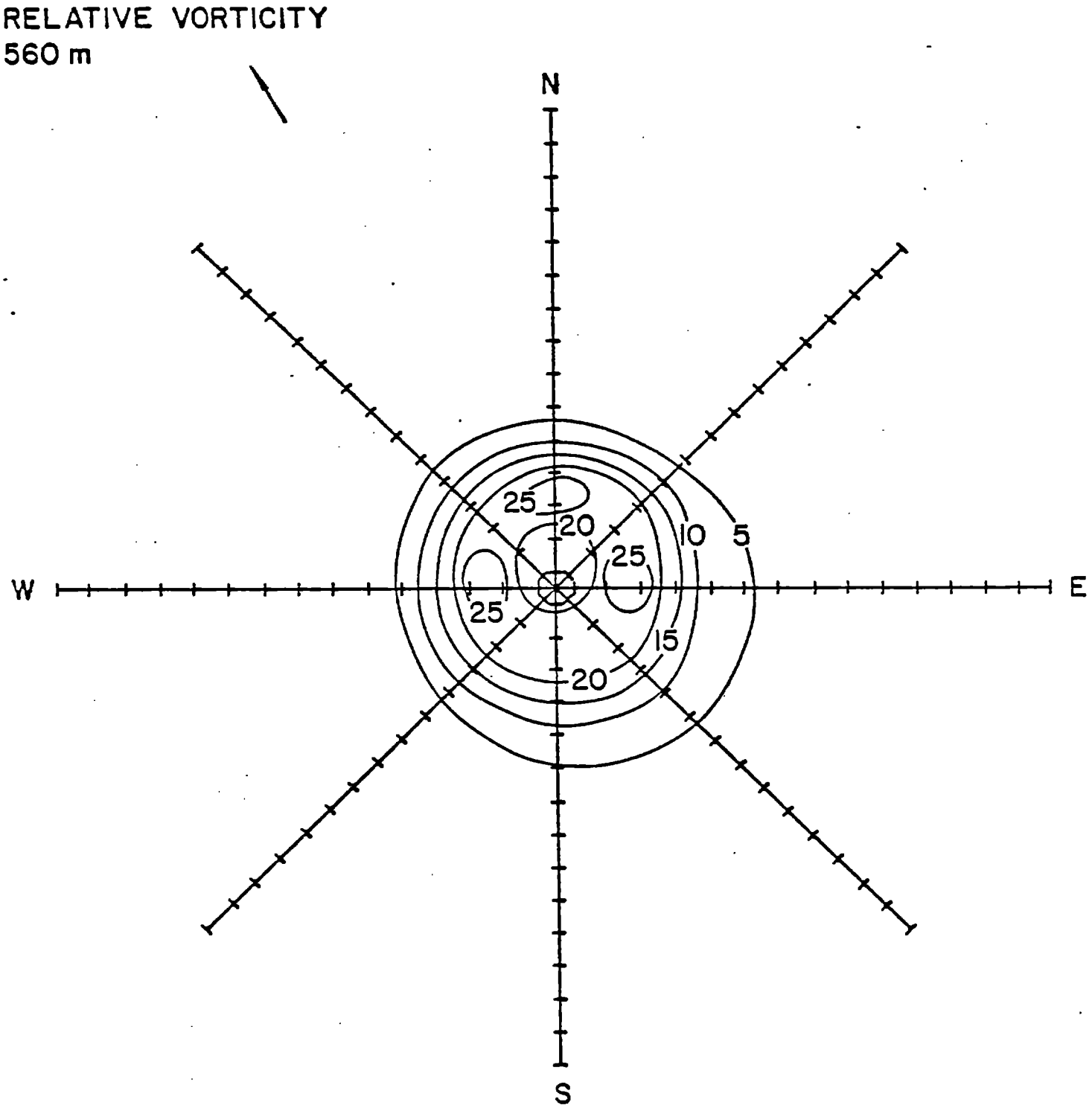

Figure A17. Relative vorticity at 560 m (x 10^{-4} s^{-1}), radially smoothed.

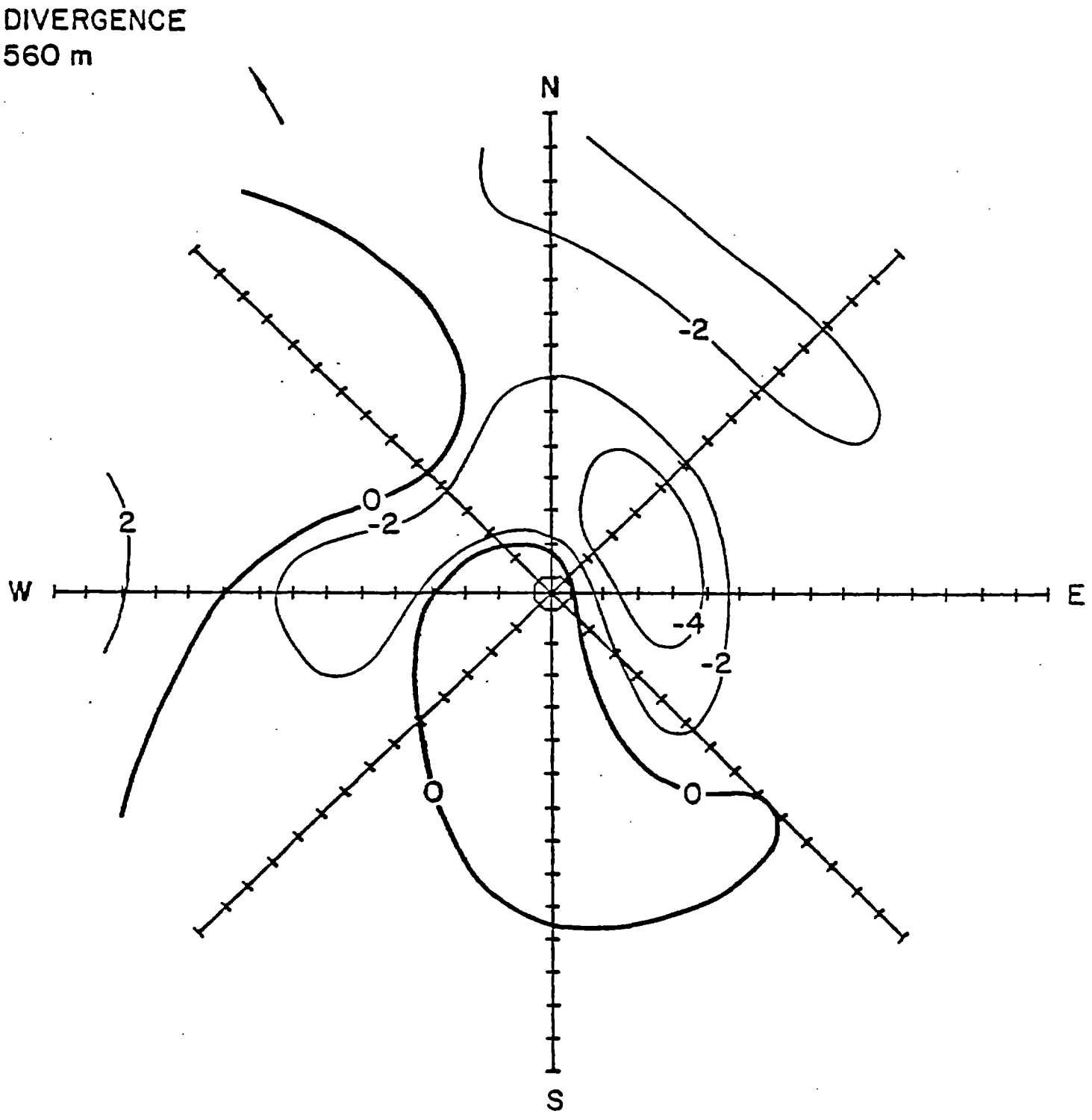

Figure A18. Divergence at 560 m (x 10^{-4} s^{-1}). Radially smoothed.

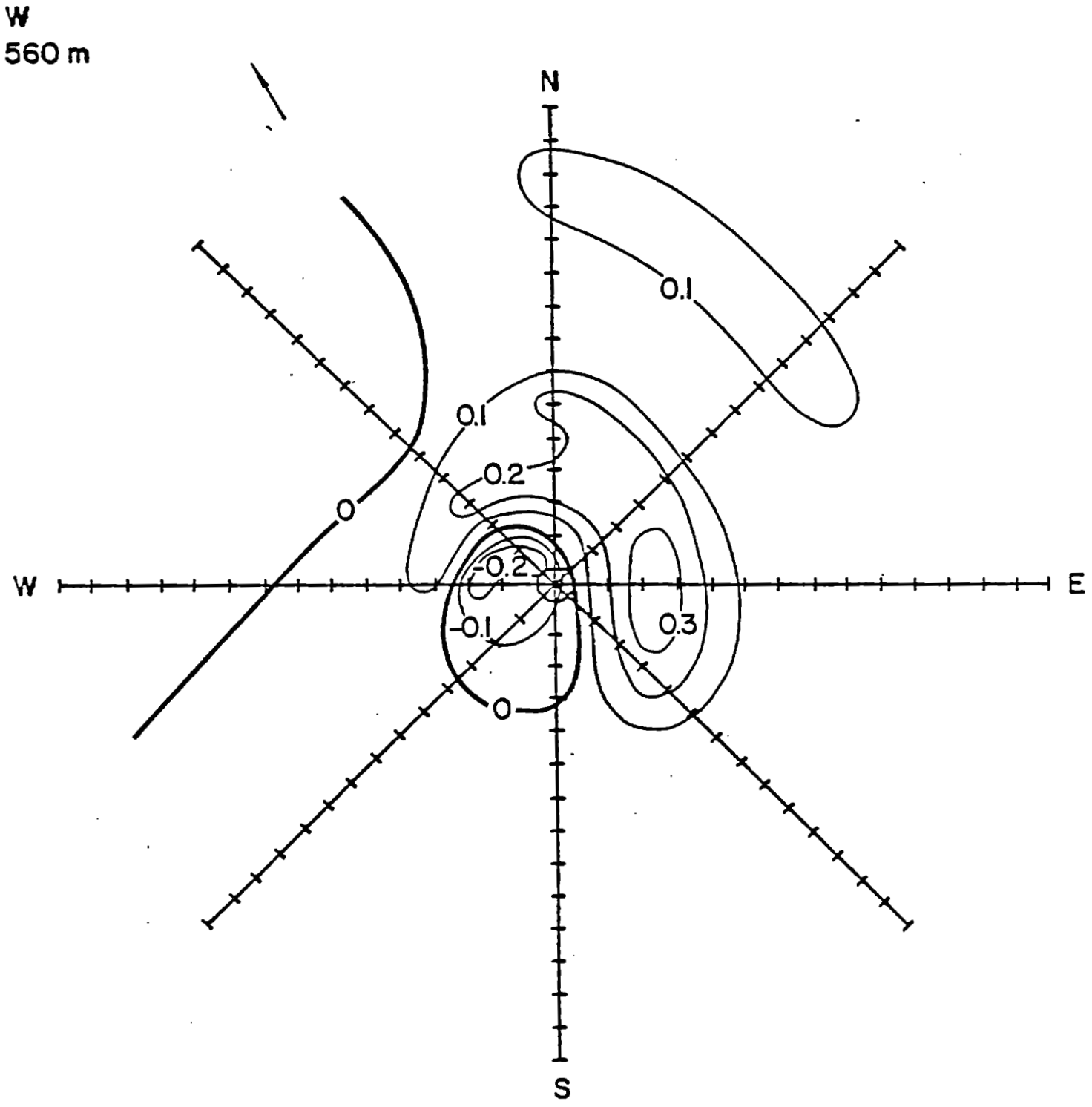

Figure A19. Vertical velocity at 560 m (m s^{-1}).

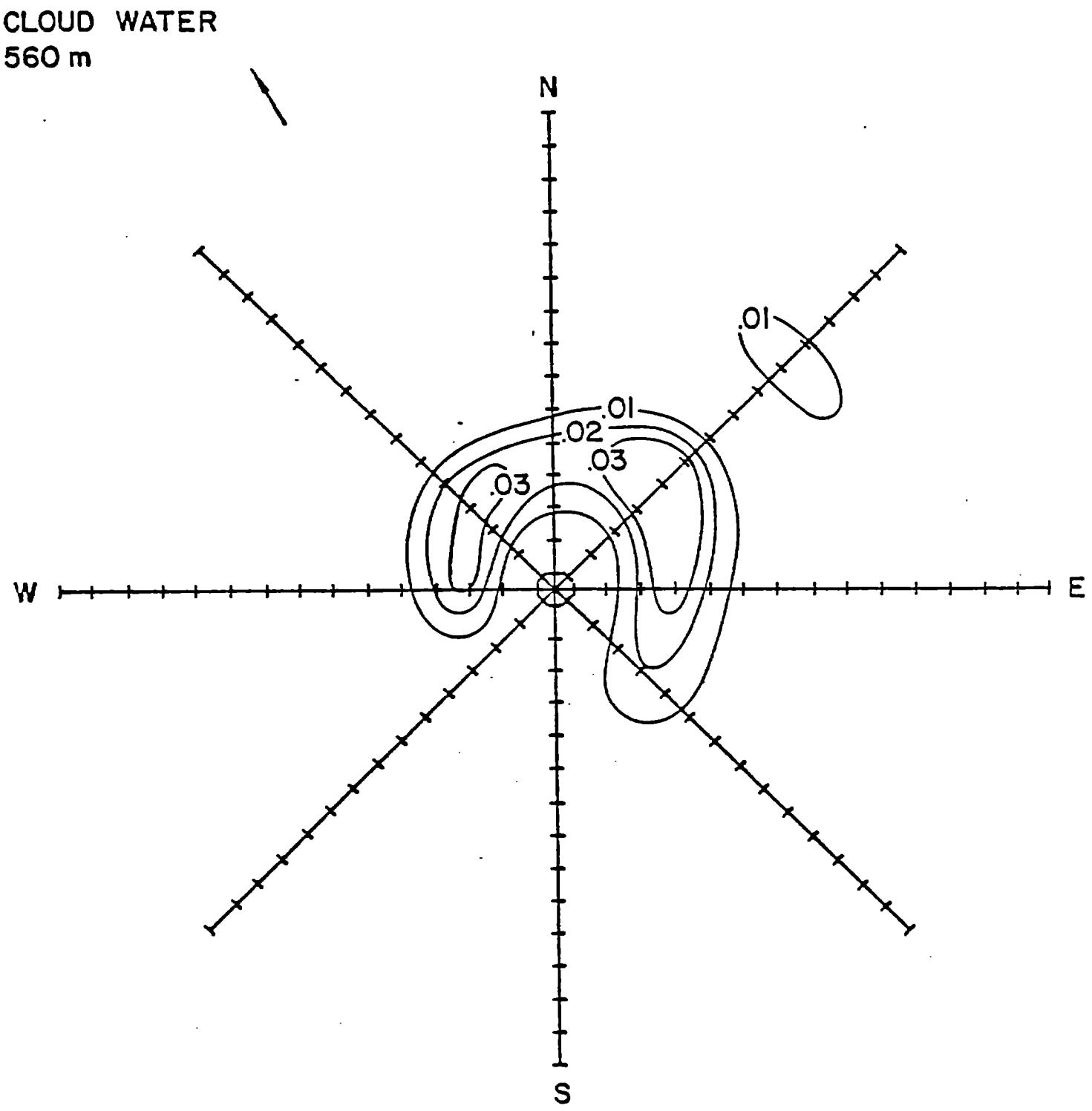

Figure A20. Cloud water at 560 m (g m^{-3}).

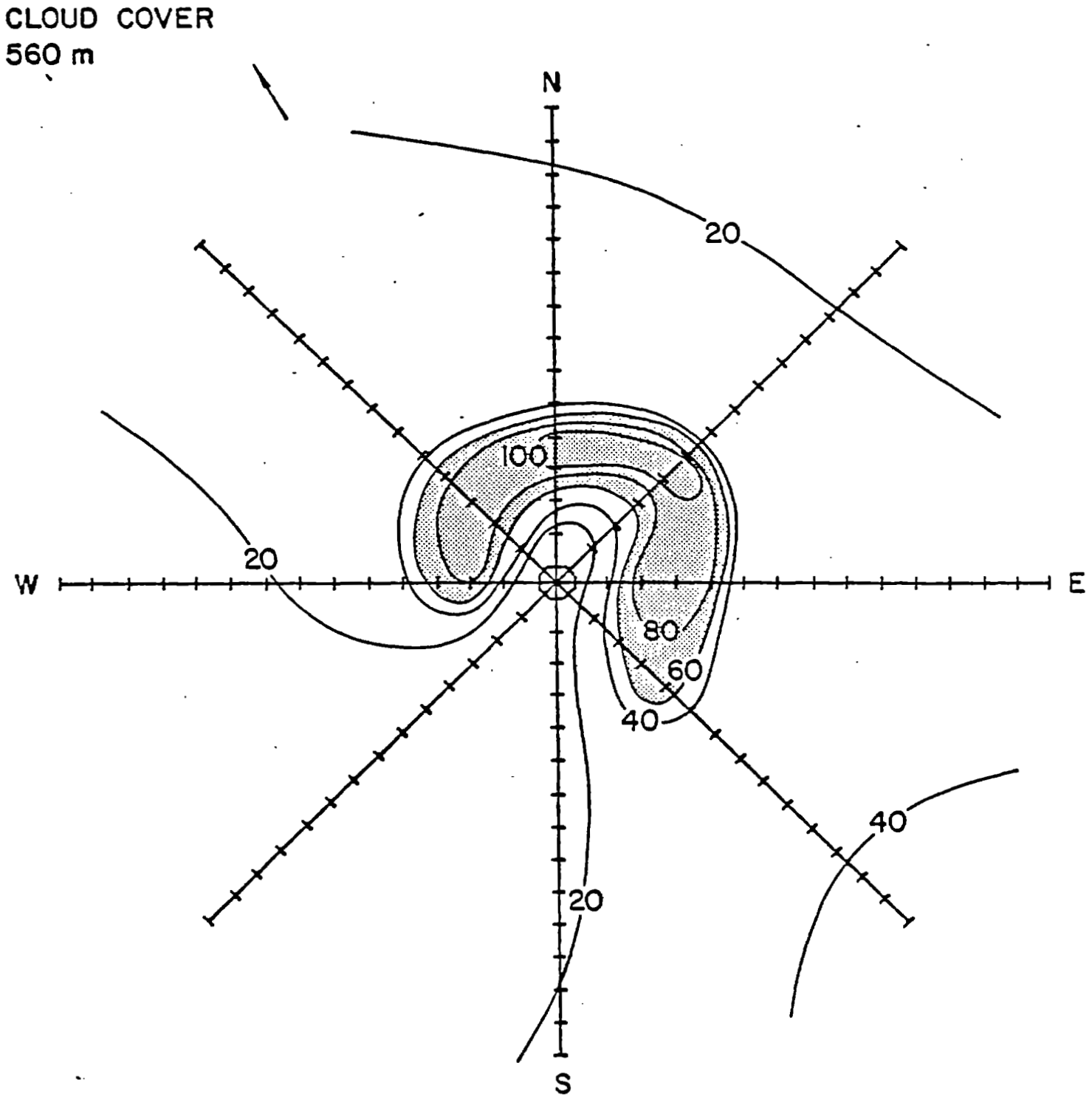

Figure A21. Percentage of 1 s observations during which cloud water was detected.